DEVELOPMENT OF A MICROFLUIDIC DEVICE

FOR SYNTHESIS OF LIPID BI-LAYER *IN-SITU*

A Thesis

by

BANNEYAKE MUDIYANSELAGE RANIL UGEESHKUMARA BANNEYAKE

Submitted to the Office of Graduate Studies of
Texas A&M University
in partial fulfillment of the requirements for the degree of

MASTER OF SCIENCE

December 2008

Major Subject: Mechanical Engineering

DEVELOPMENT OF A MICROFLUIDIC DEVICE

FOR SYNTHESIS OF LIPID BI-LAYER *IN-SITU*

A Thesis

by

BANNEYAKE MUDIYANSELAGE RANIL UGEESHKUMARA BANNEYAKE

Submitted to the Office of Graduate Studies of
Texas A&M University
in partial fulfillment of the requirements for the degree of

MASTER OF SCIENCE

Approved by:

Chair of Committee,	Debjyoti Banerjee
Committee Members,	Won-Jong Kim
	Victor M. Ugaz
Head of Department,	Dennis L. O'Neal

December 2008

Major Subject: Mechanical Engineering

ABSTRACT

Development of a Microfluidic Device for Synthesis of Lipid Bi-Layer *In-Situ.*

(December 2008)

Banneyake Mudiyanselage Ranil Ugeeshkumara Banneyake, B.Sc. Eng, University of Peradeniya

Chair of Advisory Committee: Dr. Debjyoti Banerjee

Lipid bi-layers are ubiquitous components of biological cells and are found in a variety of cell components. In biological membranes, lipid bi-layer membranes carry membrane proteins, which control transport of material and communication of signals in and out the cell. There are several disadvantages involved with patch clamping method as a way of studying biological membranes and protein interactions. Hence, artificial synthesis of bi-layer has been of great interest in basic biophysical studies, drug discoveries in pharmaceutical studies and study of protein nanopores for precise engineering applications. However, conventional lipid bi-layer synthesis techniques require skilled operators, have low repeatability (reliability), have portability restrictions and result in unstable bi-layers having a short lifetime.

In this investigation a novel microfluidic device and a method for artificial synthesis of lipid bi-layer *in-situ* are explored. In the proposed method, lipid trapped at an aperture on a Teflon sheet, is thinned to form a lipid bi-layer by a continuous flow of buffer solution on both sides of the aperture in the microfluidic device. The microfluidic

device is expected to have advantages from its compact design. Further, the new approach is expected to be repetitive and good for automation removing the requirement of a skilled operator.

The microfluidic device was fabricated using two glass substrates. Two channels of '+' shape were etched and through holes were fabricated at all four terminal ends of the microchannels on each glass substrate. A thin Teflon sheet carrying a 100μm diameter hole was sandwiched between the two glass wafers forming two sets of microchannels on both sides of the aperture. An analytical microfluid model of the microchannels was developed to investigate the nature of the flow and to select microchannel parameters. Experiments using the proposed device were performed to verify the feasibility of the novel approach for lipid bi-layer synthesis. Experimental results suggest formation of a lipid bi-layer at an aperture on the Teflon sheet but further investigation might be necessary for verification. Life time of the bi-layer is short mainly due to low quality of the used aperture.

DEDICATION

This thesis is dedicated to my Mother, Badhra, and Father, Daya, who provided a solid foundation which was not limited to my academic progression. My Mother's dedication and love have always encouraged me to aim far and achieve higher goals. This is also dedicated to my '*Loku Amma*', Malathi, for stretching a helping hand whenever I needed. If not for them I would not have been what I am today.

ACKNOWLEDGEMENTS

I would like to thank my research advisor, chair of the advisory committee, Dr. Debjyoti Banerjee, for providing continuous support and guidance with this research. My thanks go to my advisory committee members, Dr. Won-Jong Kim and Dr. Victor Ugaz, for always being prepared to help me. Further, I desire to thank the colleagues of the Multiphase Flow and Heat Transfer Laboratory for being helpful in various means during my time among them.

My thanks go to the Department of Mechanical Engineering, Texas A&M University and its staff for equipping me with knowledge to succeed in my research. I extend my thanks to the National Aeronautics and Space Administration University Research Engineering and Technology Institute (NASA URETI) for providing funding for this study. I also thank NanoMEMS Research LLC for partially supporting my graduate studies. I am thankful to Dr. Ali Beskok of Old Dominion University (ODU) for making this project possible. I would also like to thank Dr. Allison R. Ficht and Dr. Xiaofeng Kang for having useful discussions. Special thanks should be given to Dr. Jingyi Shen and other staff members of the Material Characterization Facility of Texas A&M University.

NOMENCLATURE

2D	Two Dimensional
A	Cross-Section Area of Micro-Channel
Ag	Silver
AgCl	Silver Chloride
A_L	Area of the Lipid Bi-Layer
Au	Gold
BOE	Buffered Oxide Etchant
BNC	Bayonet Neill-Concelman Connector
Cr	Chromium
D	Equivalent Diameter of Micro-Channel
d	Width of the Bi-Layer
DC	Direct Current
DI	Deionized
DPhPC	1,2-diphytanoyl-sn-glycero-3-phosphatidylcholine
DSP	Digital Signal Processing
ECDM	Electrochemical Discharge Machining
h	Height of Micro-Channel
K	Pressure Gradient along a Micro-Channel
K_0	Pressure due to Surface Tension
L	Length of a Micro-Channel

H_2S	Hydrogen Gas
H_2SO_4	Sulfuric Acid
HCL	Hydrochloric Acid
HF	Hydrofluoric Acid
KCl	Potassium Chloride
KOH	Potassium Hydroxide
m	Mass of Fluid Volume
NaOH	Sodium Hydroxide
NH_4F	Ammonium Fluoride
Ni	Nickel
p	Pressure
Q	Fluid Flow Rate in Micro-Channel
Re	Reynolds Number
RIE	Reactive Ion Etcher
t	Time
Ti	Titanium
u	Fluid Velocity along Micro-Channel (i.e. in x Direction)
USB	Universal Series Bus
UV	Ultra Violet
V	Fluid Volume in Micro-Channel
W	Width of Micro-Channel
x	Coordinate along Micro-Channel

y	Coordinate Perpendicular to Micro-Channel Bottom
z	Coordinate along the Thickness of Micro-Channel
η	Dynamic Viscosity of Fluid
ρ	Fluid Density
ρ_L	Conductivity of Lipid
υ	Kinetic Viscosity of Fluid

TABLE OF CONTENTS

Page

ABSTRACT iii

DEDICATION v

ACKNOWLEDGEMENTS vi

NOMENCLATURE vii

TABLE OF CONTENTS x

LIST OF TABLES xii

LIST OF FIGURES xiii

1. INTRODUCTION 1

2. OPERATION OF MICROFLUIDIC DEVICE 7

    2.1 Analytical Flow Model 9
    2.2 Flow Control 17

3. FABRICATION OF NOVEL DEVICE 25

    3.1 Glass Etching with HF Wet Etchants 28
        3.1.1 Photoresist Masks 29
        3.1.2 Metal Masks 39
        3.1.3 Etchants and Etching Process 42
    3.2 Fabrication of Through Holes on Glass Wafers 50
        3.2.1 Electrochemical Discharge Machining of Holes 50
        3.2.2 Drilling of Holes 53
    3.3 Preparation of Teflon Sheet 54
    3.4 Assembling 59
        3.4.1 Clamping of Layers 59
        3.4.2 Bonding of Layers Using Epoxy 65
        3.4.3 Thermal Bonding of Layers 69
        3.4.4 Tubing Connection 69

4. EXPERIMENT AND RESULTS 72

Page

4.1 Electronic Measurement System 73
4.2 Preparation for the Experiment 78
4.3 Experimental Procedure 84
4.4 Results 87
4.5 Processing and Interpretation of Results 89

5. CONCLUSION AND FUTURE DIRECTIONS 93

5.1 Conclusion 93
5.2 Future Directions 94

NOTES 95

REFERENCES 96

APPENDIX A SIGNAL PROCESSING PROCEDURE 101

VITA 114

LIST OF TABLES

Page

Table 1: Properties of fluids 15

Table 2: Channel dimensions 15

Table 3: Tandem syringe pumps used in the experiments 23

Table 4: Some trials for selecting better photolithographic conditions 34

Table 5: Electrical characteristics for DphPC lipid bi-layer 73

Table 6: Data of the used chemicals.....83

Table 7: Summery of current measurements.....89

Table 8: Resistance results 90

LIST OF FIGURES

Page

Figure 1: Lipid bi-layer illustration (not to scale) 2

Figure 2: New lipid bi-layer formation concept 7

Figure 3: Lipid bi-layer formation procedure 8

Figure 4: Cross-section of micro-channel 10

Figure 5: Effect of surface tension on pentane flow 14

Figure 6: Effect of surface tension on water (aqueous solution) flow 14

Figure 7: Variation of pumping pressure against pentane flow rate in a micro-channel for various channel heights 16

Figure 8: Variation of pumping pressure against KCl flow rate in a micro-channel for various channel heights 17

Figure 9: Variation of Reynolds number for KCl flow rate in a micro-channel for various channel heights (channel width = 0.5mm) 19

Figure 10: Variation of Reynolds number for pentane flow rate in a micro-channel for various channel heights (channel width = 0.5mm) 19

Figure 11: Velocity response of a stepper motor for a saw-tooth velocity reference input (Euclid Research) 20

Page

Figure 12: Position response of a stepper motor for a ramp reference input (Euclid Research) 21

Figure 13: Cumulative fluid flow for different gear reductions between stepper motor and syringe piston 22

Figure 14: Three-layer design of the device. a Unassembled layers. b After sandwiching Teflon sheet in between glass wafers. Closed channels are formed at each Teflon-glass interface 26

Figure 15: Dimensions (in millimeters) of the cross-channels on glass wafers. Channel depth is varied between 5μm – 10μm 26

Figure 16: SU8 process. (copyright © 2007 MicroChem Corp.) 30

Figure 17: Glass etching process using photoresist mask. A negative photo mask is used for photolithography as SU8 is a negative photoresist 31

Figure 18: Spin coater (from website of Micro Chemical Facility, Texas A&M University) 31

Figure 19: Mask aligner 32

Figure 20: 3D Microscope (from website of Micro Chemical Facility, Texas A&M University) 33

Figure 21: Profilometer system (from website of Micro Chemical Facility, Texas A&M University) 33

Page

Figure 22: Results of 5 seconds exposure time for SU8 50. a Mask. b After etching (mask still on) 35

Figure 23: Results of 15sec exposure time for SU8 50. a Mask. b After etching (mask still on) 35

Figure 24: Results of 15sec exposure time for SC1827. a Mask. b After etching (mask still on) 35

Figure 25: Etching with standard SU8 mask (obtained with Profilometer). a Effect of undeveloped SU8 debris present in the channels. b Chamber was generally of good quality 36

Figure 26: Improved SU8 50 photoresist mask with modified photolithography process. Channel edges are not firm 37

Figure 27: Channels etched with modified SU8 mask (obtained with 3D Microscope). a Smooth channels but damaged edges. b Sometimes channel edges were better 37

Figure 28: Reactive Ion Etcher 38

Figure 29: Glass etching process using metal mask. A positive photo mask is used for photolithography as SC1827 is a positive photoresist 40

Figure 30: Au/Cr metal mask 41

Page

Figure 31: Glass etched with BOE for 50 minutes. a Channel cross-section. b Central chamber 44

Figure 32: Glass etched with BOE (20:1) for 5 hours. a Channel cross-section. b Central chamber 46

Figure 33: Glass etched with 1:1:10 of HF: HCl: BOE (50:1) for 17 minutes. a Channel cross-section. b Central chamber 47

Figure 34: Pyrex etched with 1:1:10 of HF: Hal: BOE (50:1) for 150 minutes. SU8 is stripped off the channel edges. a Channel cross-section. b Central chamber 48

Figure 35: Pyrex etched with 1:1:1 of HF: HCl: BOE (20:1) for 30 minutes.....49

Figure 36: Apparatus used for ECDM process 51

Figure 37: A through hole obtained from ECDM process.....52

Figure 38: A drill hole (1 mm diameter) obtained by drilling 54

Figure 39: An aperture (400µm diameter) on Teflon obtained by punching.....56

Figure 40: Cross-section profile of an aperture (150µm diameter) on Teflon obtained by punching 56

Figure 41: Extruded Teflon sheet during hot punching 57

Figure 42: An aperture (75µm diameter) on a Teflon sheet.....58

Page

Figure 43: Colored water flow in a single cross channel test setup clamped with a G-clamp 60

Figure 44: Clamping of layers with G-clamp..... 61

Figure 45: Custom made C-shaped clamp. a Exploded view. b Assembly 62

Figure 46: Custom made new clamp (exploded view)..... 63

Figure 47: Custom made new clamp dimensions (in inches)..... 64

Figure 48: Testing of custom made new clamp for stressing the wafers 64

Figure 49: Testing of bonded layers..... 66

Figure 50: Profilometer plot showing epoxy layer thickness..... 68

Figure 51: Components of a NanoPort assembly and their dimensions (in mm) 70

Figure 52: Simplified diagram of the experimental setup..... 72

Figure 53: Schematic diagram of the apparatus with microfluidic device. The section view along the channel carrying KCl is shown (not to scale). Lipid bi-layer is shown to provide a better understanding to the reader..... 76

Figure 54: Use of a T-joint to connect the electrode into the KCl flow..... 78

Figure 55: Microfluidic device held using paper clips (aperture is visible)..... 79

Figure 56: Microfluidic device inside the Faraday cage 80

Figure 57: Experiment setup 81

Page

Figure 58: Schematic diagram of the apparatus with microfluidic device. The section view along the micro-channel carrying Pentane is shown (not to scale) 82

Figure 59: Signal observed when only KCl is present (Input voltage = 50mV; Current amplifier setting = 1Pa/1V) 85

Figure 60: Signal with noise observed after pumping of pentane (Input voltage = 50mV; Current amplifier setting = 1Pa/1V) 85

Figure 61: Stabilized signal with noise observed after pumping of pentane (Input voltage = 50mV; Current amplifier setting = 1Pa/1V) 86

Figure 62: Signal observed after breaking of lipid bi-layer (Input voltage = 50mV; Current amplifier setting = 1Pa/1V) 86

Figure 63: Expected and observed voltage variations (Input voltage = 50mV; Current amplifier setting = 1pA/1V) 88

Figure 64: Low-pass filter specifications 90

Figure 65: Model for resistance calculation 90

Figure 66: MATLAB command window 102

Figure 67: SPTool window initial view 103

Figure 68: SPTool window: creating a new filter 103

Figure 69: Low-pass filter design specifications in Filter Design and Analysis Tool ... 104

Page

Figure 70: Designed low-pass filter in Filter Design and Analysis Tool.....105

Figure 71: Visualization of low-pass filter.....106

Figure 72: Import data option in MATLAB main menu.....107

Figure 73: Import data browser.....107

Figure 74: Data Import Wizard.....108

Figure 75: Imported dataset appears in MATLAB workspace as a matrix.....108

Figure 76: Importing a dataset into SPTool.....109

Figure 77: Import to SPTool window.....109

Figure 78: Sampling frequency specification for dataset.....110

Figure 79: SPTool ready for filtering the dataset.....111

Figure 80: Signal Browser for viewing raw data.....111

Figure 81: Apply Filter window.....112

Figure 82: Filtered dataset (signal).....113

1. INTRODUCTION

Cell is the primary building box of biological systems. A biological membrane (also called the plasma membrane) defines the outline of a cell as well as some internal membranes may divide the cell into compartments (Hanke and Schlue 1993). Since the biological membranes provide the interface between cells and their surroundings, the membranes play an essential role in any biological system. Major functions of the biological membrane include facilitating communication of cell with its environment and other cells, transport of materials (e.g. ions) in and out of the cell across the membrane, enabling lateral signal flux, and cellular growth (Brown 1996; Hanke and Schlue 1993; Stouch and Bassolino 1996). Functions of the membrane are determined by its composition. The "fluid mosaic model" of biological membranes (and other similar models with modifications), treats the biological membrane to be composed of a double layer of lipid molecules, called 'Lipid Bi-layer', with associated proteins (membrane proteins) and other molecules (Hanke and Schlue 1993; Singer and Nicolson 1972). Hydrophobic hydrocarbon chains (called the "tails" of lipid molecules), form the membrane core, while hydrophilic ends ("heads" of lipid molecules) are in contact with the aqueous solutions outside the membrane (Figure 1). The observed high ion diffusion rates through the hydrophilic lipid bi-layer are possible because of the membrane proteins. The membrane proteins control the signals and ion/molecule transportation across the biological membrane (Funakoshi et al. 2006; Hanke and Schlue 1993).

This thesis follows the style of Microfluidic Nanofluidic.

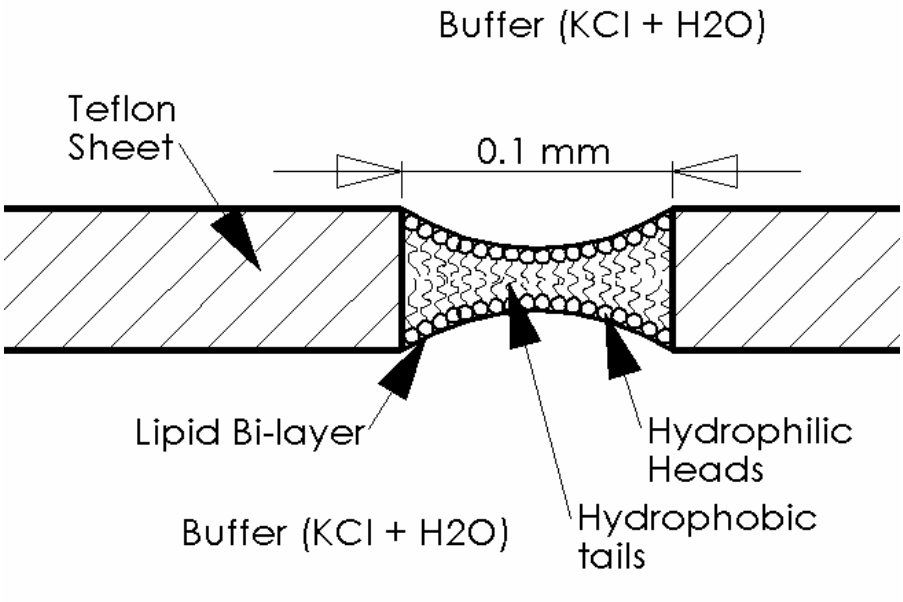

Figure 1: Lipid bi-layer illustration (not to scale)

Proteins form pores across the lipid bi-layer providing a path for ion channels. Since membrane proteins are water insoluble they are not as amenable for characterization as compared to water soluble proteins. Study of transport phenomena in living cells that are performed in biophysical studies, is also quite difficult due to heterogeneous nature of the membranes (Funakoshi et al. 2006; Hanke and Schlue 1993).

It is important to study biological membranes, their interactions with membrane proteins and the ion channels for enhanced understanding of their basic biophysics (Hanke and Schlue 1993; Malmstadt et al. 2006). Membrane proteins are the central attraction in pharmaceutical studies as drug discovery requires recognizing how membrane proteins react to drugs (Funakoshi et al. 2006; Malmstadt et al. 2006). Further, study of protein nanopores for precise engineering applications, such as

stochastic molecular sensing and DNA detection, has generated a great interest lately for investigation of membrane proteins (Kang et al. 2005; Malmstadt et al. 2006).

There are several different strategies used in ion channel studies based on microscopy, spectroscopy, biochemistry, molecular biology and electro-physiology (Hanke and Schlue 1993). Lipid bi-layer synthesis (classical methods) and the patch-clamp method (Suzuki H et al. 2004) were developed in the realm of electro-physiology, where electrical current recording of an isolated ion channel is possible. In the patch-clamp method a micropipette is brought into contact with a cell membrane and suction is applied in a way such that the membrane is sealed to the micropipette. Then by lifting the micropipette a small part of the membrane that fits into the aperture of the micropipette can be detached. This portion can be examined in isolation from rest of the membrane. Even though the patch-clamp technique has advantages such as ability to apply directly on biological systems, ease of use, stability, repeatability and high electrical resolution (Hanke and Schlue 1993), its biggest disadvantage of uncontrollable composition makes planar lipid bi-layer method preferable. In other words isolating an ion channel in the patch-clamp method is not easy or definite. Further, culture study is very time consuming and is a major drawback (Malmstadt et al. 2006).

The biological membrane is a very complicated system and complete artificial synthesis of it may not be practical. Therefore, general studies of the membranes using planar lipid bi-layer technique are limited to artificial formation of lipid bi-layer using a purified homogeneous lipid followed by introduction of a protein species, creating an aqueous pore across the bi-layer (Funakoshi et al. 2006; Hanke and Schlue 1993). In

general the artificial lipid bi-layer is formed by bringing two planar lipid mono-layers into contact. A monolayer can be observed at the lipid – aqueous interface, where hydrophilic end of the lipid molecule (also referred to as the "heads") face the aqueous solution. Classical methods of planar lipid bi-layer include the painting method and the folding method. Some variations of the patch-clamping technique have emerged at the end of the 70's (Hanke and Schlue 1993). Recently new techniques such as solvent extraction (Malmstadt et al. 2006) have been reported.

In the painting method a mechanical tool is used to spread a lipid dissolved in an organic solvent, such as decane, across an aperture connecting two compartments filled with an aqueous solution. The organic solvent and additional lipid gradually diffuse out of the membrane (solvent extraction method) until lipid bi-layer of 3 – 5nm thickness forms (Hanke and Schlue 1993). Automatic thinning occurs due to reduction in the surface tension of mono-layers resulting from: (1) the increase in chemical potential of lipid at annulus, (2) the Plateau-Gibbs border suction and, (3) London-Van der Waals attraction between the two aqueous phases on both sides of the lipid bi-layer. (Hanke and Schlue 1993). The folding method involves positioning of two mono-layers on the two sides of an aperture and bringing the two layers into contact to form the lipid bi-layer. Usually two chambers on both sides of the wall containing the aperture are filled with an aqueous solution (buffer) and the lipid solution (dissolved in a highly volatile solvent such as pentane or hexane) is added to two chambers (Funakoshi et al. 2006; Malmstadt et al. 2006). In about 5-15 minutes time the solvent evaporates leaving two lipid mono-layers formed on the aqueous solutions. By carefully elevating the aqueous solution

levels separately or simultaneously, the mono-layers are brought into contact at the aperture to form the lipid bi-layer. Since the aperture is very small the solution is restricted from flowing into the aperture and instead a monolayer is established. Hence in this method a simultaneous operation is not necessary (Hanke and Schlue 1993).

Most of the existing devices used for lipid bi-layer formation have various limitations, which includes the requirement of a skilled operator (Malmstadt et al. 2006; Suzuki H et al. 2004), short lifetime of the lipid bi-layer (Kang et al. 2007; Suzuki H, et al. 2004), low throughput resulting from bi-layer instability (Funakoshi et al. 2006) and long time to form the lipid bi-layer, limitations with size (Malmstadt et al. 2006), and low repetitiveness. There have been many studies involving improvement and extension of folding method as it is preferable over the painting method because it is more suitable for miniaturization, automation, repetition and high throughputs (Funakoshi et al. 2006; Malmstadt et al. 2006; Peterman M et al. 2002). While a lipid-wetting aperture is desired for lipid bi-layer formation, for flow of aqueous solution a hydrophilic channel is preferred. Since commonly used polymers are hydrophobic, flow control is not easy in polymer devices. However, glass microfluidic devices being hydrophilic better flow control is achieved. Therefore, devices fabricated in glass are better suited for microfluidic applications but devices fabricated in polymer substrates are easier to fabricate (Kelly and Woolley 2007). Miniaturization has been a main objective of most of the recent lipid bi-layer studies because a smaller device eases the handling steps and device operation; enables economical advantages due to reduction in usage of space as well as materials and operation fluids (reagents and analytes). Further, automation is

enabled on these microfluidic devices (Malmstadt et al. 2006) as well as portable platforms are realized (e.g., for enabling aero-space applications and space based microgravity experimental platforms). Micro fabricated apertures are expected to enable more stable lipid bi-layers (Funakoshi et al. 2006). Therefore, for the proposed microfluidic device for synthesis of lipid bi-layer - the micro-channels are fabricated in a glass substrate.

This report presents a novel approach of lipid bi-layer formation using a glass-Teflon-made microfluidic device. Scope of the study includes design and fabrication of the device, implementation of the proposed lipid bi-layer formation method, and verification of its functionality. Under this, concept of the operation and flow control issues are discussed and an analytical-flow-control-model is presented. Device fabrication methodologies and method optimization are detailed. The experimental apparatus and its electrical measurement system are explained. Finally experiment procedure, results and interpretation of the results are presented.

2. OPERATION OF MICROFLUIDIC DEVICE

The proposed method is a variant of the folding bi-layer method where the planar bi-layer formation is achieved at a miniature scale. In this method, the buffer and lipid are dissolved in n-pentane and are then flowed into two sets of channels on both sides of an aperture on a Teflon sheet (Schmitt et al. 2006). Hence this method is similar to the folding method. However, the lipid bi-layer is not formed by bringing the two mono-layers together at the aperture. Instead, lipid from two sides is brought together at the aperture to trap a bulk volume of lipid, which is then reduced in volume (and thickness) by a gradual removal of lipid using a continuous flow of buffer which finally leads to the formation of the lipid bi-layer (Figure 2). The salient steps in this method are illustrated in Figure 3.

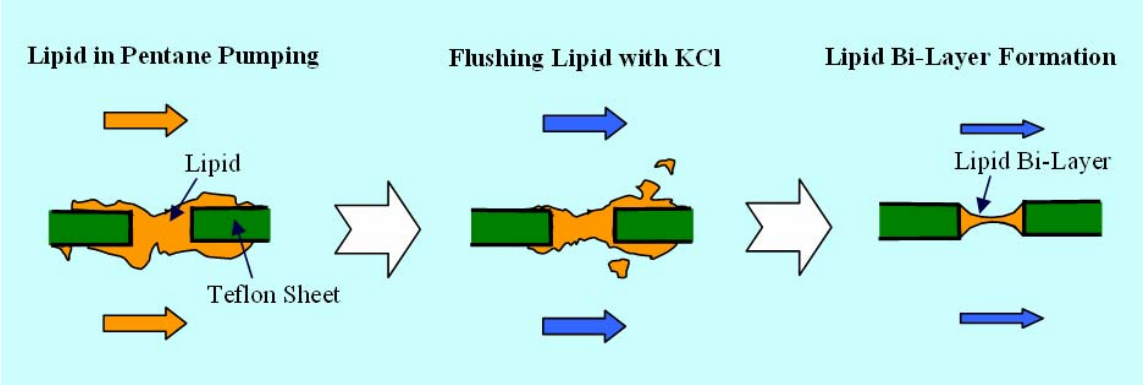

Figure 2: New lipid bi-layer formation concept

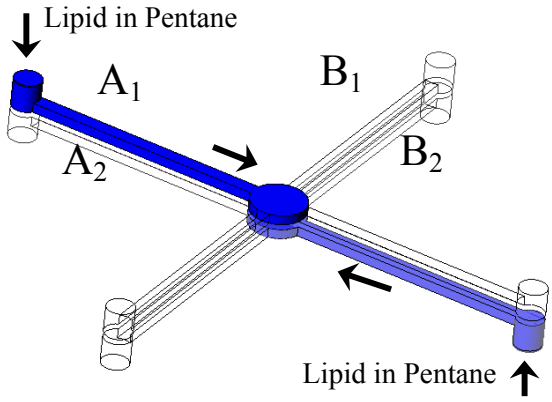

a) Pumping of Lipid dissolved in Pentane through channels on both sides of Teflon sheet.

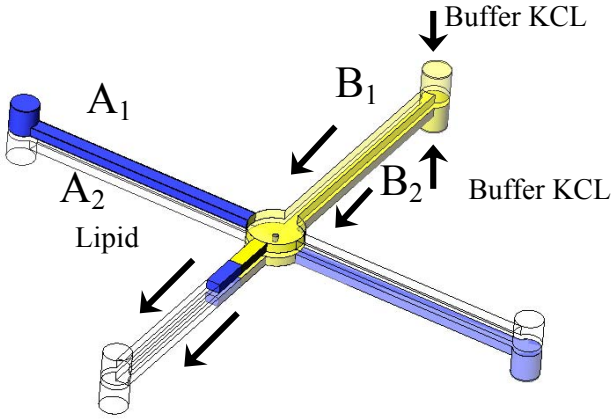

b) Pumping of KCl from channels on both sides of Teflon sheet flushing excessive Lipid.

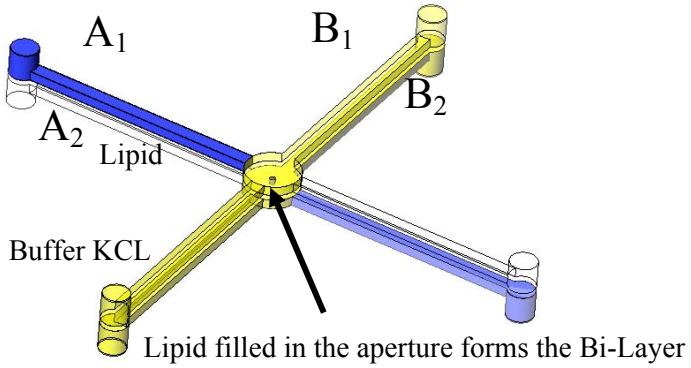

c) Pumping of KCl at a lower rate to support lipid bi-layer formation at the aperture.

Figure 3: Lipid bi-layer formation procedure

Detailed steps of the operation can be listed as follows:

1. Whole micro-channel volume is filled with 1M KCl (buffer) to wet the channel walls ensuring a smooth uniform KCl flow. This is also a necessary part in terms of electrical measurements, because KCl serves as a medium for electricity.
2. Lipid dissolved in n-pentane is filled from both sides using two channels at least up to the central chamber so that sufficient amount of lipid is trapped at the aperture (Figure 3a).
3. n-Pentane is allowed to evaporate leaving only lipid in the channels.
4. KCl is pumped on both sides using two channels gradually flushing the excessive lipid from the aperture till the lipid bi-layer is formed (Figure 3b and c).

Once the bi-layer is formed required experiments can be performed. When the lipid bi-layer breaks this procedure can be repeated starting from the step 2(mentioned before). Therefore, the repeatability requirement for the experimental procedure is satisfied in this approach.

2.1 Analytical Flow Model

An analytical model was developed to optimize the experimental conditions. This model, as shown in Figure 4, was used as the basis in determining channel depth and selecting flow rates.

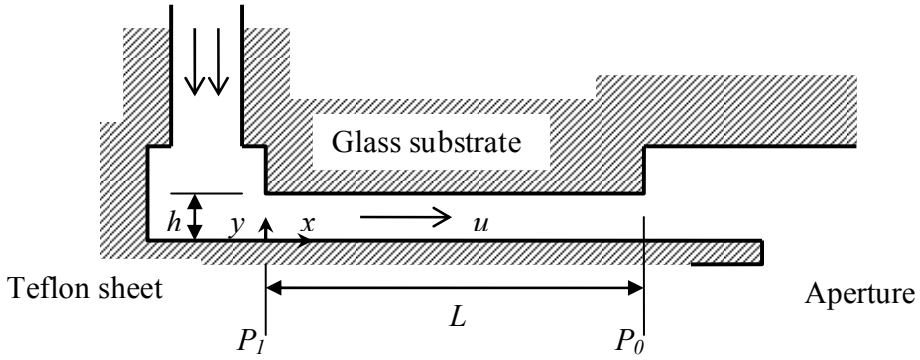

Figure 4: Cross-section of micro-channel

Following assumptions were made:

1. Incompressible fluid; Volume (V) is constant with time
2. Unidirectional; Flow is only in the channel direction (x) -no flow in y direction
3. Laminar flow; High viscosity(υ), low velocity(u in x direction) and relatively large length(L) and hence low Reynolds number, Re = u. D/ υ < 2300
4. 2-D flow; Relatively wide channels

This type of laminar flow between two stationary parallel plates is called a 'Poiseuille Flow'.

For steady state condition,

$$\frac{dm}{dt} = 0 \qquad (1)$$

which combined with $m = A.u.\ \rho$, where A is the channel area and ρ is the fluid density, yields

$$A.u.\frac{\partial \rho}{\partial t} + A.\rho.u\frac{\partial u}{\partial x} = 0 \qquad (2)$$

i.e. $\frac{\partial \rho}{\partial t} + \rho \frac{\partial u}{\partial x} = 0$

Since density does not change with time $\frac{\partial u}{\partial x} = 0$ (3)

Therefore, velocity in *x* direction, *u* is only a function of *y*.

Consider Navier- Stoke's equation (3D):

$$\frac{\partial u_i}{\partial t} + u_x \frac{\partial u_i}{\partial x} + u_y \frac{\partial u_i}{\partial y} + u_z \frac{\partial u_i}{\partial z} = -\frac{1}{\rho}\frac{\partial p}{\partial x_i} + \upsilon\left(\frac{\partial^2 u_i}{\partial x^2} + \frac{\partial^2 u_i}{\partial y^2} + \frac{\partial^2 u_i}{\partial z^2}\right) + g_i,\ i = x, y, z \quad (4)$$

Where u_i is the velocity and g_i is the acceleration in *i* coordinate direction (i.e. *u, v* or *w*), *p* is the pressure, and ρ is the density and υ is the kinematic viscosity of the fluid.

Here, all *z* terms will disappear as we assume a 2D flow.

Applying equation (4) in x direction noting flow is steady, no acceleration in horizontal direction, only u_x is non-zero and $u_x = u$ is only a function of *y*, we get

$$0 = -\frac{1}{\rho}\frac{\partial p}{\partial x} + \upsilon\left(\frac{\partial^2 u_x}{\partial y^2}\right) \quad (5)$$

i.e. $$\frac{1}{\rho}\frac{\partial p}{\partial x} = \upsilon\left(\frac{\partial^2 u_x}{\partial y^2}\right) \quad (6)$$

Since right hand side of equation (6) is not a function of *x*, pressure gradient cannot be a function of *x* and is a constant in *x* flow direction. Let it be *–K*. We get 2nd order differential equation.

$$-\frac{1}{\rho}K = \upsilon\left(\frac{\partial^2 u_x}{\partial y^2}\right) \tag{7}$$

Applying equation (4) in y direction noting $u_y = v = 0$ and g can be neglected when compared to the effect of pressure;

$$0 = -\frac{1}{\rho}\frac{\partial p}{\partial y} \tag{8}$$

Therefore, pressure gradient is constant in *y* direction.

By integrating equation (7) twice in terms of *y* we get,

$$u(y) = -(K/2\eta)\, y^2 + C_1\, y + C_2 \tag{9}$$

With the boundary conditions,

at $y = 0$, $u(0) = 0 \Rightarrow C_2 = 0$ and (10)

at $y = h$, $u(h) = 0 \Rightarrow C_1 = Kh/2\eta$ (11)

we get

$$u(y) = -(K/2\eta)\, y^2 + (Kh/2\eta)y \tag{12}$$

Pressure gradient, *K* can be written as $\Delta p/L$ and Δp is the effective pressure difference alone the channel.

Equation (12) can be rearranged to get the following:

$$u = \frac{\Delta p}{2\eta L}(hy - y^2) \tag{13}$$

u can be applied from equation (13) in the following expression:

Flow rate, $Q = \int_A u.dA$

$$= \int_0^h u.dy.z$$

$$= z\int_0^h \frac{\Delta p}{2\eta L}(hy - y^2).dy$$

$$= z\frac{\Delta p}{2\eta L}\left[\frac{hy^2}{2} - \frac{hy^3}{3}\right]_0^h$$

$$Q = z\frac{\Delta p.h^3}{12\eta L} \tag{14}$$

We can write effective pressure difference as

$$\Delta p = (p_1 - p_0) - K_0, \tag{15}$$

where K_0 represents the resistance of surface tension between the fluid and the channel walls.

When applied from equation (14), equation (15) yields

$$P_1 = P_0 + \frac{12\eta QL}{zh^3} + K_0 \tag{16}$$

For Lipid in Pentane

In the case of Pentane flow K_0 in equation (16) will be given by the following;

$$K_0 = \frac{(W + 2h).\gamma_w.\cos\theta_{p-g} + W.\gamma_w.\cos\theta_{p-t}}{Wh} \tag{17}$$

Where, $\theta_{p\text{-}g}$ is the contact angle for pentane-glass interface and $\theta_{p\text{-}t}$ is the contact angle for pentane-Teflon interface (Figure 5).

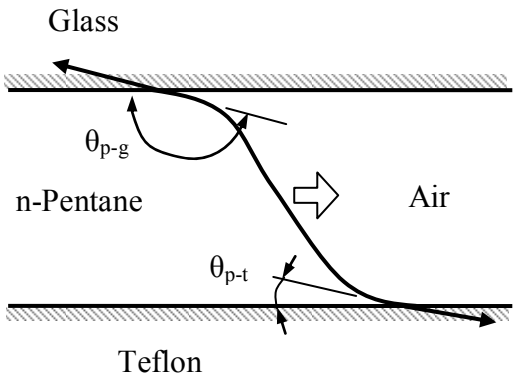

Figure 5: Effect of surface tension on pentane flow

For KCl

In the case of aqueous solution flow K_0 will be given by the following;

$$K_0 = \frac{(W + 2h).\gamma_w.\cos\theta_{w-g} + W.\gamma_w.\cos\theta_{w-t}}{Wh} \quad (18)$$

Where, $\theta_{w\text{-}g}$ is the contact angle for water-glass interface and $\theta_{w\text{-}t}$ is the contact angle for water-Teflon interface (Figure 6).

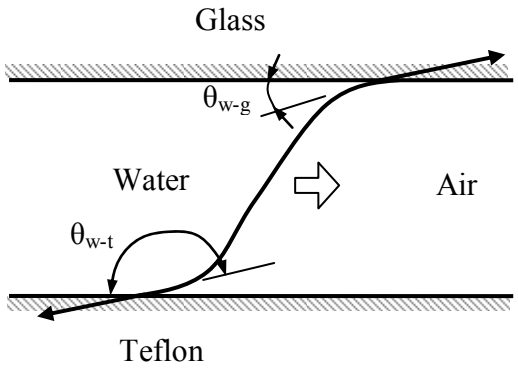

Figure 6: Effect of surface tension on water (aqueous solution) flow

The fluid properties given Table 1 and channel dimensions given in Table 2 are assumed for the simulation purposes. Channel length and width are predetermined (section 3) and depth is selected based on the simulation results of the flow model that follow.

Table 1: Properties of fluids

Fluid	**n-Pentane**	**Water**
Kinematic Viscosity at 25˚C /(10^{-7} m^2/s)	3.58	10.04
Density at 25˚C /(kg/m^3)	630	1000
Computed Dynamic Viscosity at 25˚C /(10^{-4} Pa.s)	2.255	10.04
Surface tension of the fluid, γ /(N/m)	0.01548	0.0728
Contact Angle with Glass, θ_{-g} / (degrees)	10	15
Contact Angle with Teflon, θ_{-t} / (degrees)	75	80

Table 2: Channel dimensions

Parameter	**Value**
Height, h/(μm)	50[(1)]
Width, z/ (μm)	500
Length, L/(mm)	85

Based on the defined parameters the following numerical results can be obtained from the equations given below:

For Pentane

From equations (16) and (17) the required pumping pressure, P_1 (Figure 7) is given by

$$P_1 = \frac{12\eta QL}{zh^3} + P_0 + \frac{(W+2h).\gamma_w.\cos\theta_{p-g} + W.\gamma_w.\cos\theta_{p-t}}{Wh} \qquad (19)$$

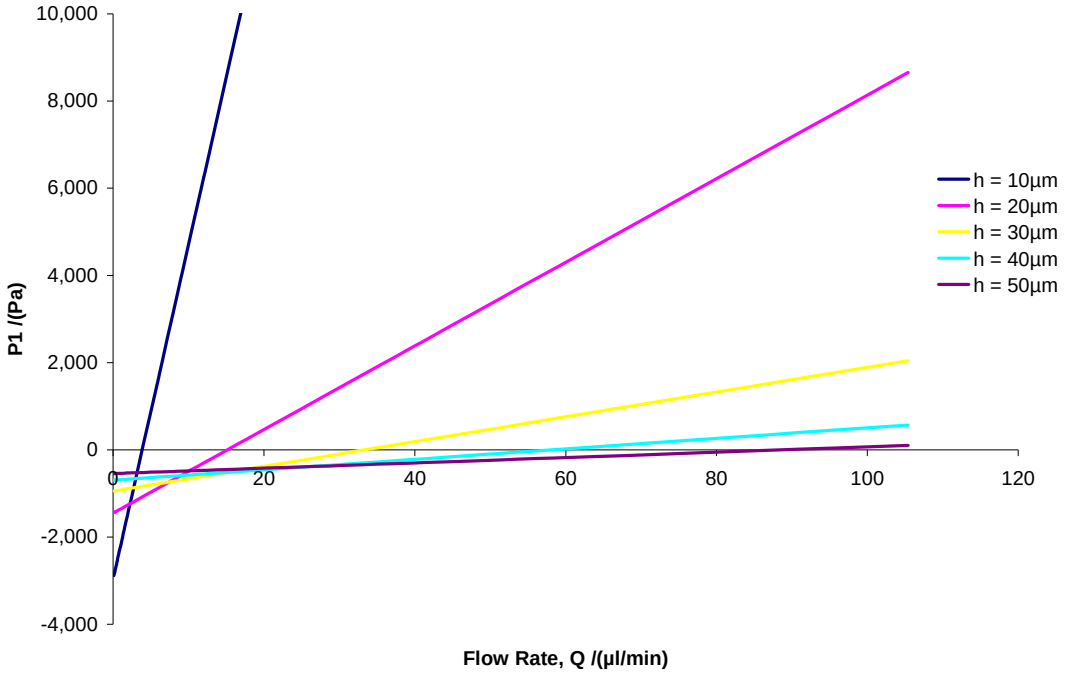

Figure 7: Variation of pumping pressure against pentane flow rate in a micro-channel for various channel heights

For KCl

From equations (16) and (18) the required pumping pressure, P_1 (Figure 8), will be given by

$$P_1 = \frac{12\eta QL}{zh^3} + P_0 + \frac{(W+2h).\gamma_w.\cos\theta_{p-g} + W.\gamma_w.\cos\theta_{p-t}}{Wh} \qquad (20)$$

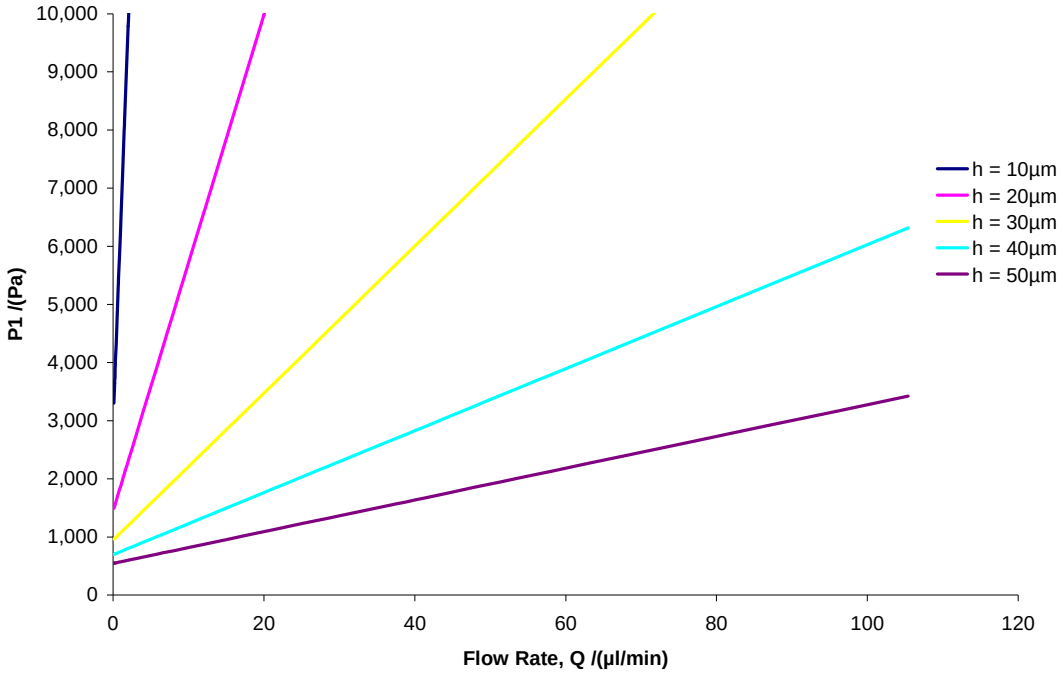

Figure 8: Variation of pumping pressure against KCl flow rate in a micro-channel for various channel heights

2.2 Flow Control

Lipid bi-layer formation is a very delicate activity as the few nanometers thick lipid bi-layer is highly sensitive to mechanical loads and even high voltages might cause damage to it. Therefore, maintaining the proper conditions and controlling the flow in channels are major considerations in the course of lipid bi-layer formation.

From Figure 7 and Figure 8 it can be seen that the pressure requirement are opposite for the two liquids, KCl solution and n-Pentane. In general, for deeper channels the magnitude of pressure is lower. Lower pressures are desirable in terms of the NanoPort connections and sealing used in the microfluidic device. However, limitations

on the channel depth were imposed by the etching capability (as discussed in section 3.1). Therefore, the channel depths close to 50 μm were selected. Based on the syringe pump (Pico Plus and Model 11, Harvard Apparatus) ratings, the pressure corresponding to this channel depth met the requirement of the experiment.

Laminar flow condition had to be maintained inside the micro-channels at all the times to avoid unexpected activities inside the channels. This was especially acute when bi-layer was forming since lipid bi-layer was highly vulnerable to mechanical vibrations. For internal pipe flow Reynolds number is defined as

$$\mathrm{Re} = \frac{D.u}{\nu} \tag{21}$$

where u is the average fluid velocity, ν is the kinematic viscosity of the fluid and D is the hydraulic diameter of the channel. For a rectangular channel, D is defined as four times the channel cross-section area divided by the perimeter of the channel cross-section. If Re < 2300 then the flow is laminar. Following graphs (Figure 9 and Figure 10) show how the Reynolds number varies with the flow rate and the channel height for the channel width of 0.5mm. Reynolds number is less sensitive to the variation of the channel height (h) but is more sensitive to the flow rate. Hence, for KCl a flow rate less than 10μl/min (Figure 9) and for pentane a flow rate less than 3.5μl/min (Figure 10) needed to be maintained. During the experiment KCl flow rate was maintained below 10μl/min and pentane flow rate was kept below 2μl/min to guarantee laminar flow conditions.

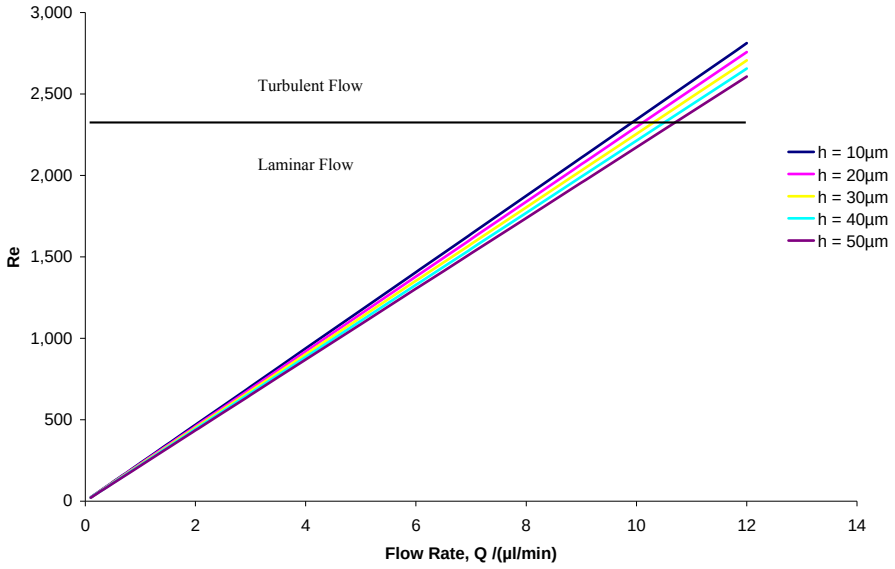

Figure 9: Variation of Reynolds number for KCl flow rate in a micro-channel for various channel heights (channel width = 0.5mm)

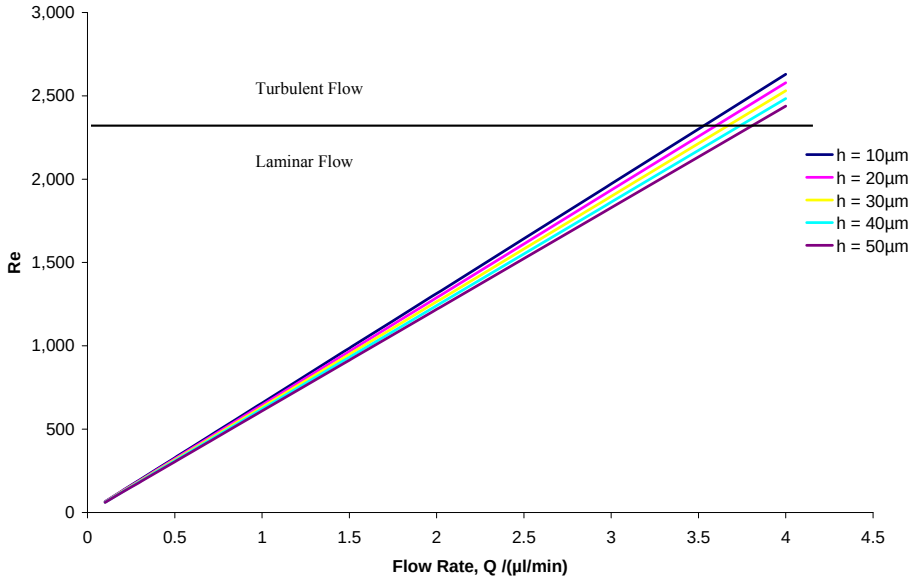

Figure 10: Variation of Reynolds number for pentane flow rate in a micro-channel for various channel heights (channel width = 0.5mm)

Typical syringe pumps employ stepper motors, where non-uniform flows are observed due to stepwise rotation of the rotor of the motor. There is a high risk of damaging the lipid bi-layer due to these high pressure surges. The easiest solution is to reduce the sensitivity of the output flow from syringe to the stepper motor. Practical way of performing this is by reducing the gear reduction from the stepper motor to the piston of the syringe mounted on the syringe pump.

Figure 11 (Euclid Research) illustrates the high variability of the velocity at low velocities and increased smoothness at high velocities using an unloaded stepper motor (micro-stepped 16:1), which is ramped in velocity up to five revolutions per second. This suggests that the stepper motors are best used at higher velocities.

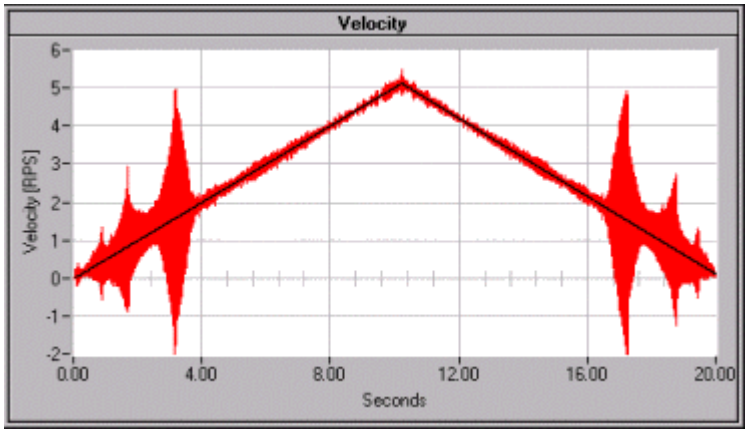

Figure 11: Velocity response of a stepper motor for a saw-tooth velocity reference input (Euclid Research)

Also stepper motors resonate at each step. In the case illustrated in Figure 12 (Euclid Research), the motor was stepped at a rate of one-half step every 200mS. It can be noticed how the motor resonates almost a full step (1.8°) after

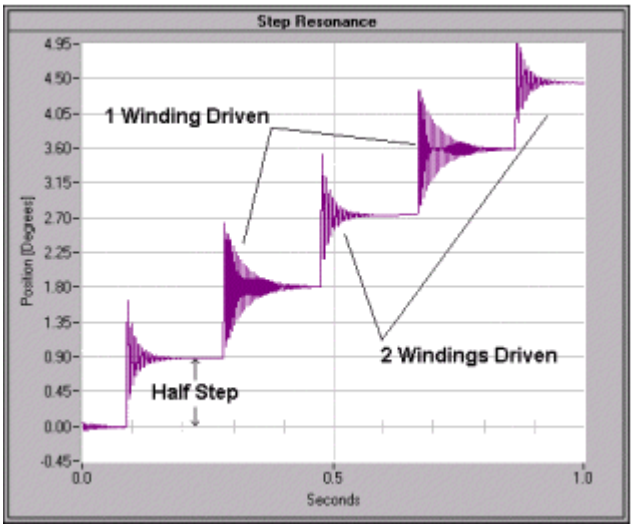

Figure 12: Position response of a stepper motor for a ramp reference input (Euclid Research)

each half step. Therefore, it is important to have a high gear reduction between the stepper motor and the syringe-driven piston to minimize the effect of this resonance. Further, this can result in a smoother flow rate as shown in Figure 13, with reduced effects of jerks due to stepping.

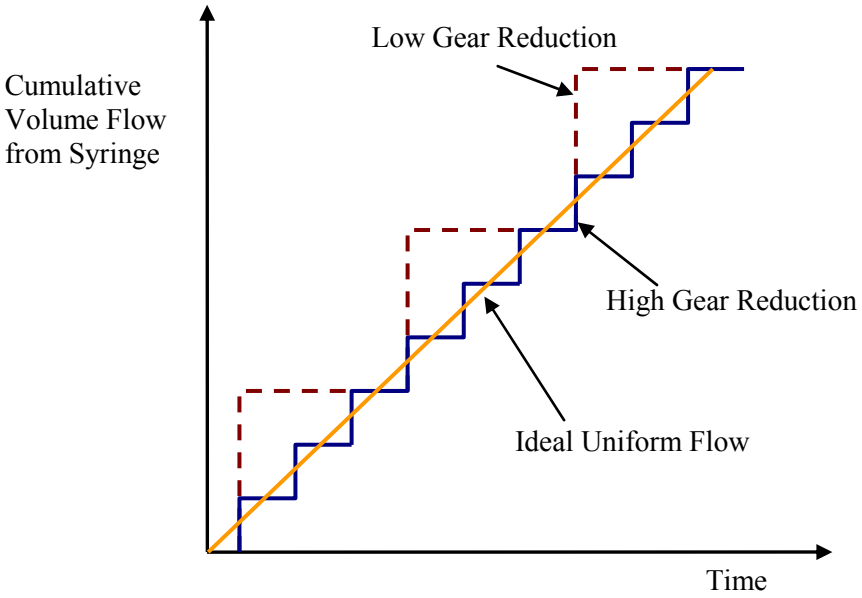

Note: Resonance effects are neglected here

Figure 13: Cumulative fluid flow for different gear reductions between stepper motor and syringe piston

It is clear that the effect of both resonance and velocity variability can be minimized if gear reduction is used between the stepper motor and the syringe piston; when operated at higher velocities velocity variability is reduced and small steps at the higher end reduce the effect of resonance. With a syringe pump with fixed gear reduction, this can be achieved by using a small diameter syringe, where the stepper motor has to rotate relatively higher number of turns to give a unit displacement at the syringe piston, when compared to a larger diameter syringe. Therefore to obtain the same flow rate, the stepper motor has to operate at higher velocities where the velocity variability is less, and due to decreased amount of volume pumped per each turn of the stepper motor the resonance effect is mitigated. The reduction ratio of the gear apparatus

(from stepper motor to the syringe actuation plunger) is proportional to the inverse of square root of the syringe diameter. For instance, to achieve gear reduction of 1/3 as in Figure 13, use of a smaller syringe with $1/\sqrt{3}$ times the original diameter is sufficient.

It can be summarized that the advantages of use of a smaller diameter syringe as:

1. Reduced effect from jerks due to motor stepping;
2. Low velocity variability;
3. Reduced effect of resonance involved with motor steps.

However, a syringe with small diameter becomes the bottle neck for performing the experiment repetitively. Best alternative might be to use an expensive pulse less pump such as PHYSIO 22 Pump from Harvard Apparatus, or an expensive micro-stepping pump.

The pumps used in the experiment are listed in Table 3. Both pumps have effective angle/step about 0.05° at the plunger. Model Pico Plus pump was selected for pumping KCl as it has a lower plunger movement than the other pump, since KCl pumping required slower pumping rates during lipid bi-layer formation.

Table 3: Tandem syringe pumps used in the experiments

Harvard Pump Model	**Step angle /(degrees)**	**Gear Ratio**	**Effective angle at pusher /(degrees)**	**Movement at Pusher per Step/ (μm/step)**	**Used in pumping**
Pico Plus	1.8	36:1	0.05	0.0444	KCl
Model 11	7.5	300:1	0.025	1.322	Pentane

For 1 ml syringe (VWR international LLC, PA) a volume of about 8×10^{-4} µl fluctuations can be expected due to resonance effect when pumping KCl at 0.2 µl/min rate used during lipid bi-layer formation stage.

3. FABRICATION OF NOVEL DEVICE

In order to overcome drawbacks imposed by the conventional instruments used in this experiment (as discussed in section 1) a small and portable device was implemented. A smaller device eases the handling steps and operation. Better economies of scale are obtained by using a smaller amount of space, fabrication materials and operating fluids (reagents and analytes). Further, automation can be enabled (Malmstadt et al. 2006). Micro fabricated apertures are considered to produce more stable lipid bi-layers (Funakoshi et al. 2006). A closed design would enable 'clean' operation due to isolation from the environment and avoid spill of analytes compared to open device designs presented by Funakoshi et al. 2006; Malmstadt et al. 2006; Peterman et al. 2002. For a very specific application (like microgravity) above features are essential and for any general application (e.g. pharmaceutical studies) those requirements are desirable.

The new design consists of a thin Teflon® sheet sandwiched between two borosilicate glass wafers as shown in Figure 14. Two micro-scale (Figure 15) cross-channels are on each glass wafer making two identical cross-channel systems on either side of the Teflon® sheet. Only connection between channels on both sides is the aperture on the Teflon® sheet at the central chamber, which is the intersection point of the cross- channels on both glass substrates. Through holes at the end of the channels facilitate connection of tubing coming from syringes to the device. NanoPort Assemblies® (Figure 14b) are used to fix tubing to

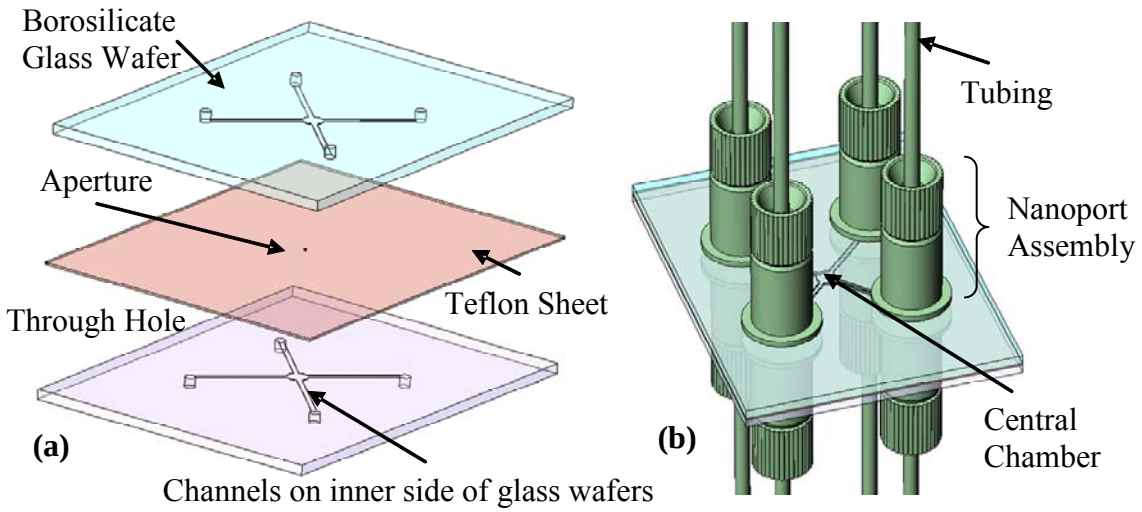

Figure 14: Three-layer design of the device. **a** Unassembled layers. **b** After sandwiching Teflon sheet in between glass wafers. Closed channels are formed at each Teflon-glass interface

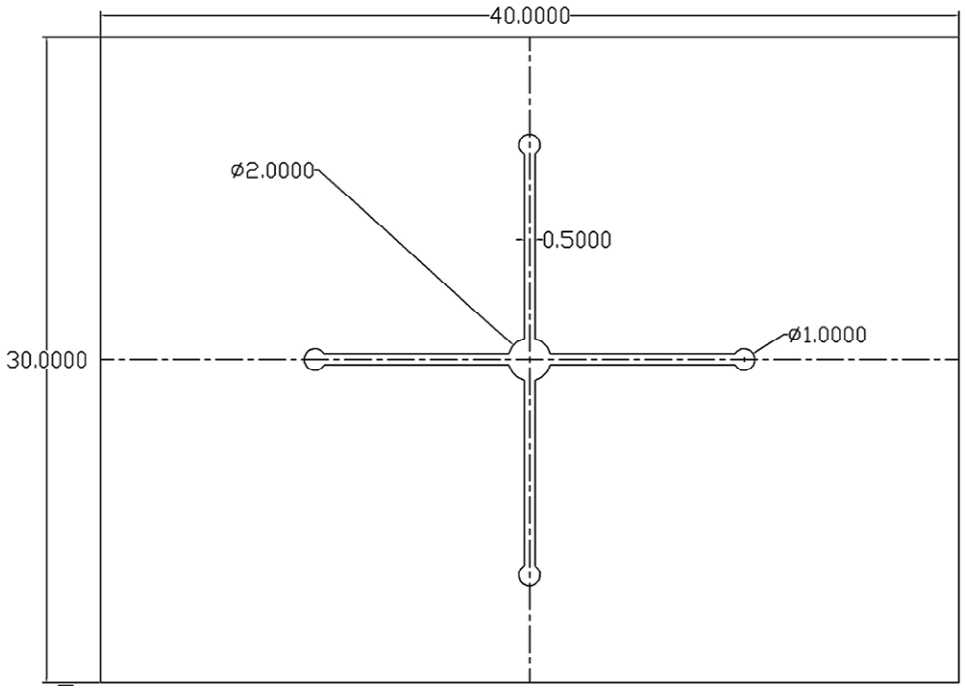

Figure 15: Dimensions (in millimeters) of the cross-channels on glass wafers. Channel depth is varied between 5µm – 10µm

glass wafers at through holes, while lure adaptors on the other end of tubing connect tubing to the syringes. This design satisfies the aforementioned requirements.

The purpose of having two perpendicular cross-channels was to allow independent control the flow of Lipid and buffer solutions. Lengths of the channels were determined based on NanoPort^{TM} base sizes (section 3.4.4). The channel width of 0.5mm has been used in a similar cross-channel configuration by Funakoshi et al. 2006, and hence the same value was selected as channel width for the new design. Aperture size of 100μm was selected as most of the previous work had used aperture sizes in the same order (Kang et al. 2007; Malmstadt et al. 2006). Tilting the channels with respect to glass wafer edges, more room for NanoPort^{TM} Assemblies was acquired (Figure 14 and Figure 15).

Teflon® is used in conventional lipid bi-layer formation applications (Hanke and Schlue 1993; Kang et al. 2007; Kang et al. 2005; Schmitt et al. 2006) due to the good testability of organic solutions such as lipids. Wetting of the aperture by lipid is essential for spontaneous self-assembly of lipid bi-layer at the aperture. Further, having high melting point, being inert to many active chemicals and possessing high strength, it is an ideal candidate for applications involving chemical interactions (Resnick and Buck 1999). However, non-adhesive nature and less deformability of Teflon® introduced major problems at the time of assembly process (as discussed in section 3.4). Since Teflon® part of the channels resists the flow of aqueous solutions like buffer (KCl), it is required that the other parts of the channels be hydrophilic (glass satisfies this requirement). Further, glass does not react with organic chemicals and buffer solution

used in the process. In general for microfluidic flow control applications glass is preferred over polymers (Kelly and Woolley 2007). However, glass fabrication is more challenging and rigorous compared to polymer fabrication, especially in micro-applications. Borosilicate glasses were used in fabricating the device as were readily available and cheap. Even though Pyrex® has about ten-time better surface roughness than borosilicate it was not a successful candidate for this study. Pyrex was hard to etch using wet glass etching and very slow etching rates were observed. Also, the etch masks could not withstand high concentration etchants that were required for etching Pyrex. In addition, the extremely high cost of Pyrex glass was disadvantageous compared to low cost of borosilicate glass.

Fabrication process consisted of fabricating channels and drilling holes on glass wafers, making aperture (in Teflon), sandwiching the three layers, and connecting tubing. Next few paragraphs will discuss the fabrication process.

3.1 Glass Etching with HF Wet Etchants

Hydrofluoric acid was used for wet etching of glass to fabricate micro-channels (Mourzina et al. 2005). Absence of suitable machinery micro-machining of glass was not an option. When etching with Hydrofluoric (HF) acid wet etchant, an etch mask was required to protect the glass surface where no etching was desired. Two types of etch masks commonly used with HF based glass etching are photoresist and metal mask (Bien et al.2003; Mourzina et al. 2005).

3.1.1 Photoresist Masks

A photoresist is a photosensitive material usually composed of a resin, a photosensitizer, and some additives (Matsuzawa 1987). When the photoresist is exposed to light the photosensitizer undergoes changes in structure causing it either to dissolve or not dissolve in a developer solution. A photoresist, which becomes stronger by absorbing energy to develop a cross-linked structure, is termed 'Negative photoresist' (Darling, Negative Photoresist). In 'Positive photoresist', exposure to light causes already existing cross-links to break (Darling, Positive Photoresist). Positive Photoresist gets its name as it acquires the same pattern as the photo mask. A photo mask is a transparent sheet with the required pattern, which is used between the light sources and the photoresist. This optical process of transferring the mask pattern onto a substrate is called 'photolithography' (Darling, Photolithography). Figure 16 illustrates a typical photolithography process.

Two negative photo resists SU8 50 and SU8 2050 from MicroChem were used as etch masks because SU8 is resistant to HF based etchants. SU8 can be used to obtain up to 2mm thick masks (Guerin, SU8 Homepage) while SU8 50 and SU8 2050 can yield thicknesses only up to 50μm. With of SU8 100, which can result in 100μm thicknesses, finer details could not be achieved. Being cross-linked by Ultra Violet (UV) near light already used in the Material Characterization Facility of Texas A&M University, SU8 photoresists were easier to use. Beforehand the photolithography process the photo mask had to be designed using AutoCAD® software and obtained from a 35mm negative film. The process used for SU8 50, a variation of the standard method given in MicroChem

SU8 50-100 Datasheet (MicroChem), was as follows (Figure 17): First the borosilicate glass wafer was cleaned with acetone and isopropylene respectively to remove any impurities and dust particles present on the surface. Then the glass wafer was preheated for 5 minutes at 200ºC on a hotplate to vaporize alcohol solutions. Next SU8 50 was poured onto the glass wafer so that all the areas were covered and no air bubbles were present, and the

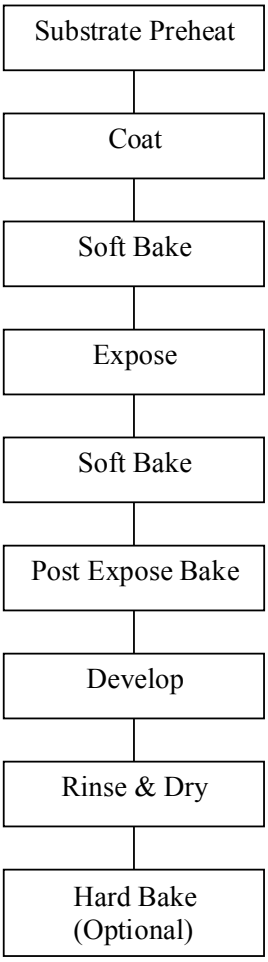

Figure 16: SU8 process. (copyright © 2007 MicroChem Corp.)

glass wafer was spun on a spin coater (SCS p62041 (8 in bowl) Non-programmable Spin Coater, Special Coating Systems, Figure 18) at 4000rpm for 40seconds to get an even SU8 50 layer of nearly 40μm in thickness.

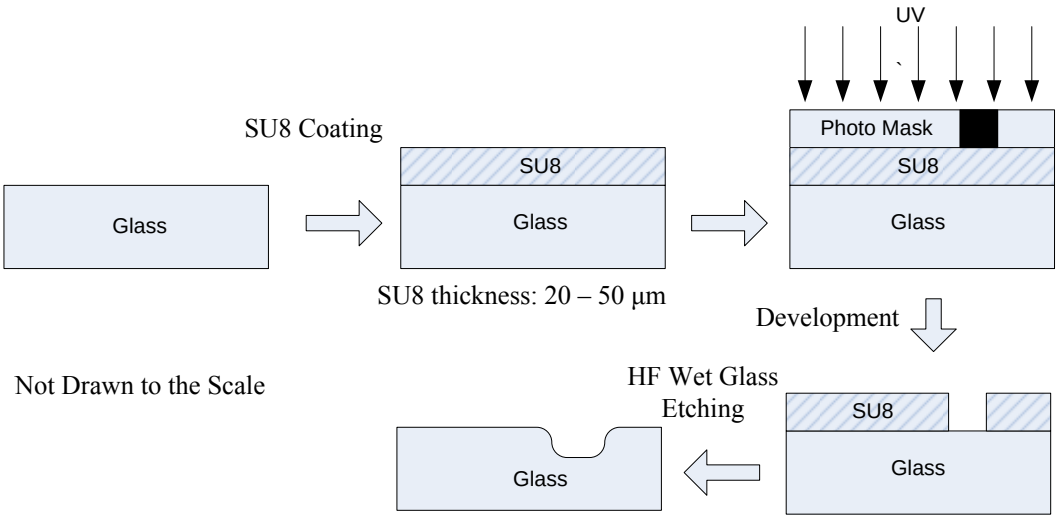

Figure 17: Glass etching process using photoresist mask. A negative photo mask is used for photolithography as SU8 is a negative photoresist

Figure 18: Spin coater (from website of Micro Chemical Facility, Texas A&M University)

In the next step glass wafer was soft baked at 65ºC for 5minutes and at 95ºC for 15minutes respectively on hotplates. After placing the photo mask on the Mask Aligner (Quintel Mask Aligner Q4000-6IR, Figure 19), the glass wafer was loaded and exposed for 5 seconds to UV light (365nm wave length) of 9.2 milliwatt/cm^2 energy density (4 seconds with 11.2 milliwatt/cm^2). Then it was baked again at 65ºC for 1minute and at

Figure 19: Mask aligner

95ºC for 5minutes respectively on hotplates followed by soaking in the SU8 developer solution (MicroChem Corp., MA) for 6 minutes. It was essential to leave the glass wafer to cool down before developing to avoid surface cracks due to thermal stresses. This process ended with rinsing with deionized (DI) water, drying, and inspecting under the 3D microscope (MX -5040RZ, Hirox 3-D Microscope System, Hirox-USA Inc., NJ, Figure 20). Profilometer (Dektak 3 Stylus Profilometer, Figure 21) was used to measure

the depth and the quality of the micro-channel patterns in SU8. If on visual inspections an insufficiently developed photoresist was detected, it was then developed further. This

Figure 20: 3D Microscope (from website of Micro Chemical Facility, Texas A&M University)

Figure 21: Profilometer system (from website of Micro Chemical Facility, Texas A&M University)

process is obtained by modifying the standard process specified by MicroChem SU8 50-100 Datasheet (MicroChem) to get better quality channels.

Table 4 lists (Figure 22, Figure 23 and Figure 24 illustrate) some initial trials performed to select a better photoresist and to obtain better processing conditions for photolithography. The etchant used in these was the standard glass etchant (5:10:85 of

Table 4: Some trials for selecting better photolithographic conditions

Photoresist	**SU8-100**	**SU8-50**	**SU8-50**	**SC1827**
Type	Negative	Negative	Negative	Positive
Exposure/(sec)	40	15	5	20
Nature of Mask	-Thickest - No channels	-Thick -Shallow channels	-Thick -Good features	-Thin -Superior features
Result after Etching (10min)	-No effect	-Shallow channels	-Rough channels	-Damaged mask

BOE: HCl: H_2O). Even with very short exposure times, such as 4 and 5 seconds, SU8 100 could not replicate micro-channel features, because the effect of UV light refraction at edges of the photo mask on SU8 100 was relatively high due to the thickness of the SU8 100 layer. Exposure time was critical to get sharp and adequate features. An exposure time of 5 seconds (Figure 22) resulted in a considerably good profile of the patterns when compared to over cross-linked photoresist mask that resulted when a 15-second (Figure 23) exposure time was used. Even though, the mask made of SC1827 (MicroChem Corp, MA), a positive photoresist, yielded finer features (Figure 24), it could not withstand glass enchants being consistent with Mourzina et al. 2005. SU8 2050 (an improved

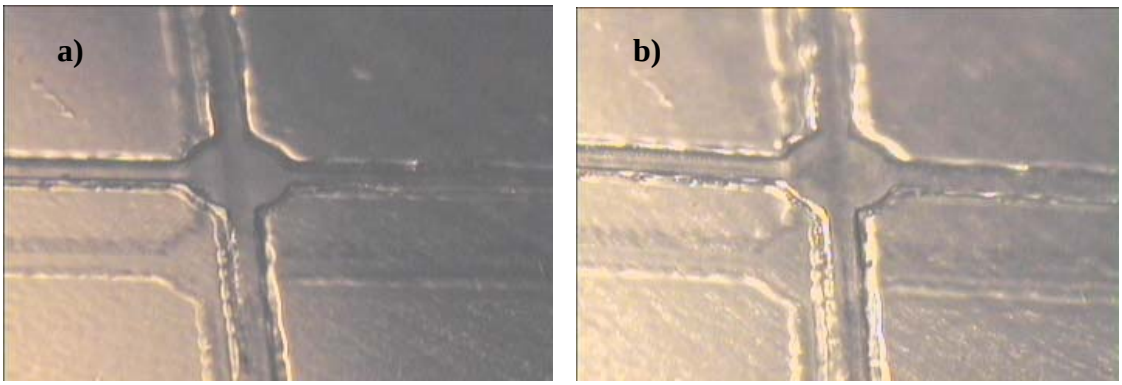

Figure 22: Results of 5 seconds exposure time for SU8 50. **a** Mask. **b** After etching (mask still on)

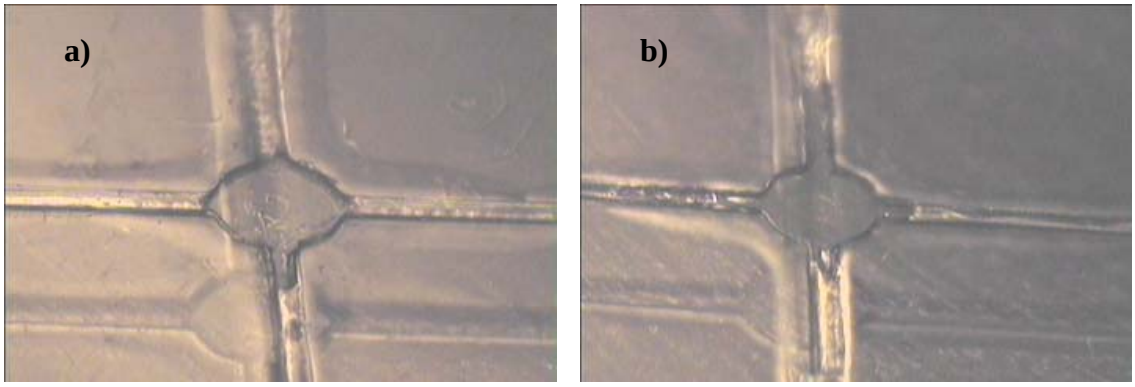

Figure 23: Results of 15sec exposure time for SU8 50. **a** Mask. **b** After etching (mask still on)

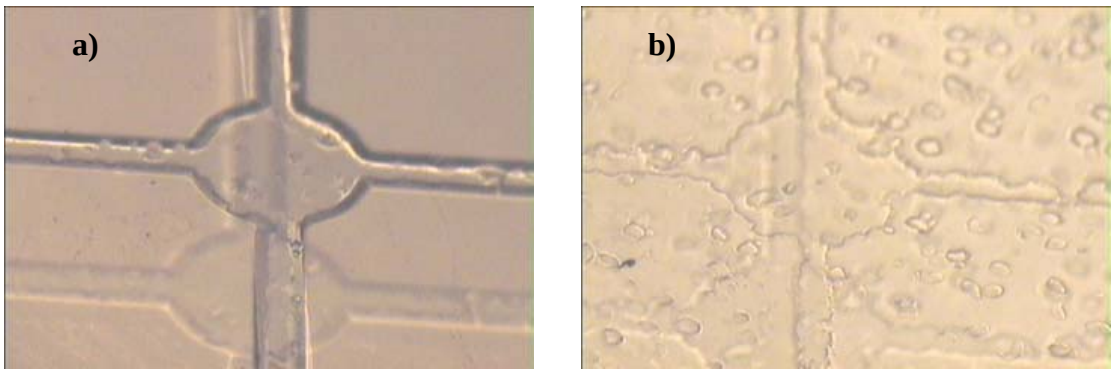

Figure 24: Results of 15sec exposure time for SC1827. **a** Mask. **b** After etching (mask still on)

version of SU8 50) with an easier photolithography process, was used subsequently in a similar process, replacing SU 50.

Undeveloped SU8 debris was resulted on the channel areas when the standard process specified by MicroChem SU8 50-100 Datasheet (MicroChem) was used. Photoresist debris in channels obstructed etching of channels during the glass etching giving rise to very rough channels (Figure 25). Better SU8 photoresist mask (Figure 26) and better results for channel quality (Figure 27) were obtained by increasing the spinning rate to 4000rpm from the specified value of 3000rpm (for SU8 2050, to 3000rpm from 2000rpm) but with reduced photoresist thickness of about 25μm and a partially damaged photoresist layer at channel edges (Figure 26). The concept behind this process improvement was the reduction of the effect of UV refraction with thinner photoresist layer. However, the reduced photoresist mask thickness made the mask at channel edges vulnerable causing them to be easily stripped off by the etchant.

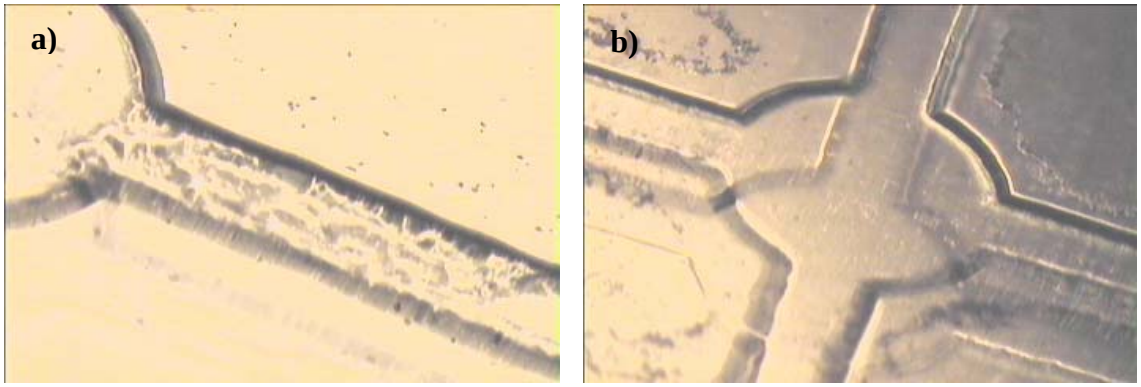

Figure 25: Etching with standard SU8 mask (obtained with Profilometer). **a** Effect of undeveloped SU8 debris present in the channels. **b** Chamber was generally of good quality

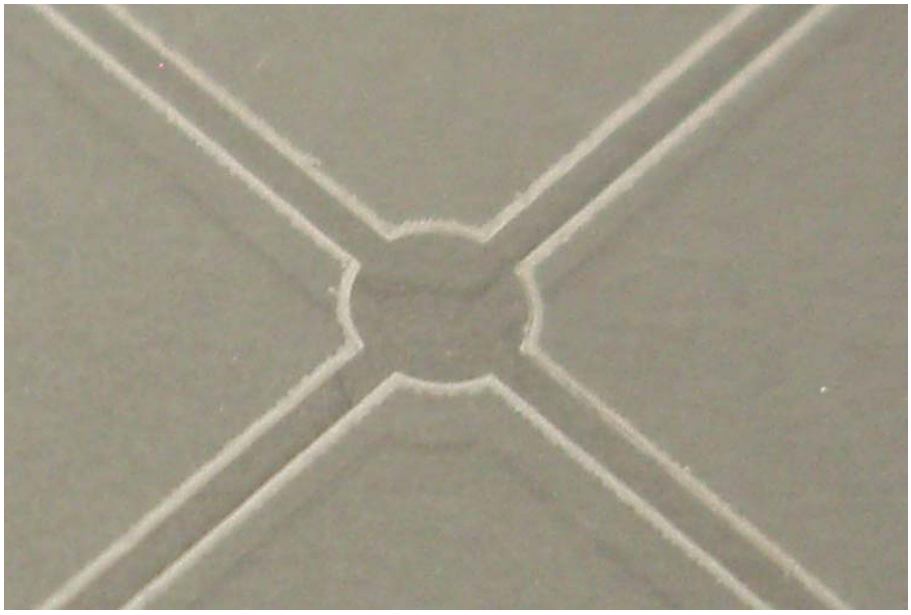

Figure 26: Improved SU8 50 photoresist mask with modified photolithography process. Channel edges are not firm

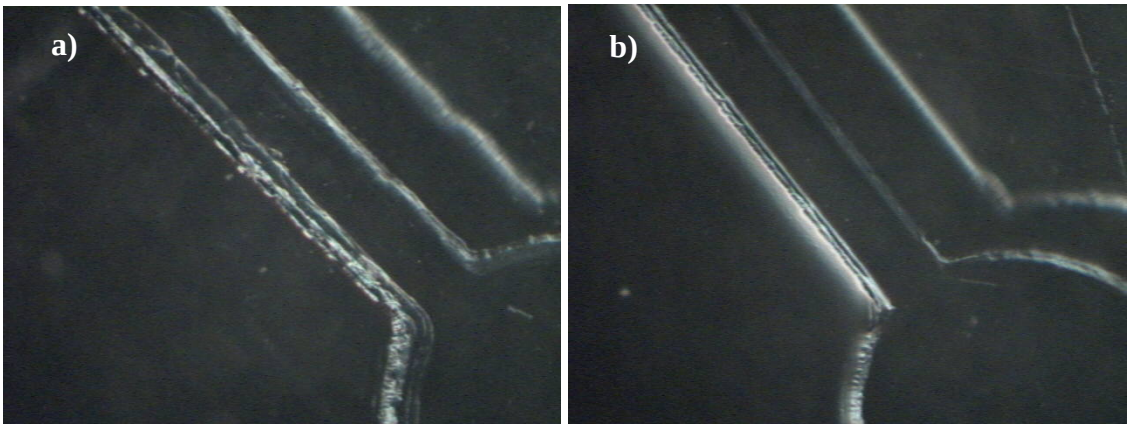

Figure 27: Channels etched with modified SU8 mask (obtained with 3D Microscope). **a** Smooth channels but damaged edges. **b** Sometimes channel edges were better

Instead of reducing photoresist thickness, cleaning of the glass wafers using March Plasma Systems Model CS-1701 reactive iron etcher (Figure 28) was performed

for 300seconds to get cleaner channels. The power was set to 350W, Gas flow rate was set to 20, the end point value was set to 100 and rate was set to 80. However, Reactive Ion Etching (RIE) process damaged photoresist at channel edges and reduced the thickness of the photoresist. When hard baking was performed to improve the strength of the photoresist, after RIE treatment, the channel quality was observed to deteriorate the same way with normal hard baked SU8 50 masks. The reason was that RIE could remove only the debris having thickness below a certain value. Photoresist masks obtained from increased spin rates were better in quality than RIE treated standard SU8 50 masks.

Figure 28: Reactive Ion Etcher

Hard baking was tested as a method of hardening the etch masks so that higher etching depths could be achieved. However, while the photo resist in the area, where etching had to be avoided, was getting harder as intended due to hard baking, thin SU8 leftovers/debris at channel areas also was growing undesirably harder. Therefore, RIE cleaning and hard baking were avoided from use. After etching glass, SU8 masks were

removed using PG remover (Nano Remover PG, MicroChem Corp, MA) by dipping the glass wafer with SU8 photoresist for about 30mins. By heating the PG remover solution to 70ºC, SU8 stripping process could be accelerated, i.e. SU8 was removed within 5minutes. Further, sonication process followed by RIE cleaning was used to remove the remaining SU8 particles. The sonication involved mechanically excitation of SU8 particles in a liquid medium using sonic waves.

3.1.2 Metal Masks

Gold (Au) and Nickel (Ni) metal coatings have been widely used as etch masks in glass etching (Mourzina et al. 2005) because of their ability withstand HF etchants to a good extend. Au was tested to be used as the etch mask in channel-etching on glass wafers. A Chromium (Cr) adhesion layer was required to use between the glass wafer and the Au layer to increase the adhesion. However, Cr alone could not be used as the etching rate on Cr is relatively high (Corman et al. 1998). Comparatively long process time and cost of Au were major concerns with metal masks. An attempt to use aluminum instead of Au proved unsuccessful.

Fabrication of metal mask begins with metal deposition followed by photolithography and metal etching (Figure 29). Au and Cr layers were deposited using the metal evaporation chamber (Auto 306 vacuum coater for research and development, Boc Edwards). Glass wafers were cleaned beforehand using acetone and isopropylene to remove any impurities. It was important to let the metal coating to cool down inside the metal evaporation chamber to avoid thermal cracking. Metal etching with a photoresist

mask was used to make the pattern on Au-Cr layer. SC1827, a positive photoresist from MicroChem, was used over SU8 as it was easier to coat, easier to remove and better in transferring finer mask patterns. Exposure time of 20 seconds was used for UV light (365nm wave length) of 9.2 milliwatt/cm^2 energy density. Gold etchant with 25°A/second etching rate (gold etch type TFA, Transene company, Inc) and chromium etchant with 14°A/second etching rate (CR-14S, Cyantek corporation) were used to etch metals. Etching times were calculated based on their respective etching rates. However, twice the calculated times had to be used for metal etching to achieve complete etching.

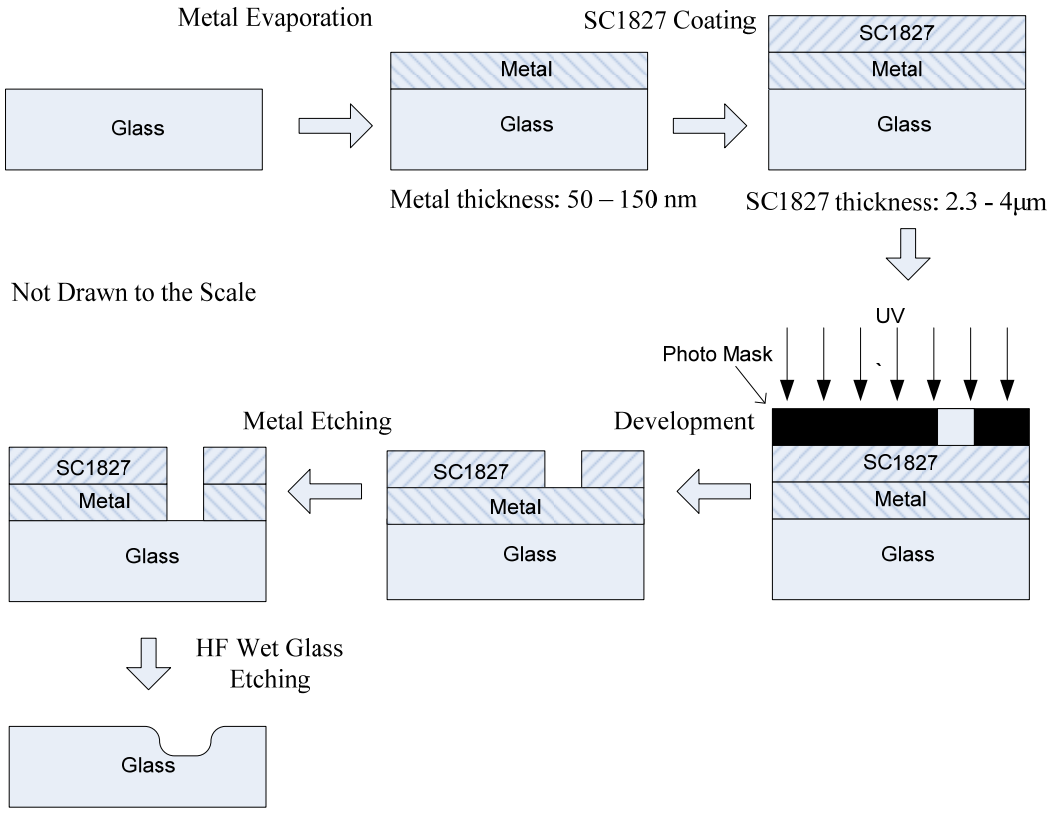

Figure 29: Glass etching process using metal mask. A positive photo mask is used for photolithography as SC1827 is a positive photoresist

Instead of a single layer several alternative layers of Au and Cr were deposited to increase the strength of the Au-Cr mask. Various layer thicknesses were initially used. However, the resultant 53.5nm thick mask could not withstand the etchant: 10nm of Cr, 17.4nm of Au, 16nm of Cr and 10.1nm of Au. Even with the following 145nm thick (30nm of Cr, 30nm of Au, 11nm of Cr, 31nm of Au, 10nm of Cr, and 35nm of Au) metal mask small pin holes were found to occur (Corman et al. 1998). However, Au-Cr mask was superior for etching finer details (Figure 30) as it gave smother sharp features when compared to SU8.

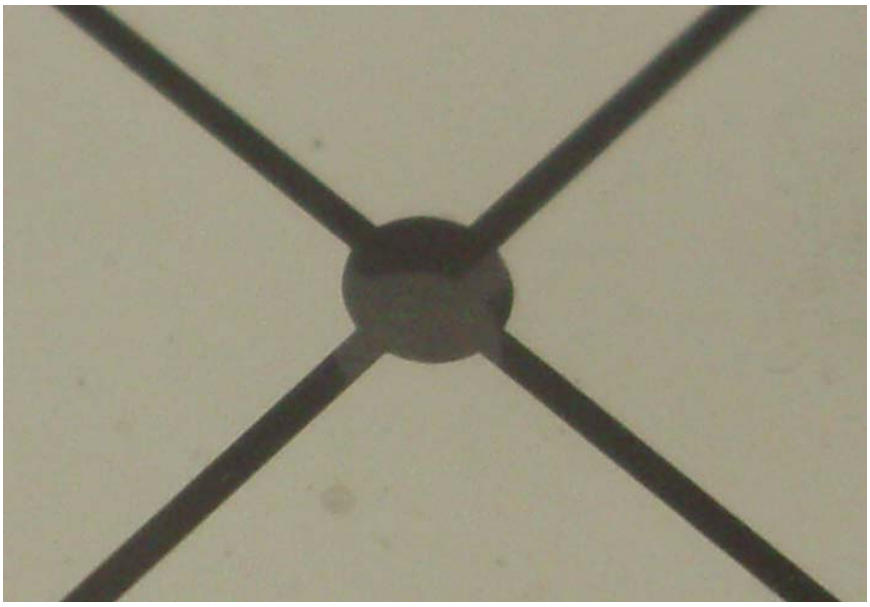

Figure 30: Au/Cr metal mask

Even though metal masks yielded finer pattern, need of a very thick mask for deeper channel etching and the high cost were barriers for extensive use of metal masks in the glass etching process. The quality achieved with SU8 masks was satisfactory for

the device, given its comparatively lower cost and lower processing time. Removal of metal masks involved alternative etching with relevant etchants.

3.1.3 Etchants and Etching Process

HF based wet glass etchants, a commonly used etchant, was selected for etching channels on glass because of its simplicity to use, cost effectiveness and versatility (Kelly and Philipsen 2005). Undercut (the sideway etching of side walls) is a major drawback involved with wet glass etching due to isotropic etching when compared to anisotropic etching in dry etching processes. However, it was not a major concern as the etch depth in the design was negligible compared to the pattern dimensions.

Etching was performed inside a fume hood, and etchant body contact and vapor inhale had to be avoided. Neoprene glows, a mask, a full headgear and a lab coat were to be worn by the operator all the times. The etching procedure started with preparation of the etchant to be used. Always Teflon containers were used and a high acidic solution was poured into a low concentrated solution. Then a Teflon container carrying about 200ml of etchant was placed on a magnetic stirrer and the magnet (covered with Teflon) was placed inside the container. It was observed that uniform etching and high etching rates were obtained when the etchant solution was stirred during the etching process. The stirring improved the contact between glass surface and etchant. Next the substrate to be etched was submerged in the etchant in a way the surface to be etched was faced up and at the same time a timer was activated. It was important to ensure that no air bubbles were formed on the glass surface where etching was necessary; otherwise those

areas under the air bubbles were under-etched. Commercial BOE solutions with added surfactants were effective in avoiding bubbles on the glass surface. After the end of the predefined etching period the substrate was lifted from the etchant using a Teflon tweezer, washed in DI water and dried by blowing compressed air. Reduced etching rates were observed with time as the strength of the etchant decayed during the etching process. During the etching process the operator had to be present to avoid any accidents. The 'buddy system', having a second person with the operator, was a good practice to reduce the involved risk. Etch depth was measured by taking Profileometer measurements in two perpendicular directions.

Even though etching rates as high as 8μm/min were possible to achieve with the direct use of 49% HF (as confirmed by Bien et al.2003) it simply stripped off SU8 50 etch masks within a minute. The use of dilute HF alone increased possible health hazards to non-experienced users. Also the high etching rates limited the control over the accuracy of the etching depth. Therefore, BOE (Buffered Oxide Etchant) glass etchant, which was extensively used for silicon etching, was modified and used for glass etching. BOE was prepared by mixing 6:1 mass ratio of 40% Ammonium fluoride (40% NH_4F) and 49% HF. It is reported to etch silicon dioxide roughly at 1μm/min rate (Bachman M 2000). BOE alone etched borosilicate glass at around 0.4μm/min rate (Figure 31). Diluted BOE forms, namely BOE (50:1) and BOE (20:1) from J.T. Baker, NJ, were also used in deriving etchants. A standard glass etchant was prepared to start with by mixing 5:10:85 of BOE:HCl:H_2O (Bachman M 2000). However, it gave a very low etching rate of about 0.15μm/min. Therefore, the percentage of HF in the etchant had to be increased.

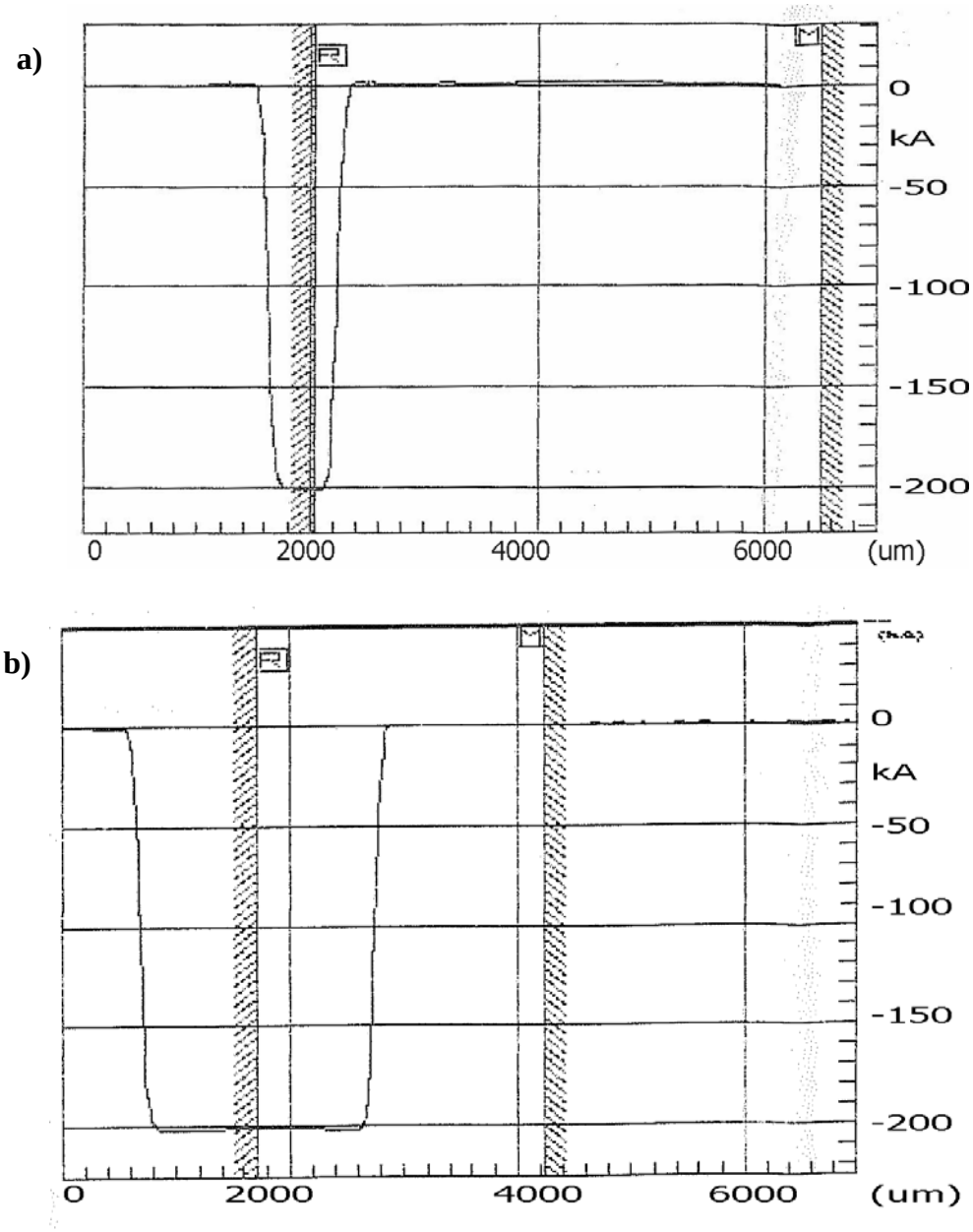

Figure 31: Glass etched with BOE for 50 minutes. **a** Channel cross-section. **b** Central chamber

With use of less HF concentrated etchants SU8 mask remained intact and adhered to the glass surface for a longer time. However, it was stripped off after sometime. In areas where SU8 50/SU8 2050 was stripped uneven surfaces were formed making it impossible to assemble a device without leakages. Usually 50μm was the limiting depth. Etching depth was limited to below 50μm to avoid damages to the photomask. To find the balance between etching rate and etch quality, combinations of HF and BOE had to be tested. Since BOE (50:1) and BOE (20:1) were commercially available it was easier to use those over BOE for deriving etchants. BOE (50:1) and BOE (20:1) alone etched borosilicate at 0.05μm/min and 0.16μm/min (Figure 32) rates. Even though, the resulted surface finish was good, to achieve higher depths several hours of etching was necessary. Long etching times were not preferred because of the increased cost and the risk. When establishing the etching rate of an etchant, a section of a glass wafer was dipped in the etchant for a set time and measured the depth using the Profilometer. However, based on the type and quality of the photomask, the etching rate for the same etchant varied considerably. Therefore, etching was performed on the glass wafers with photomasks on to see how well a photomask and an etchant were combined.

Etchant with 3:1 of BOE (50:1): 49% HF etched at 3.3μm/min etching rate and 10:1 ratio mix yielded 0.6μm/min etching rate. However, the resulting surfaces were relatively rough. HCl was added to improve the roughness of the etched surface. Since HCl dissolves the insoluble products of etching (CaF2, MgF2 or AlF3), addition of HCl ensures consistent contact between the glass surface and the etchant (Ciprian 2007).

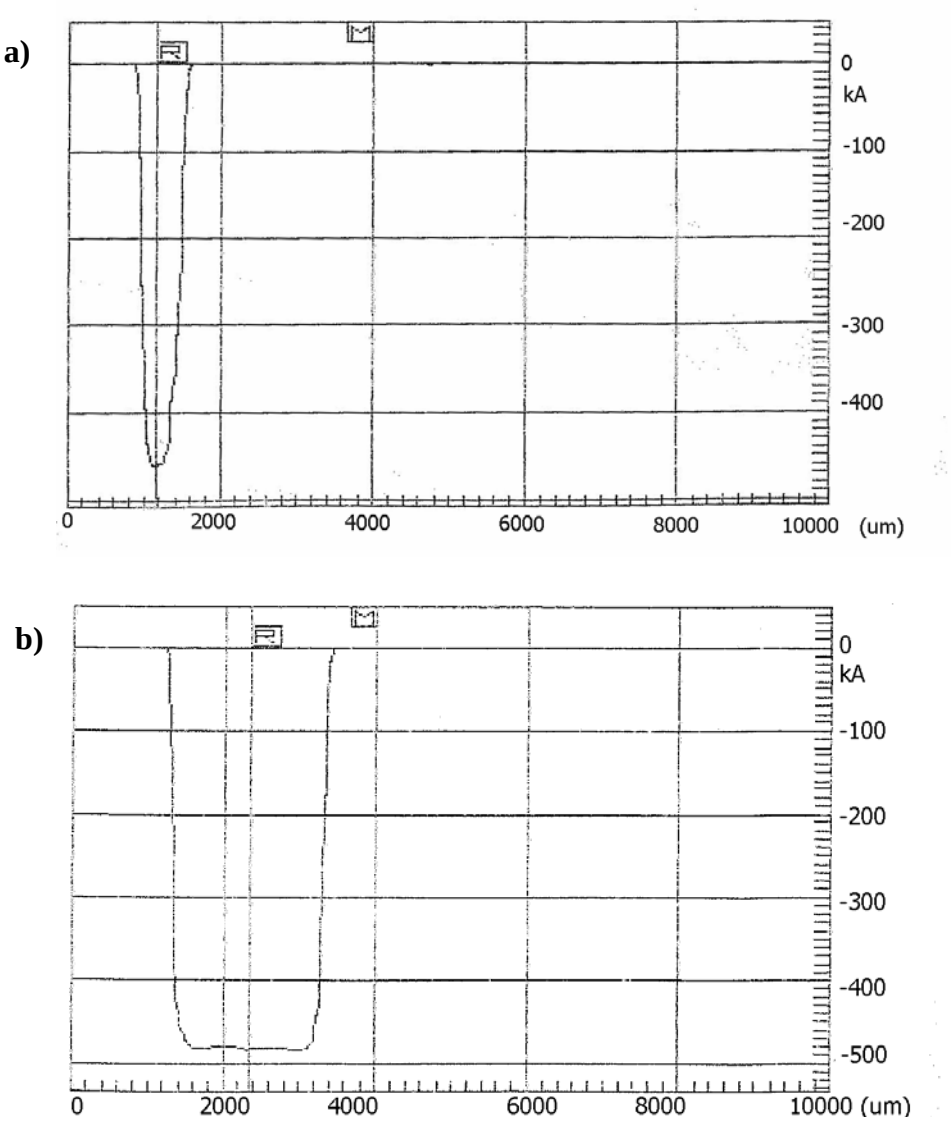

Figure 32: Glass etched with BOE (20:1) for 5 hours. **a** Channel cross-section. **b** Central chamber

After testing various combinations of HF, HCl and BOE (50:1) moderate etching rates could be achieved; Etchant with 1:1:10 of 49% HF: HCL: BOE (50:1) and etchant with 1:1:4:6 of 49% HF: HCL: BOE (20:1): water etched at 1μm/min (Figure 33). When used

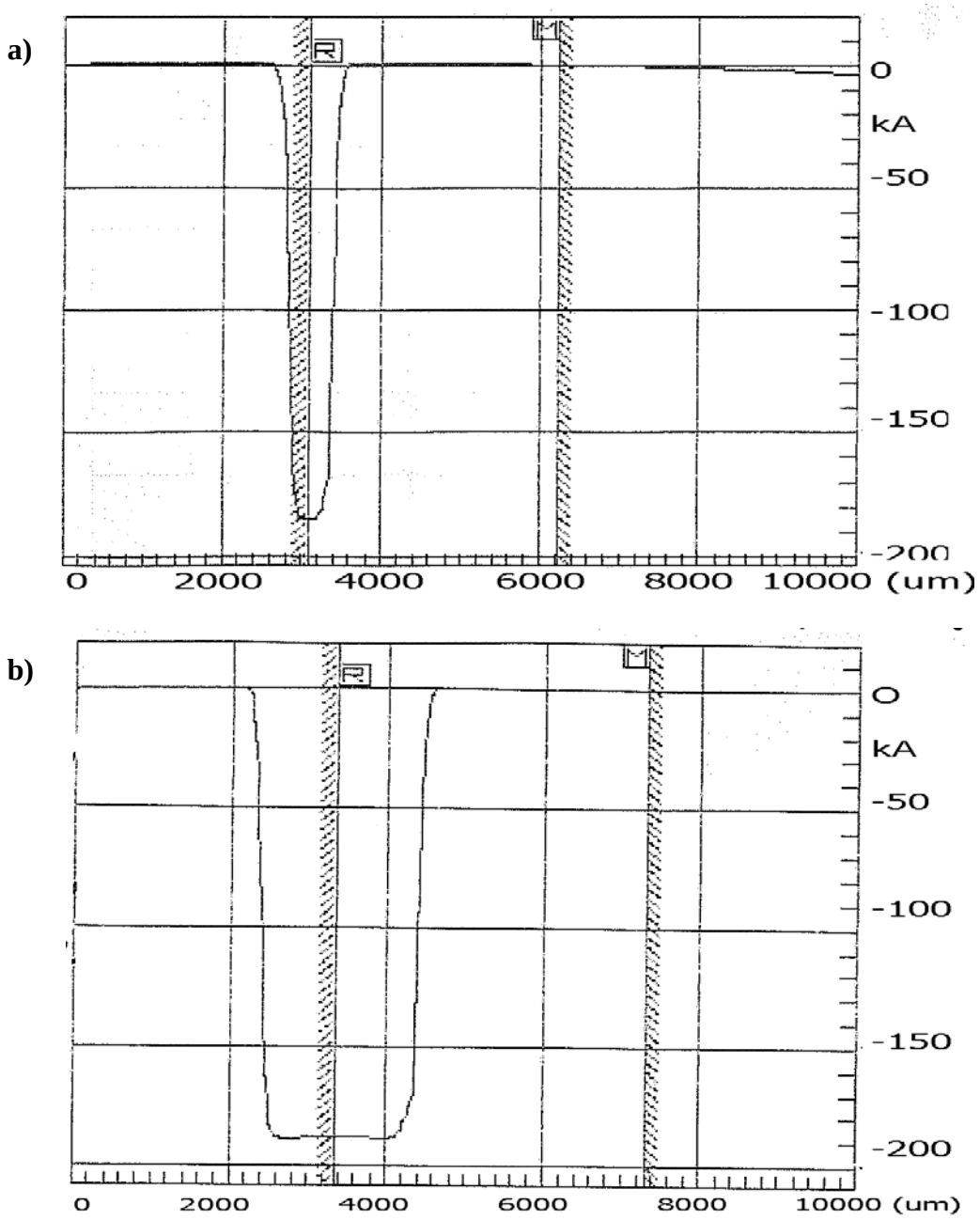

Figure 33: Glass etched with 1:1:10 of HF: HCl: BOE (50:1) for 17 minutes. **a** Channel cross-section. **b** Central chamber

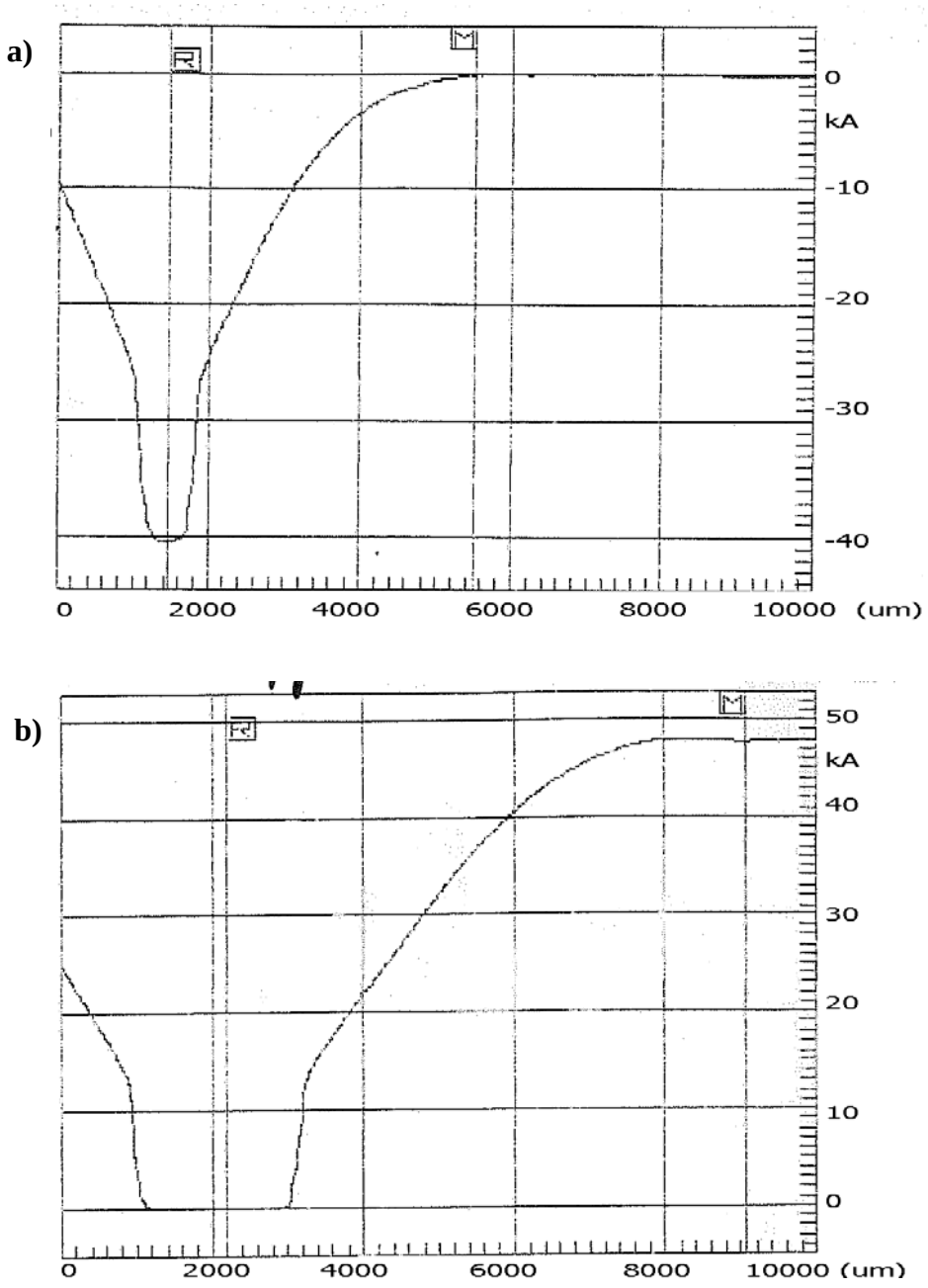

Figure 34: Pyrex etched with 1:1:10 of HF: Hal: BOE (50:1) for 150 minutes. SU8 is stripped off the channel edges. **a** Channel cross-section. **b** Central chamber

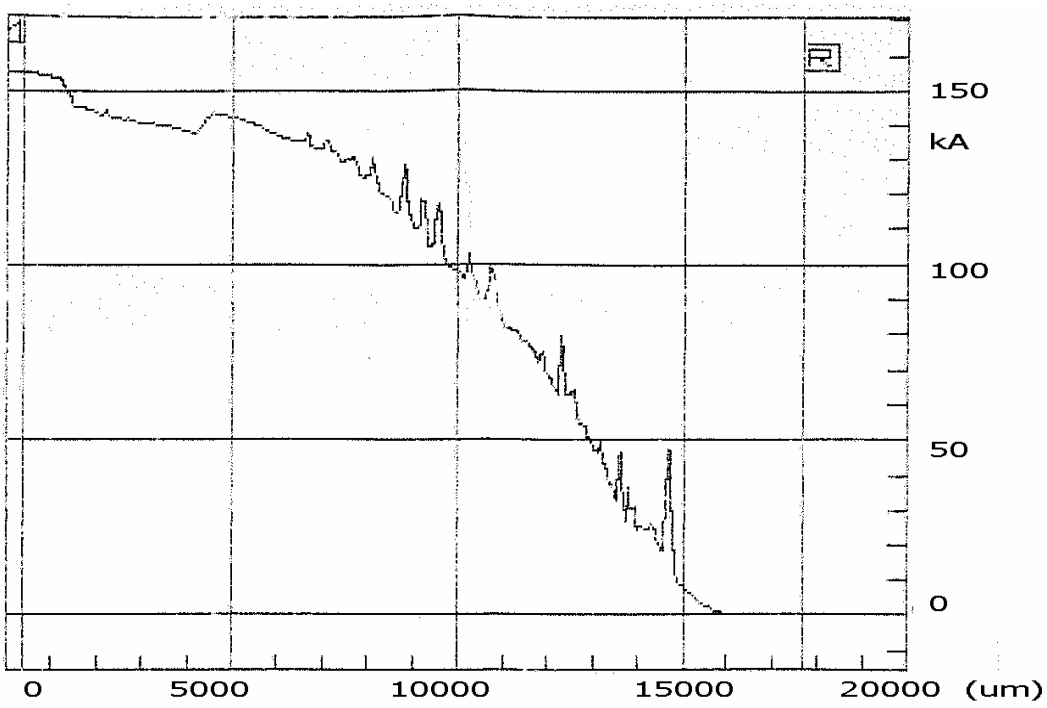

Figure 35: Pyrex etched with 1:1:1 of HF: HCl: BOE (20:1) for 30 minutes

the same etchants to etch Pyrex® it was found that the etch rates were 20 times lower, and when etched for a longer time (i.e. 150 minutes) SU8 mask was completely stripped off at channel edges and the uncovered glass surfaces were etched (Figure 34). The etchant derived by mixing 1:1:1 of 49% HF: HCL: BOE (20:1) etched Pyrex® at 0.5μm/min (Figure 35). However, the 53.5nm thick metal mask was completely stripped off within just 1 minute and SU8mask was stripped off within 5 minutes as mentioned before.

3.2 Fabrication of Through Holes on Glass Wafers

For making the connection between channels and tubing through holes had to be fabricated on the glass wafers (4 on each side). Wet glass etching was discarded for deeper depths as considerable undercut would result affecting the size of a hole. Drilling small holes on glass was a challenging task because of high brittleness of glass. An attempt to drill a hole failed damaging the drill bit and the glass wafer. Therefore, as an alternative method, electrochemical discharge machining was experimented. However, better glass drilling process was implemented subsequently.

3.2.1 Electrochemical Discharge Machining of Holes

Electrochemical discharge machining (ECDM) is a cheaper and easier alternative to high quality laser beam machining (Zheng, et al. 2007). In this method high temperature and chemical etching cause the removal of glass. Electrolysis of NaOH results in H_2 generation at the cathode. This isolates the cathode from the electrolyte (NaOH), increasing the current density in it. When current density exceeds a critical value discharge occurs causing localized heating, burning of H_2 or local sputtering (Li 2006; Zheng, et al. 2007). When implementing the ECDM process, 50% NaOH was selected as the electrolyte. A syringe needle was used as the cathode (the negative electrode). The apparatus is illustrated in Figure 36.

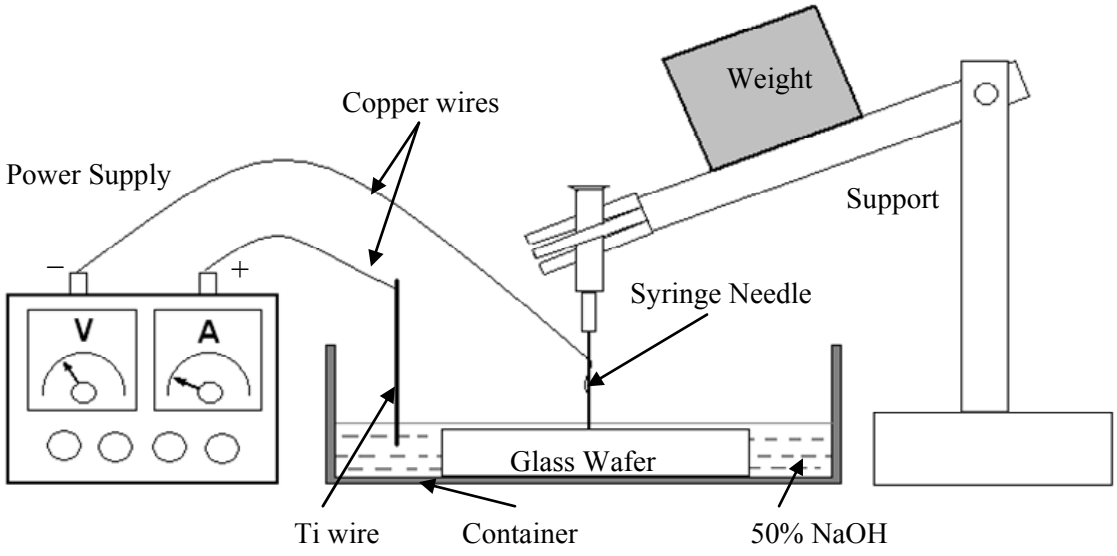

Figure 36: Apparatus used for ECDM process

A weight was mounted on the needle to automatically drive the needle down during the short period (about 2 seconds) of etching. A copper wire was initially used as the anode (positive electrode) but high oxidation hindered smooth operation. Later a titanium (Ti) wire was used. When a voltage of about 30V was applied between the two electrodes with the needle just touching the NaOH surface, sparking was found to occur. For making the holes a needle was submerged in NaOH solution to a depth of about half a millimeter. 1mm holes could be drilled within 5seconds (Li 2006 managed to achieve a maximum rate of 0.133mm/min rate). The resulting surfaces of the holes were very rough and had many possible crack initialization points (Figure 37). Probably slower feeding rate for the needle might have resulted in a superior surface finish but there was no easy way of controlling the feed rate as the weight mounted on the support arm was

used for driving the syringe. Feeding with hand would have been an option but was not feasible due to the high direct current used.

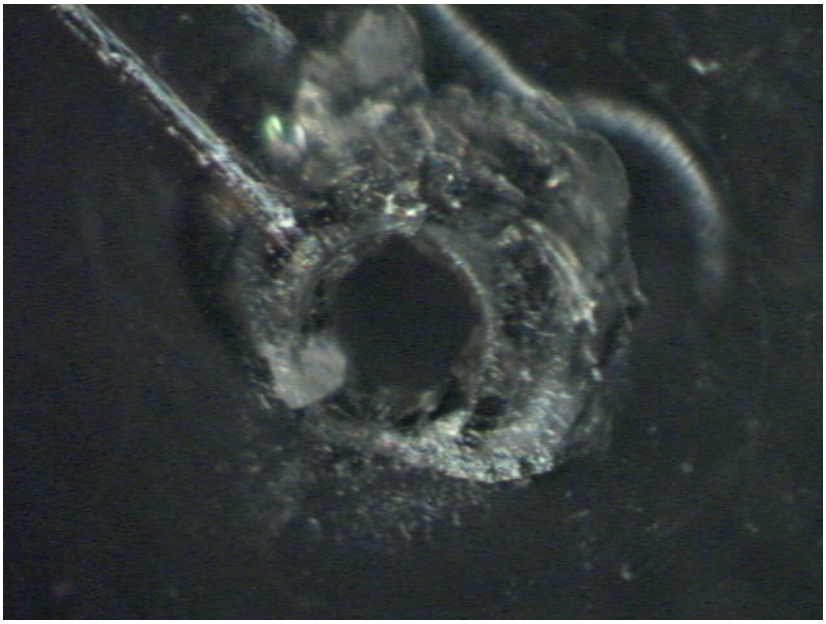

Figure 37: A through hole obtained from ECDM process

Even though the holes were fabricated in a very short period of time, glass wafers had a very high chance of shattering with this method. Since 4 holes per a glass wafer were required to be made, this method was not very reliable. A related observation was that the holes could be obtained even after reversing the polarities of two electrodes. Glass erosion at this setting might be due anodic etching as explained in Zhuang and Edgar 2005.

3.2.2 Drilling of Holes

Drilling holes on glass requires use of special drill bits, very high tool speeds, very slow feed rates and continuous cooling. Overall process generates high temperatures and hence continuous cooling is essential. Drill with less vibration is desirable to avoid fracture of glass due to fluctuating stresses.

Diamond drill bits (4ED10, 1mm diamond solid drills, Ukam Industrial Superhard Tools) were used on Sears Craftsman 8" drill press to drill holes of 1mm in diameter. During the drilling process glass wafer at the drilling point was covered with water to provide cooling. This was done by placing the glass wafer in a plastic Petri dish and then filling in water. Points were marked with a fine point marker on both sides of the glass wafer (for easy alignment). The marked points were properly aligned with the drill bit before filling in water, because after wetting it was not easy to achieve an accurate alignment. The drill bit was fed very slow that it took around 2 minutes to drill a hole on a 1mm thick glass wafer. It was necessary to occasionally withdraw the drill bit to allow water filling into the drill hole during the drilling process. The glass wafer was kept on a wooden plate so that vibrations were minimized and the drill bit could drill through without getting damaged. When the feeding rate was changed during the manual feeding the glass wafers cracked. However, drilling was a much better option considering the glass wafers breaking frequency during ECDM process. In general chipping of the glass wafer from the opposite surface was observed when the drill bit almost drilled through the glass wafer. It would have been avoided with a reduced feed

rate but which was not feasible with manual feeding based on visual observation. A typical hole drilled on a 1mm thick glass wafer is shown in Figure 38.

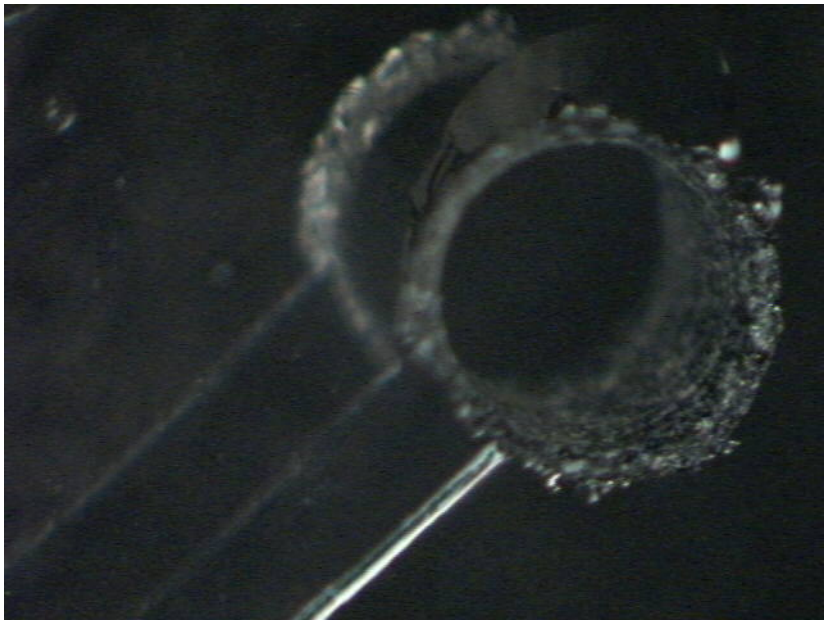

Figure 38: A drill hole (1 mm diameter) obtained by drilling

Better quality hole-walls are visible in this figure. However, a small chipping is observed at the top. Usually drilling was performed from the side of the channels so that the chipped surfaces could be avoided in the channels.

3.3 Preparation of Teflon Sheet

The thinner the Teflon sheet the better for the bi-layer as the curvature of the bi-layer at aperture edge decreases. In folding bi-layer experiments, Teflon sheets of 25μm in thickness have been used (Kang et al.2007). A 25μm thick Teflon sheet

(FP301200/10, Polytetrafluoroethylene (PTFE), Goodfellow Corp., PA) was cut into the size of 40mm × 50mm size and an aperture was made at the center. It needed to be larger than a glass wafer for the purpose of sealing with silicone. It was important to avoid wrinkling of the thin Teflon sheet when handling.

The best way of making an aperture on a Teflon sheet is by burning the Teflon sheet with a high voltage spark as detailed in Hanke and Schlue 1993. In this method a voltage pulse of about 10kV was applied across the Teflon film for a fraction of a second (10ms). In the absence of required equipments to set up such a system, an easy an economical hole punching method (Hanke and Schlue 1993) was adopted. In this method the hole was punched using a sharp circular tool, which can be manufactured from a thin syringe needle. Conventional syringe needle are too large for this application Therefore, special thin syringe needles (RN NDL (33/1.5”/3)S, Hamilton Com., NV) were used for the purpose. However, sharpening of the edge of the needle was not possible. Mechanically punching of an aperture was not very successful as it caused deformation to the thin sheet; after punching a hole by pressing a needle on a Teflon sheet kept against a soft wood surface, the Teflon sheet was no longer flat (Figure 39 and Figure 40). Further this method was not feasible with thin needles, since the needles could not support large punching forces.

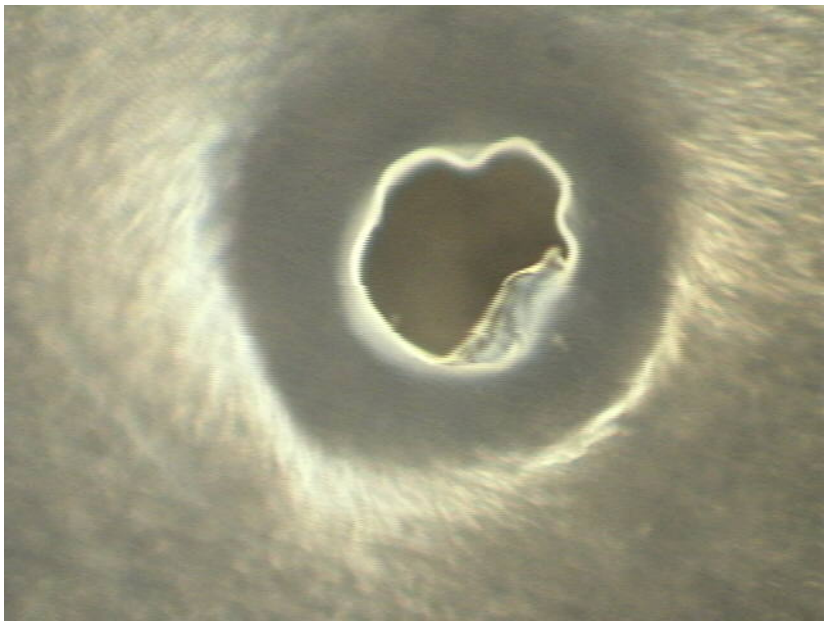

Figure 39: An aperture (400µm diameter) on Teflon obtained by punching

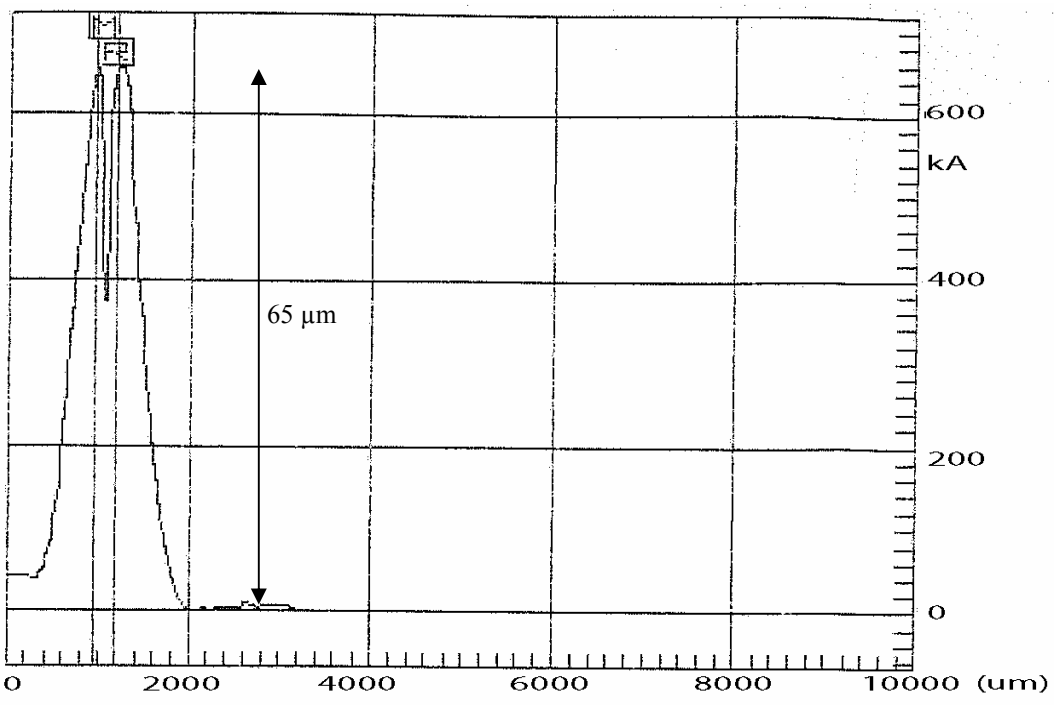

Figure 40: Cross-section profile of an aperture (150µm diameter) on Teflon obtained by punching

Hence, the needle was heated using a blue flame before punching. This will be referred to as ‘Hot Punching’ in this text. However, since the needle was so small, it lost the heat as soon as the flame was withdrawn. Therefore, needle needed to be heated until just prior to punching. If the punching was not done quickly, the Teflon sheet was extruded after melting due to heat (Figure 41).

Figure 41: Extruded Teflon sheet during hot punching

Finally the following procedure was established: Needle was heated up and while holding the Teflon against a hole of 2mm in diameter the needle was struck fast onto the sheet. Even though it was practically difficult to perform, this method was relatively successful. Care had to be taken to not to let the heat from the flame affect the Teflon sheet. Needle did not have to be very strong and the aperture size was smaller than the

used needle side due to deflection back of the aperture walls. Therefore, small diameters of the range 100μm could be fabricated. However, the aperture edge was prone to be wrinkled making it not suitable for lipid bi-layer formation. Not always circular smooth apertures could be achieved. Figure 42 shows an aperture of very good quality obtained from this method. This was used n the final device.

Figure 42: An aperture (75μm diameter) on a Teflon sheet

The Teflon sheet needed to be kept clean and hence the apertures were hot punched in a cleanroom. When assembling the device, Teflon sheet was cleaned with Acetone and isopropylene, and air dried.

3.4 Assembling

Sandwiching the Teflon sheet in-between glass wafers and making of the tubing connections are described in this section. NanoPort™ Assemblies had to be connected to glass wafers before sandwiching to get the final form of the device. At the beginning the tubing was directly connected to the holes drilled on the glass wafers simply by forcing an adaptor into the drill holes. However, this connection was not reliable and could not take adequate pressure. After initial testing, only on selected glass wafers NanoPorts were glued.

Clamping of three layers together using large paper clips was attempted initially but there was no clear flow along the channels, instead water (which was used for testing the device before the experiment stage) leaked all over the glass – Teflon interface. Given the roughness level (about 5μm change in profile per 10mm) of borosilicate glass wafers and low elasticity (high resistance to elastic deformation) of Teflon, it was initially theorized that bonding of glass to Teflon might be a better option than clamping. Thermal bonding and bonding using epoxy were explored for bonding the Teflon sheet to the glass wafers. Later, sandwiching by clamping was revisited and new clamps were designed.

3.4.1 Clamping of Layers

Initially two G-clamps (1415 – 1 ½ inch) were used to clamp as shown in Figure 43 and Figure 44. Several layers of papers (68310-206, 4" × 4" vipers, VWR international LLC, PA) were placed between the glass surface and the anchor of the G-

clamp to avoid localized stresses on glass wafers. Verification of the approach was performed by clamping a Teflon sheet (without aperture) between a glass wafer with 60µm deep etched channels and a blank glass wafer held against a wooden block. Figure 43 illustrates flow of water (dyed in blue solution) along a channel. This result was highly encouraging with almost no leakages outside the channels (Figure 43).

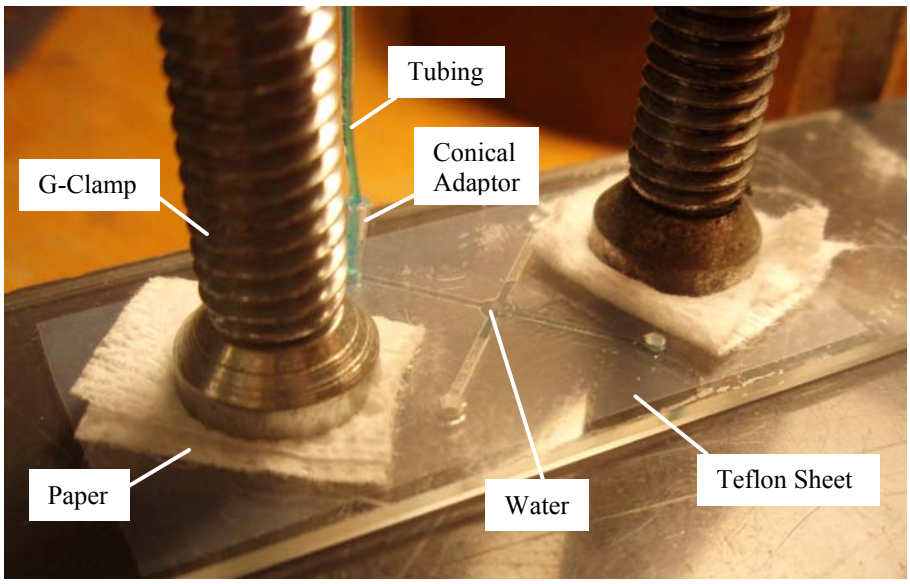

Figure 43: Colored water flow in a single cross channel test setup clamped with a G-clamp

As the next step, all three layers were clamped using a G-Clamp and tested (Figure 44). Even though low level leakages were present outside the channels, major flow was along the channel. However, it was not possible to use G-clamps in the device for the following reasons:

1. Large size and weight of G-clamps violated the requirements for miniaturization;

2. Several glass wafers were broken while handling due to twisting of glass wafers due to the torque developed by large G-clamps;
3. The large surface are of the anchors, interfered with the placement of the NanoPorts.

A custom made C-shaped clamp (Figure 45) was manufactured to apply pressure from sides of the area containing channels, replacing G-clamps. Even at very high clamping pressures very large leakages were observed with this clamp. Further, application of high pressure caused the glass wafers to crack at the area of pressure application. It was observed that glass wafers between the areas of pressure application bowed outward generating a large space between the glass surface and the Teflon sheet.

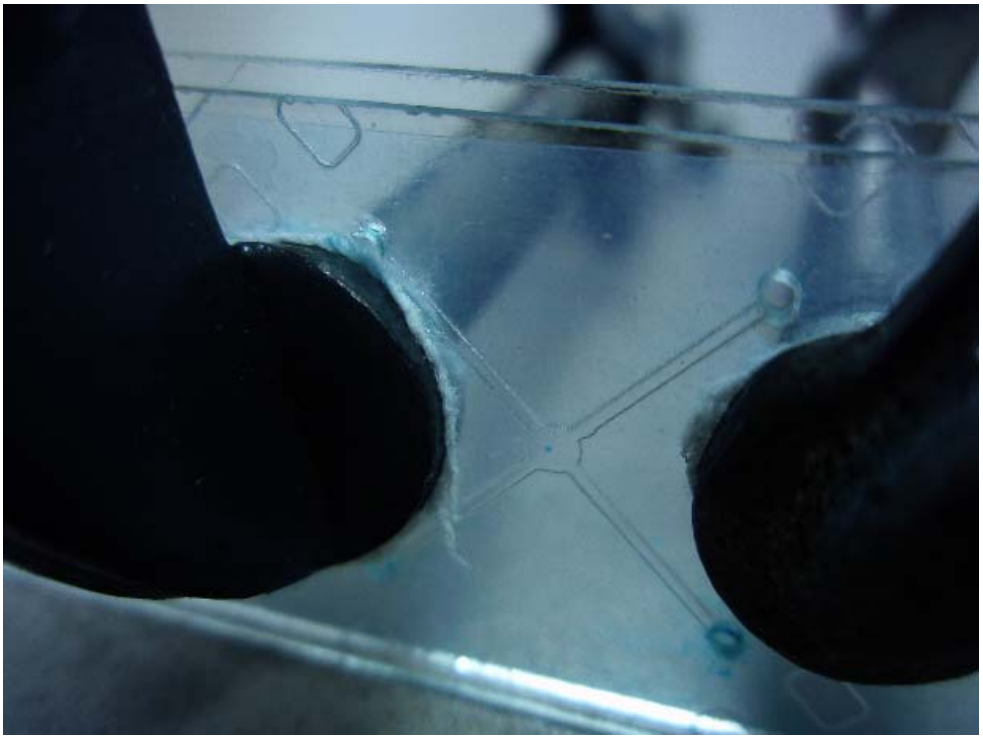

Figure 44: Clamping of layers with G-clamp

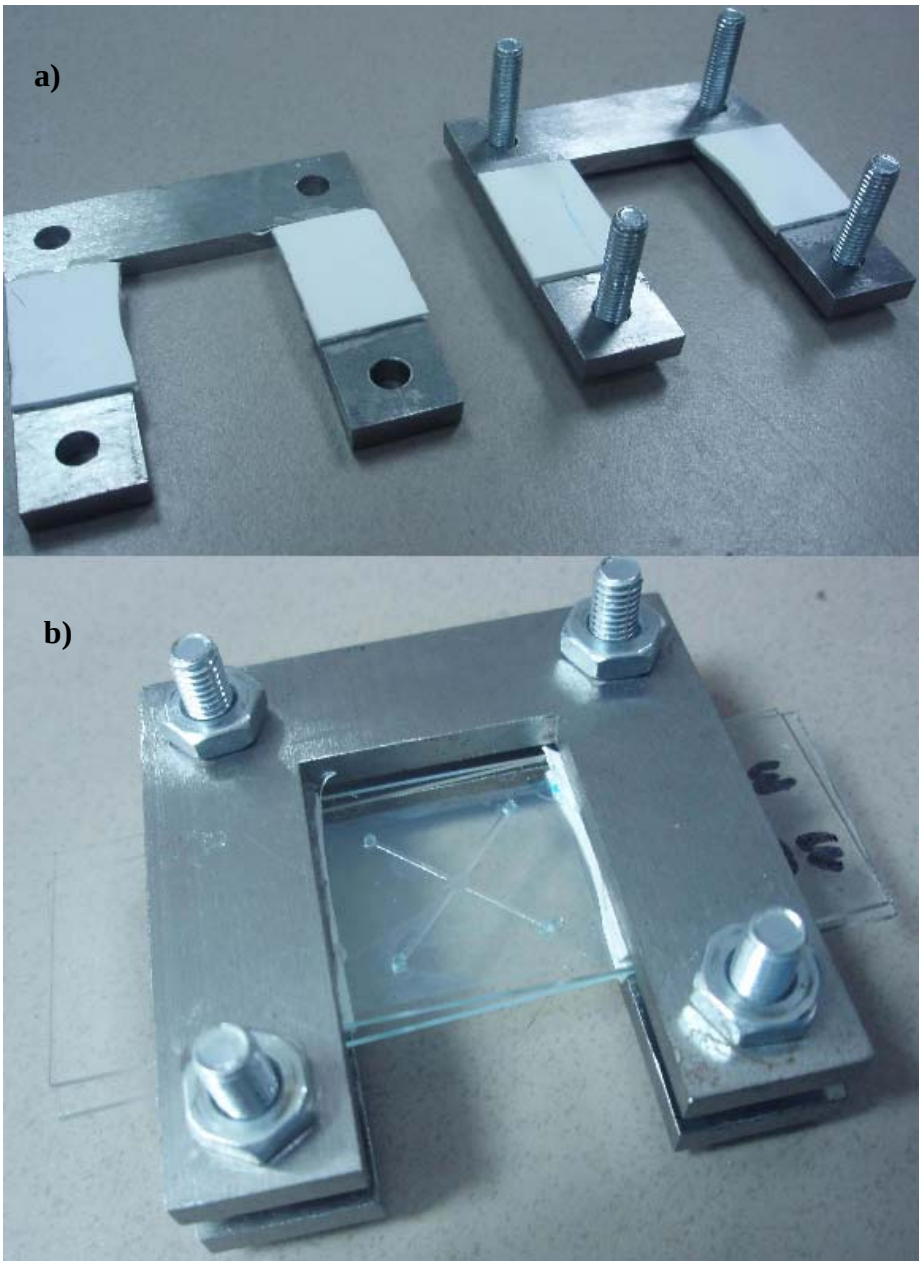

Figure 45: Custom made C-shaped clamp. **a** Exploded view. **b** Assembly

The clamp had to be redesigned to apply the clamping pressure as close as possible to the channels so that leakages could be avoided with a lower holding pressure. It was desirable the clamp should not obstruct the view of the central chamber for

observation of the lipid bi-layer in the event of such a necessity. A simple to manufacture clamp design, which satisfies all the above requirements, was developed as shown in Figure 46, Figure 47 and Figure 48. It was fabricated with Mild Steel (Figure 48) in the following manufacturing steps:

1. Square shaped pieces were cut out of mild steel plates using plasma cutting;
2. Thickness was reduced to the desired level and edges were smoothened using shaping operation;
3. Holes were drilled at required locations.

The new clamp was proved to be effective during the initial testing. Figure 47 gives the dimensions of the new clamp and Figure 48 shows the fringe patterns on glass wafers when clamped. A silicone sheet (Figure 46) was cut into the shape of the cross-with-a-hole shape where the contact takes place. Smooth fringe patterns without sharp corners were targeted to avoid stress concentrations.

Figure 46: Custom made new clamp (exploded view)

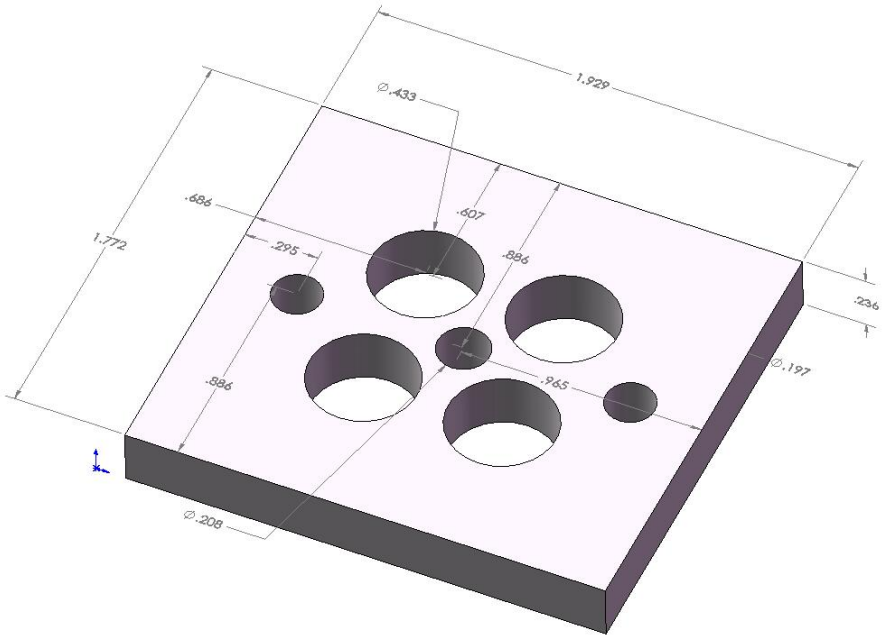

Figure 47: Custom made new clamp dimensions (in inches)

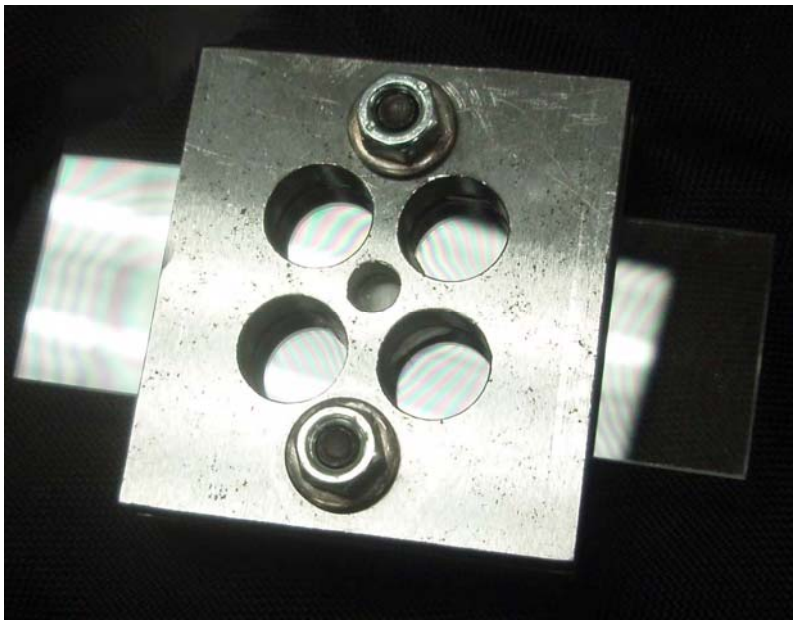

Figure 48: Testing of custom made new clamp for stressing the wafers

When clamping the layers, care had to be taken to equally tighten the bolts to avoid high local stressing due to unbalance holding forces. New clamps were better than the C-shaped clamp. It was easier to balance two sides (with two bolts) and guaranteed high holding pressure in the area with the channels. The stress applied by the clamp was controlled by measuring the gap between two plates of the clamp. Since this gap is dependant of the thicknesses of the two silicone layers, the thickness of silicone layers under the holding pressure had to be determined beforehand clamping the actual glass wafers. Two plain glass wafers identical to the glass wafers with channels were clamped between two plates of the clamp and the bolts were gradually tightened in sequence. Initially, bolts were tightened by about 45° angle but when the required torque went high the rotation was reduced to about 10°. After each rotation, the gap at the bolt was measured and adjustments were made to keep the gaps at two ends in the same order. The critical gap was found when the glass wafers cracked. This critical gap was verified with at least two pairs of plain glass wafers. When clamping the etched glass wafers, clamped-gap was kept at least 0.1 mm above the critical gap.

3.4.2 Bonding of Layers Using Epoxy

Bonding of glass wafers was considered as a method of sandwiching the layers. Major arguments supporting bonding over clamping were that the surface properties were critical only near the aperture, cheap borosilicate could be used, no etching problems anticipated and Teflon did not have to deform to the shape of the glass wafer surface to seal any gaps.

A principle characteristic of Teflon is inability to stick. It seemed impossible to find something to glue Teflon to Glass. However, after several trials it was observed that satisfactory attachment was obtained between Epoxy mixture (100:50 of EPON^{TM} Resin 828: EPI-CURE^{TM} Curing Agent from Hexion Specialty Chemicals, Inc) and Teflon. This might be due to the forming of week bonds at the interface and the shaping of epoxy to perfectly fit into imperfections on the Teflon. Even though epoxy bond alone could not withstand the analytes pumping pressure (Figure 49), with help of external pressure applied with clamps, the glue could hold the layers together.

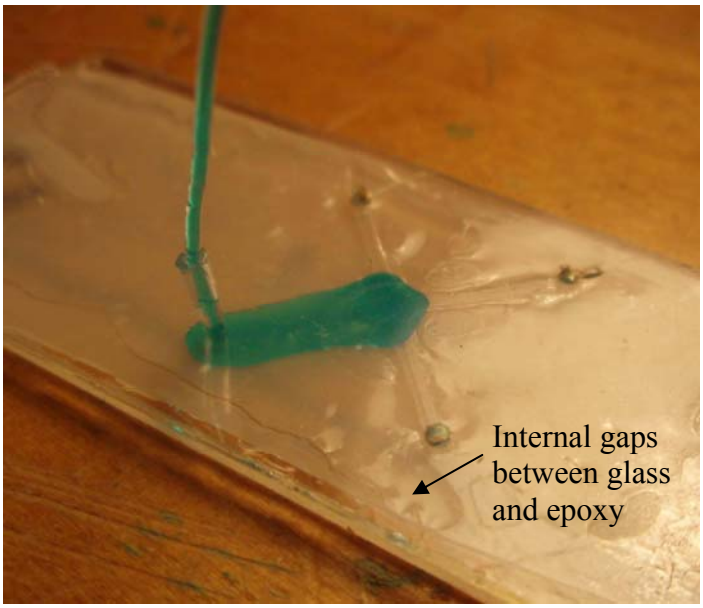

Figure 49: Testing of bonded layers

However, there were gaps between the epoxy layer and the glass wafer especially near the channel (Figure 49). This was mainly due to flowing of epoxy into channels and partially due to air bubble formation.

Following is the procedure used in gluing glass wafers:

1. A Polyethylene sticker was cut into the shape of the channels and pasted on the channels on glass wafers.
2. Epoxy mixture was prepared by adding 50ml of Epi-Cure Curing agent to a small beaker with 100ml of Epon Resin 828.
3. Epoxy mixture was heated up by submerging the beaker in water at 70°C to reduce the viscosity so improve spreading of epoxy while spinning resulting in a thinner epoxy layer (Tu et al.2005). Water was heated with its container on a hot plate and monitored with a thermometer.
4. Glass wafer was heated to 70°C on a hotplate to maintain the viscosity of the epoxy mixture after dropping on it.
5. When the epoxy mixture became viscous, a thin layer of epoxy mixture was quickly applied on glass wafer avoiding air bubble formation
6. Glass wafer was spun at 4000rpm for 60seconds to get an epoxy layer of thickness 30μm (Figure 50).
7. Using a fine-end tweezer the sticker was lifted from glass wafer leaving only the epoxy outside the channels.
8. Glass wafer was slightly pressed into Teflon sheet, which was kept against a blank glass wafer to avoid folding, until the shape of the cross channel was clearly defined by the outline of the epoxy-glass interface.
9. Assembly was maintained for 24hours at room temperature until the epoxy was set.

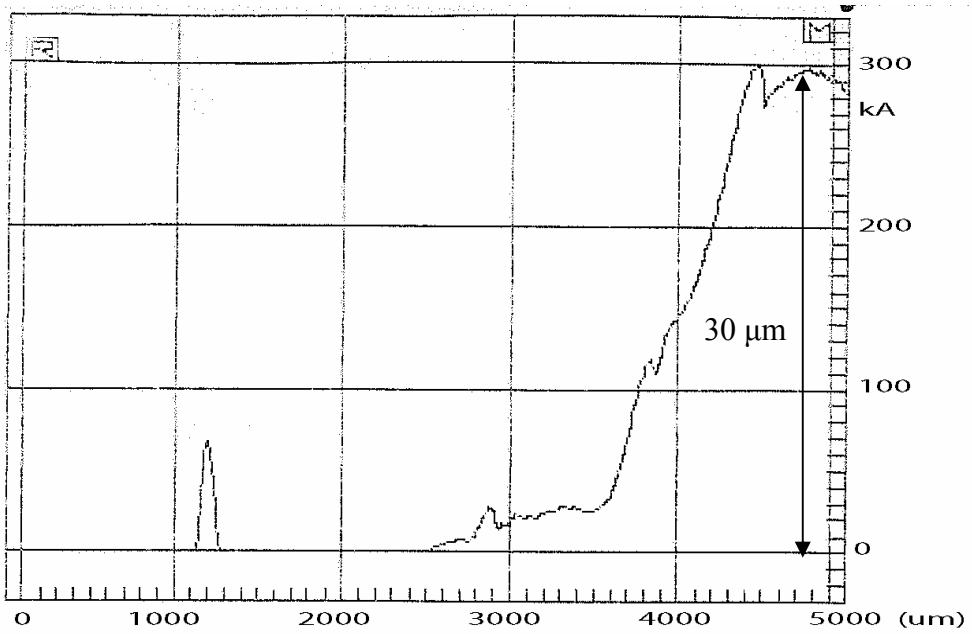

Figure 50: Profilometer plot showing epoxy layer thickness

Major problems encountered in this approach included the difficulty of getting a thinner (<10µm) epoxy layer as needed for making channels shallow, and the lack of control in making the contact between the epoxy layer and the Teflon sheet giving rise to distorted or narrow channels and voids. Large thickness of epoxy led to the use of epoxy alone, without glass etching, to define channels but this was not preferred, since channel profile needed to be smooth for better fluid control. Possibility of epoxy reacting with the lipids and analytes appeared as the biggest concern. Finally this method of sandwiching of layers had to be discarded for this particular application. Glass to glass bonding (Jia et al. 2004) was considered as an alternative but it had to be discarded as it did not provide the required high sealing pressure between the Teflon-glass interface.

3.4.3 Thermal Bonding of Layers

Thermal bonding of the Teflon sheet to the glass wafers was the third option considered in sandwiching of layers. The underline concept was deformation of Teflon sheet to form into the shape of the glass surface. A Teflon sheet compressed between two glass wafers was heated in an oven near the melting point of Teflon for about 10 minutes and allowed slow cooling to the room temperature within the oven. The procedure resulted in low strength bonding to glass, and hence the name. Various sources give different melting points for Teflon; 327°C according to McGeer P and Duus H, 1952 and around 360 °C according to the technical data given by the supplier of Teflon sheets (Goodfellow). Experiments carried out at 360 °C, 332 °C and 204 °C. With 360 °C, some parts of Teflon sheet were burnt hence a lower temperature of 332 °C was explored. Several attempts resulted in Teflon cracking along the micro-channels. The temperature was further reduced to 204 °C to avoid damages to the Teflon sheet. With 360 °C considerably high bonding was observed due to melting and solidification of Teflon. With 204 °C, even though the Teflon sheet was well intact, leakages were present as usual. Thermal bonding had to be discarded as a successful way of sandwiching Layers. However, this approach would be suitable for Teflon coating for insulation purposes.

3.4.4 Tubing Connection

During the preliminary testing of cross-channel functionality tubing was connected to drilled holes on glass wafers using conical adaptors cut out of polyvinyl

chloride Pipettes. This setup was sufficient to initialize a flow along channels but after filling a fraction of the input channel, analytes started leaking at the conical adaptors. For fully closed high pressure operation NanoPort^{TM} assemblies (N-333, 6-32 Coned Assembly, Inc., WA) were used. A NanoPort assembly consists of a nut, a ferrule, a NanoPort and a gasket (Figure 51). The purpose of the ferrule is to adapt the tubing end to fit into the NanoPort. The nut supplies pressure to seal the ferrule-NanoPort interface. Purpose of the gasket is to seal the glass-NanoPort interface. On the NanoPort bottom, an epoxy was applied excluding the gasket area when bonding with the NanoPort. The gasket avoids analytes from coming into contact with the epoxy.

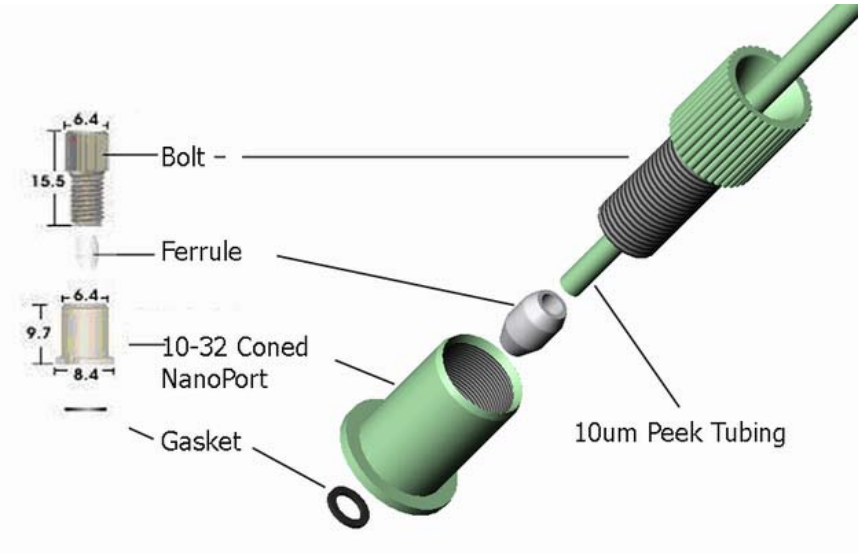

Figure 51: Components of a NanoPort assembly and their dimensions (in mm)
(2-D image from Upchurch Inc., WA)

Two types of epoxies for gluing Nanoports to another surface were available from Upchurch Inc. First was a ring of a thermoset epoxy (Adhesive Ring, N-100-01,

Upchurch Inc., WA), which required curing at 165°C to 177°C for 1 hour. While curing, the NanoPorts had to be forced onto the glass wafer using medium size paper clips. Resulting bond was very strong and durable. Other option was an epoxy gel (N-008, 2-part Epoxy Adhesive Gel-Room Temperature Cure, Upchurch inc., WA). This was required to be used immediately after the epoxy and resin were mixed, before the epoxy was set. Under the room temperature it took 24hours to set and this time would have been reduced to an hour by curing at 49°C. The resulting bond was not very strong and could easily be removed. However, since the adhesive rings would be affected when reheated, NanoPorts connected at a later stage had no other option but to glue with the epoxy gel. Therefore, it was important to glue all the four NanoPorts on a glass wafer at the same time using adhesive rings. However, it was not an easy task to align and clip all four NanoPorts at the same time, while ensuring equal force distribution over the glass wafer. PEEK^{TM} tubing with 10μm internal diameter (1531, Upchurch inc., WA) were used (P-659, Upchurch Inc., WA) between the NanoPorts and adaptors (P-659, 10-32 Female to Female Lure, Upchurch inc., WA) for syringes. Peek tubing was connected to the adaptor via a ferrule and a nut (F-330NX, Nano Tight Fitting Long PEEK, Upchurch inc., WA).

4. EXPERIMENT AND RESULTS

The primary objective of the lipid bi-layer synthesis experiments was to demonstrate the feasibility of the chosen design and experimental configuration. The designed device together with the continuous KCl flow approach was expected to form the lipid bi-layer at the aperture on the Teflon sheet.

Main constituents of the experiment apparatus are as follows (Figure 52):

1. Lipid and Analytes pumping system
2. Microfluidic Device
3. Electronic Measurement System

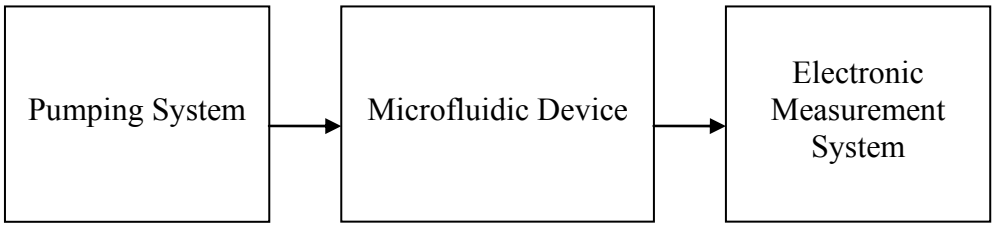

Figure 52: Simplified diagram of the experimental setup

Pumping system comprises of two tandem syringe pumps, which are explained in section 2.2, each carrying two syringes. The syringes delivered working fluid to the two sides of the microfluidic device. The microfluidic device has been discussed in great detail in section 3. Electronic measurement system captures the current signal through the aperture/lipid bi-layer for a given voltage signal as detailed in the following section. Experiment procedure is outlined in the section 4.3.

4.1 Electronic Measurement System

Planar lipid bi-layers are about 4 nm (or two-molecule) thick as discussed before. Hence a reliable way of monitoring the process of the planar bi-layer formation in the micro scale aperture is required. Two conventional methods used to monitor the process of lipid bi-layer formation are optical method and electronic measurement method. The optical method is used with painted bi-layer formation method as explained in Hanke and Schlue 1993. In contrast electronic measurements are used with almost every lipid bi-layer formation methods.

Lipid bi-layer is modeled as a resistor and a capacitor in parallel (Hanke and Schlue 1993). In Hanke and Schlue, 1993 the following simple equation is used to calculate the resistance of the lipid bi-layer:

$$R = \frac{V}{I} \tag{22}$$

Typical electrical characteristic values for planar lipid bi-layer from folding method are listed in Table 5.

Table 5: Electrical characteristics for DphPC lipid bi-layer

No.	Reference	Area/ (μm^2)	Resistance/ ($G\Omega$)	Specific Resistance/ ($\Omega . m^2$)
1	Malmstadt et al. 2006	43,374[3]	15[2]	650[3]
2	Malmstadt et al. 2006	3500[2]	70[2]	245[3]
3	Peterman et al. 2002	491[3]	2.5[2]	4.6[3]

The standard expression for resistance given in equation (23) can be rearranged to get equation (24), where R is the resistance of the bi-layer, ρ_L is the resistivity of the membrane material, d is the bi-layer thickness and A is the bi-layer area.

$$R = \rho_L \frac{d}{A} \tag{23}$$

$$R.A = \rho_L .d \tag{24}$$

The right hand side of equation (24), specific resistance, is literally constant for a given membrane material. However, the parameters k, d and ρ_L can change due to environmental factors such as temperature, pressure, type of buffer used and buffer concentration.

The electronic measurement system is a very important part of the lipid bi-layer formation experiment as it provides a mean of understanding the nano-scale phenomena occurring on the lipid bi-layer. Design of electronic measurement system for a lipid bi-layer formation apparatus is very challenging given the range of involved current is in the Pico-Ampere (pA) range (Funakoshi et al.2006; Malmstadt at al.2006). Measurements are difficult due to low signal to noise ratio.

Most critical issue in designing the measurement system was the current obtained after applying a very low voltage of about 50mV across the lipid bi-layer. Operational amplifiers were seen as a cheap and easy solution but with a simple circuitry unwanted resistances and capacitances would have been introduced to the measurement system. Further, to achieve a very high amplification factor at least two stages of amplification was necessary and hence there was a chance of more unwanted impedances being added.

Another option was off-the-shelves high sensitive voltage amplifiers. However, since the signal to be measured was current, current amplifiers were preferred. The selected Low Noise Current Amplifier (SR570 – DC to 1MHz Current Preamplifier, Stanford Research Systems, CA) had 1pA/V maximum gain and 5fA accuracy at maximum gain.

In addition, the electronic measurement system was equipped with two Ag/AgCl electrodes (EO05,World Precision Instruments, Inc., FL) of 0.5mm diameter, a function generator (33220A, 20MHz Function/Arbitrary Wave Form Generator, Agilent, CA) and an Oscilloscope (TDS 2012B, Tekronix, TX) with 2mV/div max resolution. The oscilloscope supported storage of screen captures in a USB drive. Even though it had a computer interface, which might have been used for automation, it required Microsoft Windows® Enterprise Edition. Therefore, data capturing had to be performed manually. Equipments are connected as shown in Figure 53. Two probes were used to connect the oscilloscope and the current amplifier to the electrodes. Between the current amplifier and the oscilloscope was a 50Ω BNC cable. In order to minimize electro-magnetic-interference (emi) from the ambient, all the cables and KCl tubing were wrapped with aluminum foils and the microfluidic device was placed inside a 14” × 7”× 7” custom made galvanized steel Faraday cage. Faraday cage was manufactured by bending a pattern cut out of 0.5mm thick galvanized steel sheet (24 × 36 – 26 Galv Sheet). It was essential to ensure complete electromagnetic isolation for the electronic measurement system or else very large noises were observed, especially 60Hz frequency noises due to

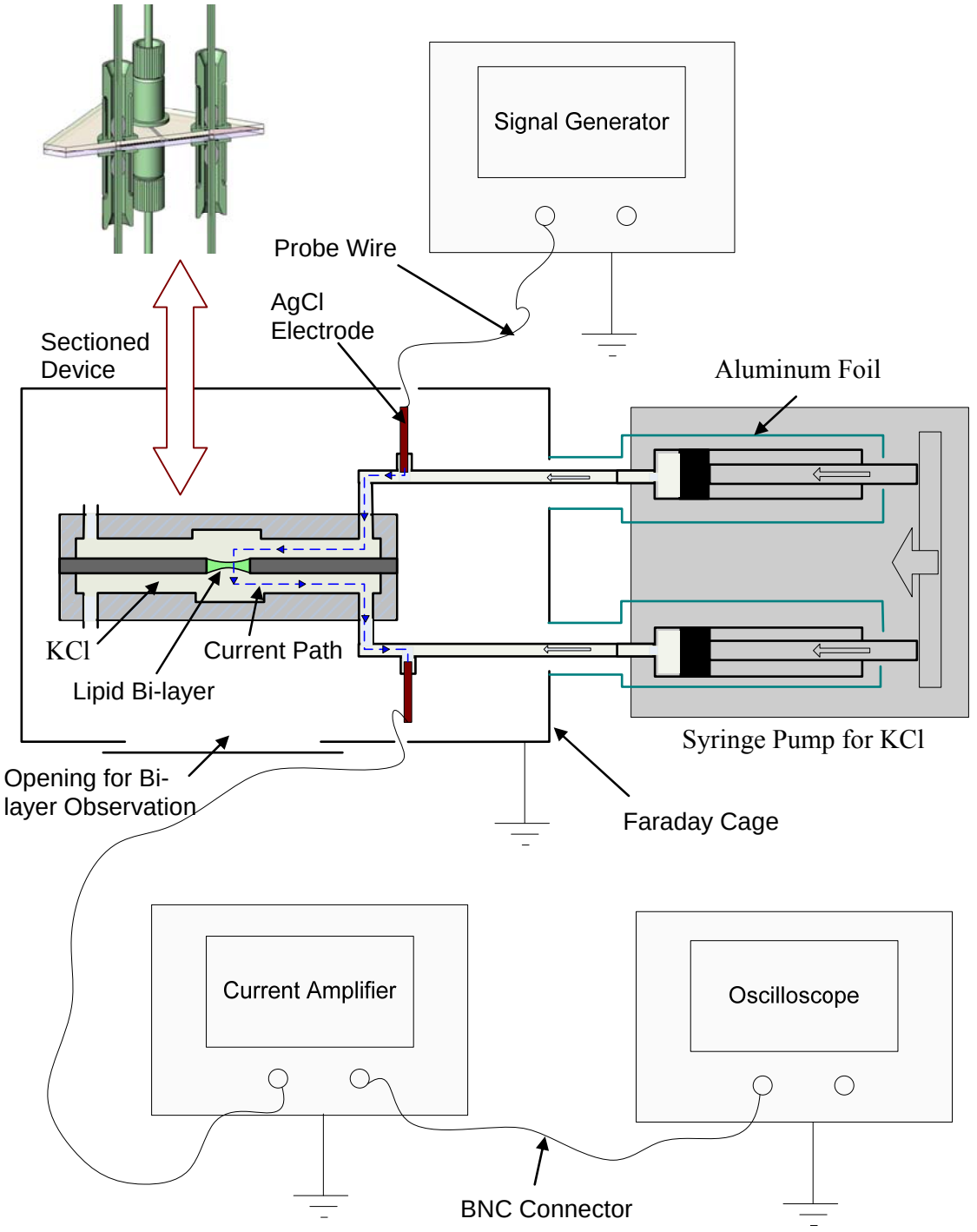

Figure 53: Schematic diagram of the apparatus with microfluidic device. The section view along the channel carrying KCl is shown (not to scale). Lipid bi-layer is shown to provide a better understanding to the reader

electronic equipments in the laboratory. Other source of noise was the electronic equipments themselves. A sharp signal of 60Hz was introduced into the measurement system. Even though it would have been possible to remove this knows noise signal later on with digital signal processing (DSP) tools, this signal hindered the visual monitoring, which was vital for the manually performed data capturing. Therefore, a high-pass filter at 1kHz was imposed on the system using the options available on the current amplifier. This filtered the 60Hz high amplitude system noise, and allowed 1kHz experiment signal with high frequency low amplitude noises into the system. Therefore, the signal observed on the oscilloscope had a fuzzy form. During the processing of the captured data by using a band-pass filter only the source frequency (1kHz) signals were extracted.

The Ag/AgCl electrodes were inserted into tubing sleeves (F-244X, Slv FEP Nat 1/16 × 0.021, Upchurch Scientific inc., WA) so that they can be tight fit into NanoPorts or T-joints. Connection of electrodes into separate NanoPorts was tested but was unsuccessful due to a long current path through KCl in a micro-channel other than the ones used for directly pumping KCl. Removal of pentane and lipids from micro-channels (not in the KCl flow path) was very slow and were prone to trap air bubbles. Introduction of T-joints (P-632, Tee Assy Tefzel 1/16in – 0.020 thru, Upchurch Inc., WA) into the KCl tubing just before the NanoPort for mounting the electrodes resolved the problem (Figure 54). However, care had to be taken to ensure that the electrodes were in contact with the KCl flow.

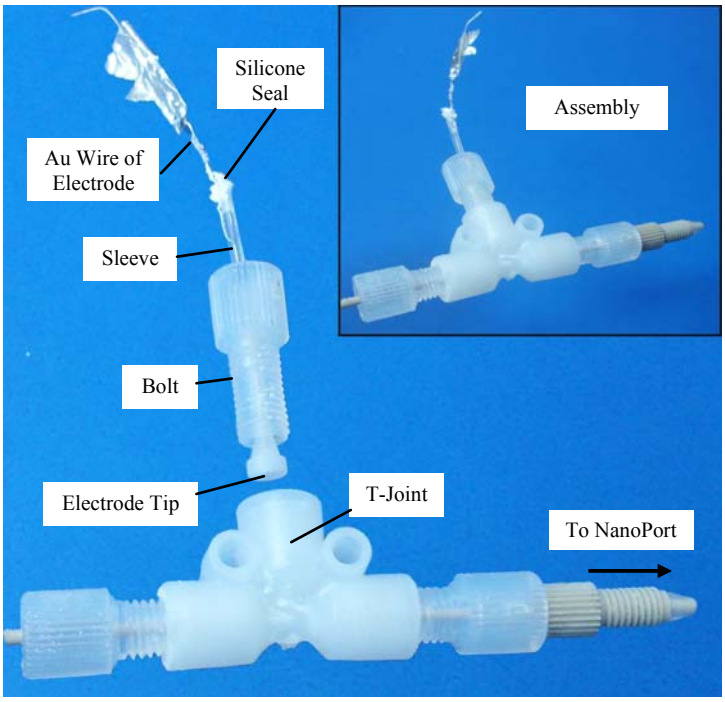

Figure 54: Use of a T-joint to connect the electrode into the KCl flow

4.2 Preparation for the Experiment

Microfluidic device was cleaned by pumping DI water through the channels at a higher rate, at about 10 ~ 15 µl/min, for about 5 minutes. If the glass wafers were heavily contaminated with a KCl powder coating then the clamp was taken apart and the glass wafers were cleaned. Device was dried first by exposing to compressed air flow and then keeping under a table lamp for a couple of hours.

Two large paper clips were used to hold the device in the vertical position as illustrated in Figure 55 and Figure 56. This was essential for pumping in pentane and analytes from both sides simultaneously, and for maintaining similar conditions on both

sides. Channels used for pumping KCl were kept vertically to reconstruct conventional folding method, even though a novel method been adopted. However, it might not be required for this method as lifting of monolayers is not involved in this procedure.

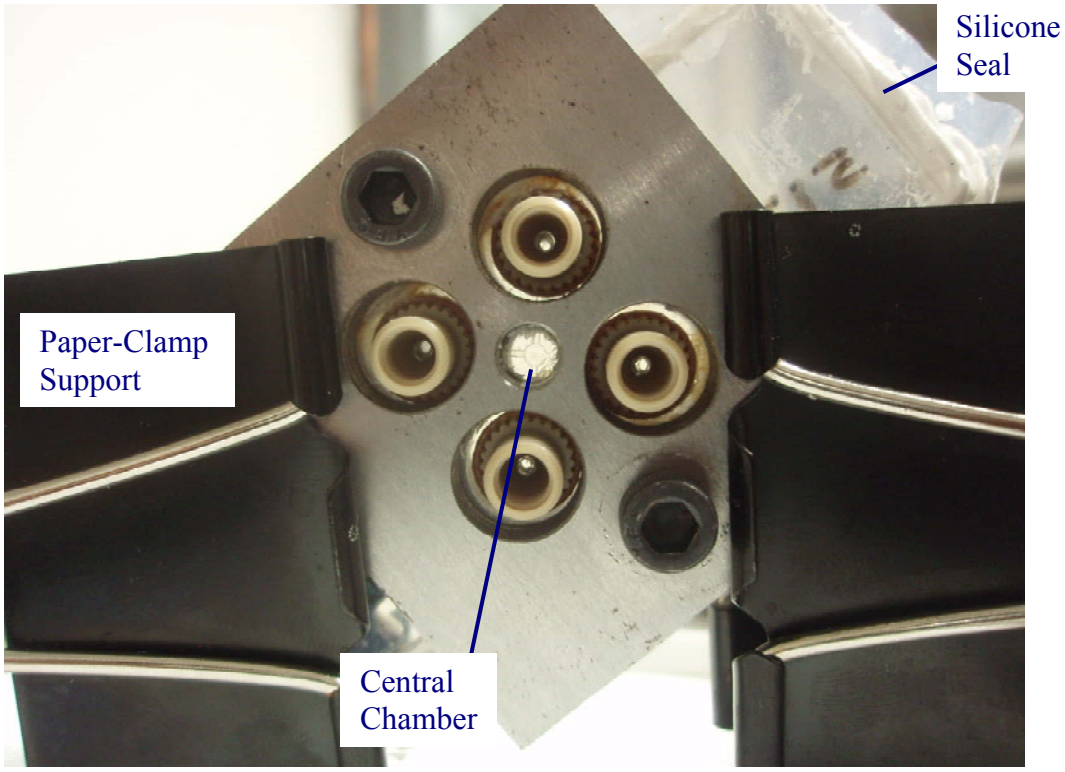

Figure 55: Microfluidic device held using paper clips (aperture is visible)

Microfluidic device was placed on a sheet of silicone (of orange color in Figure 56) inside the Faraday cage. Silicone sheet served several purposes, namely, electrically isolating the device from the grounded Faraday cage to avoid short circuit of current if KCl leakages occurred, providing mechanical damping and protecting Faraday cage surface from corrosion induced by KCl. The Faraday cage (which serves the purpose of

electromagnetic isolation of the device from the surrounding) was placed on a table with tuned damping (RS2000, Avewport). Between the table and the Faraday cage a layer of packaging foam (light blue color material in Figure 57) was employed to provide further mechanical damping.

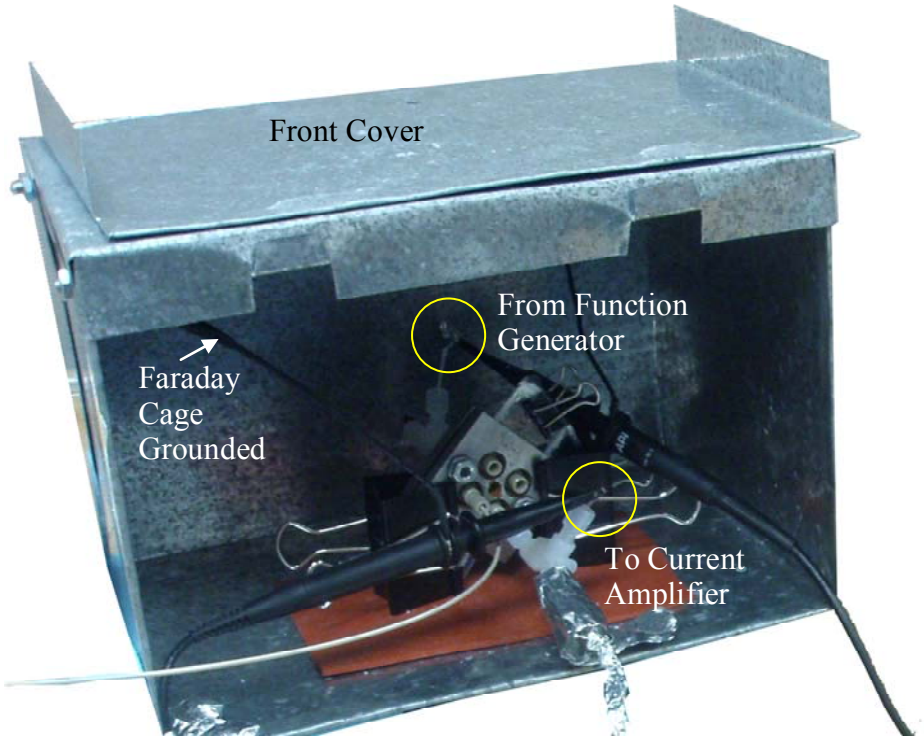

Figure 56: Microfluidic device inside the Faraday cage

Meticulous planning was necessary before performing the lipid bi-layer formation experiment to avoid any mechanical impacts during the operation. All the tube connections had to be checked before starting the experiment to avoid mechanical interference and to prevent air bubble formation in the micro-channels by air infiltration. However, Pentane mixing with KCl at low concentrations was observed, which reduced

the electric conductivity of KCl. Syringe pumps were placed on a separate platform so that the only connection between the pumps and the device was the tubing. The experimental setup is shown in Figure 56, Figure 57 and Figure 58.

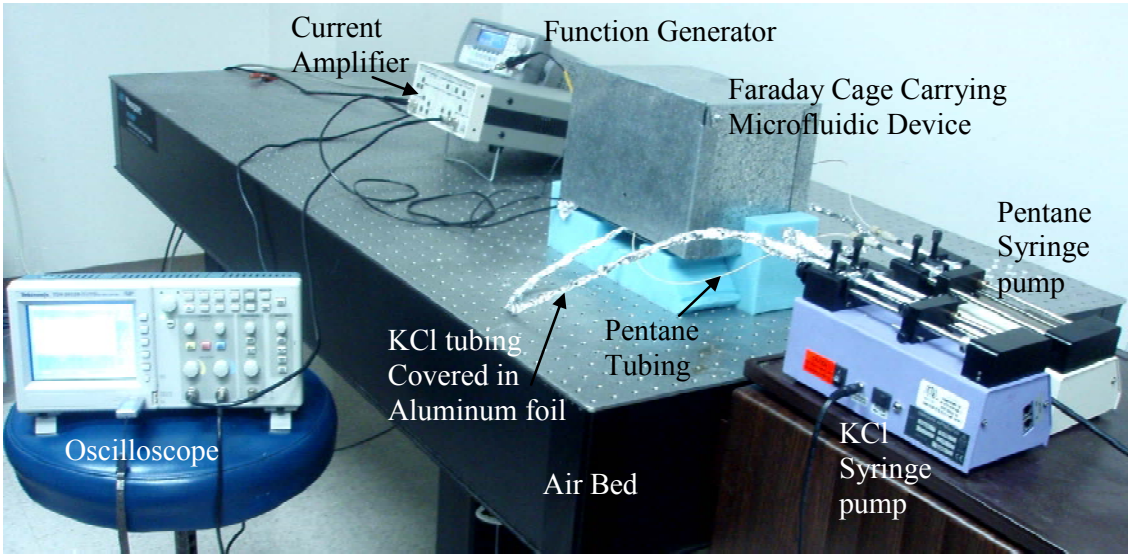

Figure 57: Experiment setup

1M KCl buffer solution was prepared by dissolving 74.55g of KCl powder in 900ml of DI water and then increasing the solution volume to 1000ml by adding more water. The solution was stirred for on a stirrer for about 20 minutes until KCl powder was entirely dissolved. The solution was stored at room temperature. Two 1ml syringes were fully filled with 1M KCl and connected to PEEK^{TM} tubing with 10µm internal diameter (1531, Upchurch inc., WA) via adaptors (P-659, Upchurch Inc., WA). These two 2.5 feet long tubes had two T-joints connected at the other end carrying the AgCl electrodes (section 4.1). Two syringes and the connected tubing were completely

covered by wrapping an aluminum foil (Figure 56 and Figure 57) for magnetic noise isolation. Syringes were mounted on a syringe pump (model Pico Plus) and the pistons were pushed to force KCl to fill up the entire tubing length. After making sure that the two pistons are equally in contact with the plunger of the syringe pump the tubing was connected to the NanoPorts. Plugs (P-551, Col Plug PEEK Natural 10-32, Upchurch Inc., WA) were used to close unused NanoPorts of Pentane channels. Only the top NanoPorts (i.e. of KCl channels) were used as outlets.

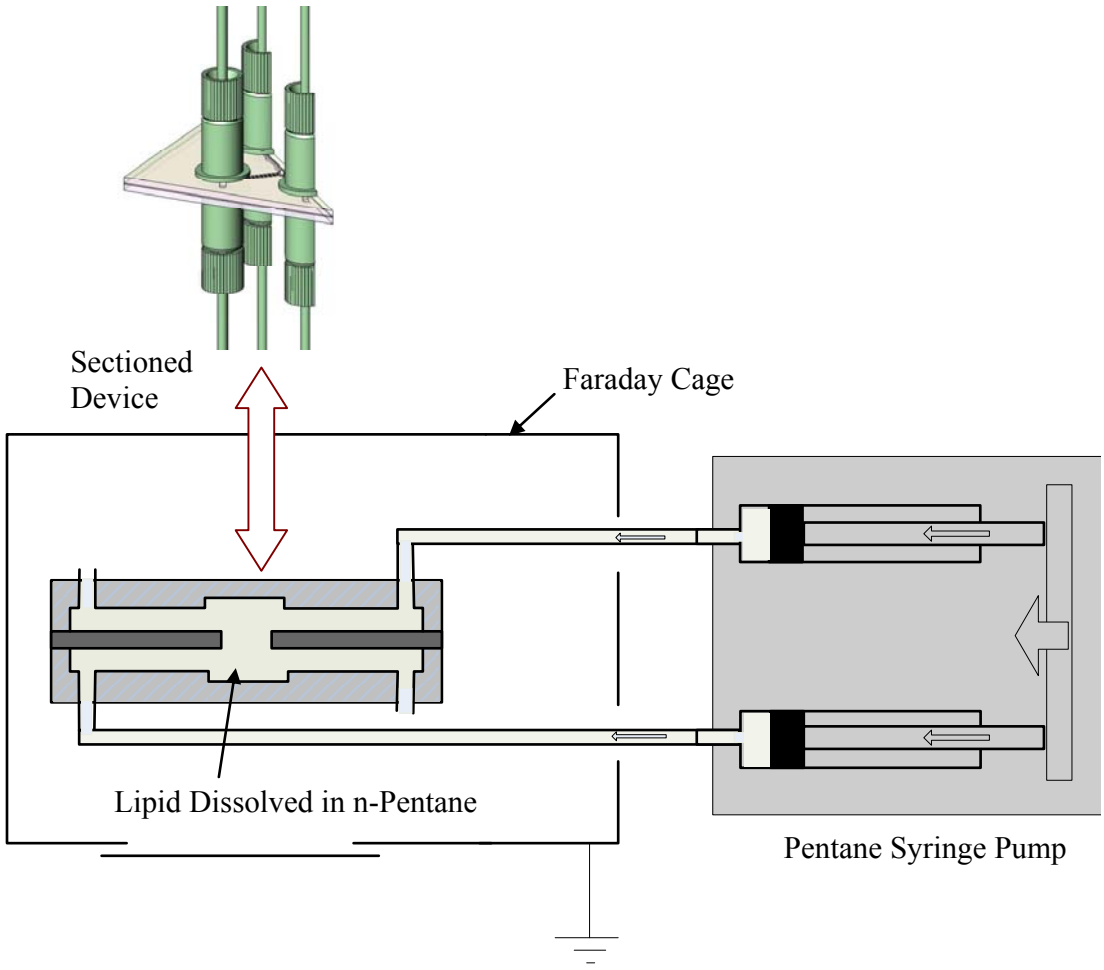

Figure 58: Schematic diagram of the apparatus with microfluidic device. The section view along the micro-channel carrying Pentane is shown (not to scale)

12% DPhPC lipid (Table 6) in n-pentane was prepared by dissolving 12mg of DPhPC (initially stored at -20°C) in 100ml of n-pentane at the room temperature. About 0.2 ml of Pentane (with lipid) was filled into each of the two 1ml syringes. After connecting syringes to PEEK^{TM} tubing with 10µm internal diameter via adaptors and mounting on a syringe pump (model 11), syringe pistons were pushed the same way as with KCl until each syringe was left with 0.1ml pentane and the pistons are balanced on the plunger. Tubing was connected quickly to NanoPorts as pentane tended to evaporate rapidly. It was important to connect Pentane to the device just before starting of the experiment to avoid evaporation of pentane into the micro-channels.

Table 6: Data of the used chemicals

Compound	Commercial Name	Supplier
Lipid (powder)	DPhPC (1,2-diphytanoyl-sn-glycero-3-phosphatidylcholine)	Avanti Polar Lipids, Inc
KCl (Powder)	KCl	VWR international, PA
n- Pentane	n-pentane	Sigma Aldrich, MO

Function generator, current amplifier and oscilloscope were connected (as explained in section 4.1). A detailed description of the electronic measurement system can be found in section 4.1.

4.3 Experimental Procedure

The experimental procedure starts with filling of the micro-channels with buffer KCl so that the current path is established and the glass walls are properly wetted for a smooth flow of KCl later on. A flow rate of about 5µl/min was maintained for about 5minutes until a clear signal can be viewed on the oscilloscope. A 50mV sinusoidal signal with a high frequency of 1kHz was generated by the function generator. The main reason for selecting a high frequency was to enable filtering the low-frequency high-amplitude system noise by using a high-pass filter in the current amplifier. However, high frequency low amplitude noise was detected in the output signal from the current amplifier (Figure 59).

Then 0.5ml of Pentane was pumped at 0.1ml/hour (1.67µl/min) rate into the horizontal channels on both sides, from holes at opposite ends (Figure 58). With this approach it was expected that the lipid-pentane solution wetting the Teflon sheet would meet at the aperture by completely covering it. If pentane were pumped at the same end on the both sides the aperture would not be covered completely. The high pumping rate was used to reduce the required negative pressure (as described in section 2.2). As Pentane was pumped the current signal was observed to fade off to a very low amplitude signal, and was almost (or completely) hidden in the low-amplitude high-frequency noise (Figure 60). About 15minutes was allowed for the pentane to vaporize leaving lipid in the channel. Next KCl buffer pumping started with the intention of flushing off excessive lipids from the channel, especially, from the aperture. Initially KCl was

pumped at around 2µl/min for about 20 minutes and then at 0.2µl/min till the end of the experiment.

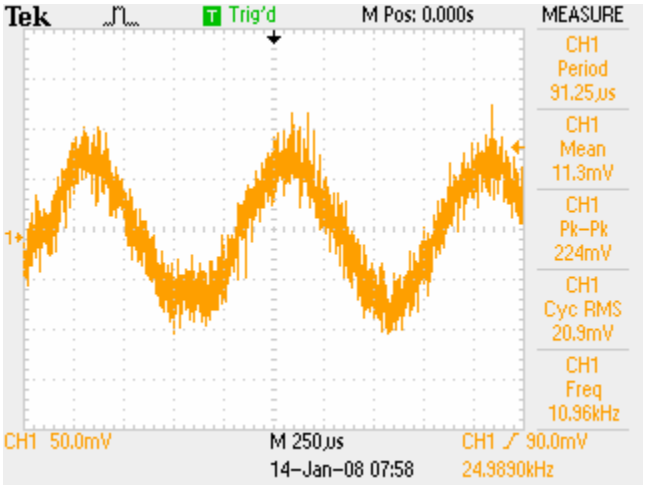

Figure 59: Signal observed when only KCl is present (Input voltage = 50mV; Current amplifier setting = 1Pa/1V)

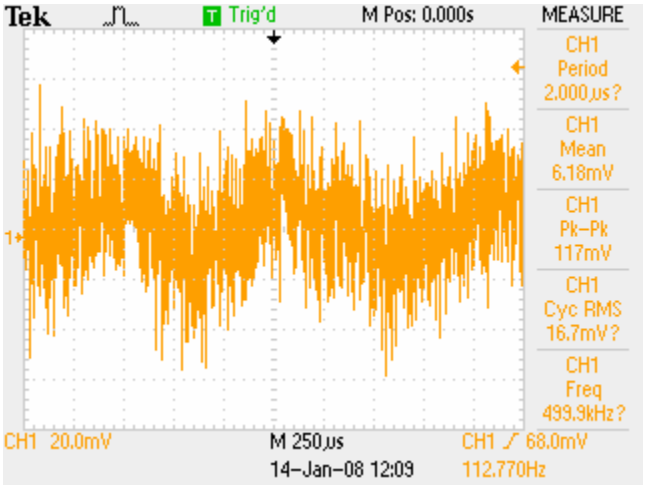

Figure 60: Signal with noise observed after pumping of pentane (Input voltage = 50mV; Current amplifier setting = 1Pa/1V)

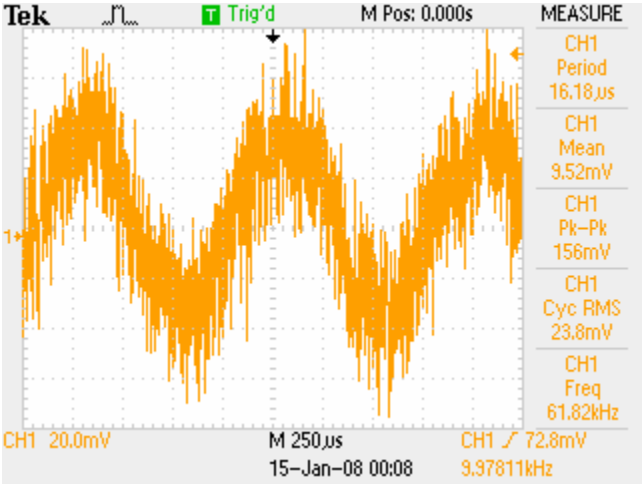

Figure 61: Stabilized signal with noise observed after pumping of pentane (Input voltage = 50mV; Current amplifier setting = 1Pa/1V)

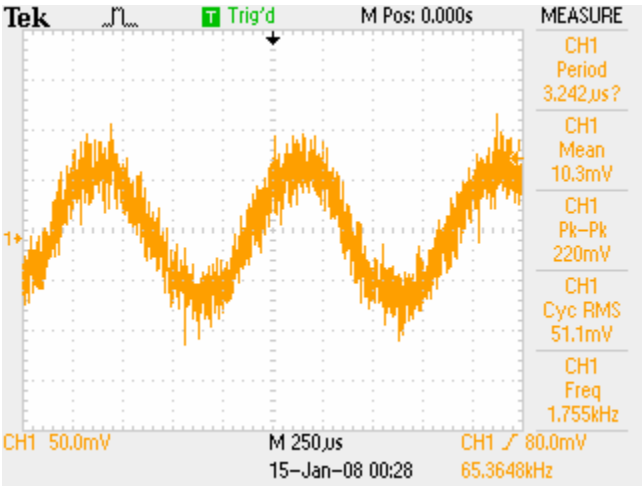

Figure 62: Signal observed after breaking of lipid bi-layer (Input voltage = 50mV; Current amplifier setting = 1Pa/1V)

After some time the signal Formation of lipid bi-layer was verified by analyzing the signal to calculate the resistance across the aperture (section 4.1). A typical signal at this stage is shown in Figure 61. After about 20 minutes the signal was observed to

suddenly increase (Figure 62) to the initial magnitude recorded at the beginning with KCl alone (Figure 59). This was recognized as the break down of the lipid bi-layer and the experiment was concluded.

4.4 Results

Since continuous recording was not possible, time-discrete measurements were taken manually, initially at close time intervals, then at 15minuted intervals and finally at hourly intervals. From the successful experiments it was observed that the time required for formation of bi-layer ranged from 8 hours to 15 hours. It took about 20minutes for the lipid bi-layer to break.

The observed voltage profile representing the variation of current through the aperture was fitted into the expected voltage variation (shape), and is shown in Figure 63. The voltage used here is filtered for noises as described in section 4.5. The expected shape is not quantified based on empirical data but scaled to fit into the observed data. This voltage captured by the oscilloscope can be converted into the corresponding current by multiplying by the current amplifier sensitivity reading (1 pA/V for Figure 63).

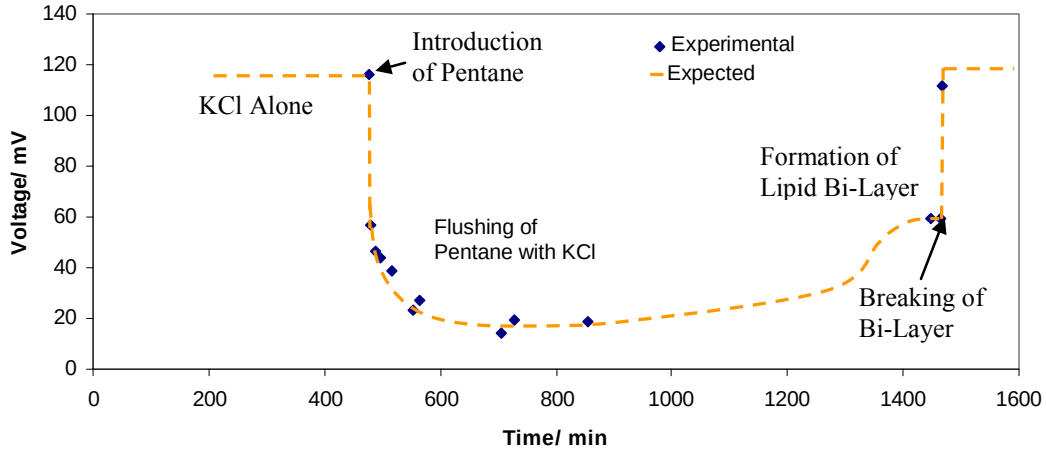

Figure 63: Expected and observed voltage variations (Input voltage = 50mV; Current amplifier setting = 1pA/1V)

At the beginning of the experiment with KCl buffer alone, highest current level was expected across the aperture due to high conductivity of KCl, which occupied the aperture. With the introduction of n-Pentane, conductivity along the current path was supposed to reduce drastically allowing a very low current across the aperture. With the flushing of pentane by pumping KCl, conductivity of the buffer medium was anticipated to increase gradually with the removal of dissolved pentane and lipids. After some time only lipid presence in the current path was expected at the aperture and the lipid bi-layer formation was supposed to commence. During the lipid bi-layer formation current was expected to increase relatively faster in a manner similar to inverse exponential variation and finally settle at a certain value. At this stage the lipid bi-layer was supposedly formed. Breaking of the lipid bi-layer results in sudden increase of the current through

the aperture to the value observed when only KCl was present in the beginning of the experiment.

The resultant current across aperture was used to calculate the resistance across the aperture and by comparing the resistance with conventional values formation of the lipid bi-layer was verified. Table 7 lists the current values (after noise filtering) observed when KCl alone was present and when the lipid bi-layer was supposedly present. The accuracy of amplifier was 0.5% (or for sensitivity of 1pA/V variation was ±5fA) and the accuracy of the function generator was ±1mV (i.e. 2% for 50mV).

Table 7: Summery of current measurements

Stage	**Experiment 1**	**Experiment 2**
KCl Alone	0.112 pA	0.138 pA
Lipid Bi-Layer Expected	0.060 pA	0.046 pA

4.5 Processing and Interpretation of Results

As explained earlier the high frequency low amplitude noise was not filtered in the electronic measurement system during the experiment. Therefore, the captured data had to be filtered for high frequency (> 1kHz) noise. For Digital Signal Processing (DSP) SPTool in MATLAB was utilized. A low-pass filter with the specifications given in Figure 64 was used to filter the current measurements. A detailed description of DSP using SPTool is given in Appendix A.

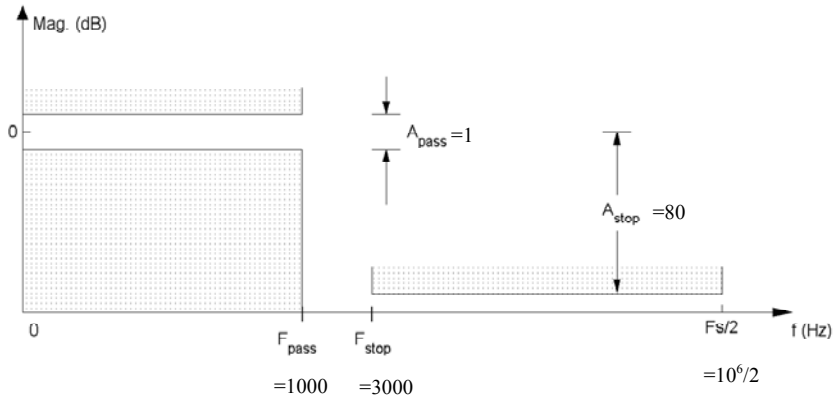

Figure 64: Low-pass filter specifications

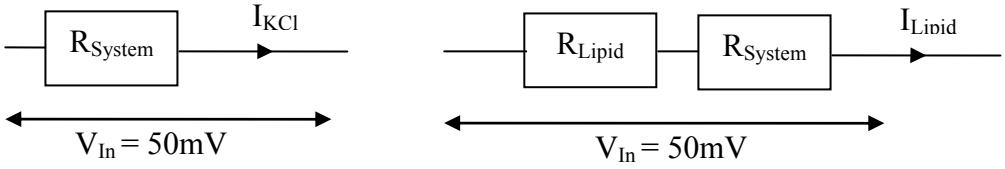

Figure 65: Model for resistance calculation

Resistance was calculated based on the model shown in Figure 65. The accuracy of the resistance calculations based on the accuracies of the function generator and the current amplifier is ± 2.5%. Calculated resistances were multiplied by aperture area assuming lipid bi-layer has the same area. Results are listed in Table 8.

Table 8: Resistance results

Stage	**Experiment 1**	**Experiment 2**
KCl alone	447.8 ±11 GΩ	362.3 ± 9 GΩ
Lipid Bi-Layer Expected	838.5 ± 21 GΩ	1087.0 ± 27 GΩ
Resistance of Bi-Layer[4]	390.7 ±10 GΩ	724.6 ±18 GΩ
Specific Resistance[5]	1726 ± 43 Ω.m^2	3201± 80 Ω.m^2

When comparing resistance by area value (specific resistance) for the bi-layer resulted from the experiments (Table 8) and extracted from other literatures (650 $\Omega.m^2$), the experimental values seem to be three times and five times the values from other sources. This might be due to several possible reasons:

1. Having a smaller effective bi-layer area than the area of the aperture (due to edge effect)
2. Change in conductivity of lipid due to entrapment of pentane
3. Measurement errors

Due to the curvature of the lipid bi-layer near the edge thinning is restricted to the central part of the aperture. This edge effect is dominant for smaller diameter apertures and thicker Teflon sheets. To find the real effective area observation with a microscope can be performed (Hanke and Schlue 1993). With the available experiment setup this is not possible as for this purpose a special Faraday cage, which can facilitate a microscope, is required. Further, not to disturb the highly sensitive lipid bi-layer a special arrangement is required for an observer to view through the microscope without touching it. This might be possible if the microscope can capture and directly feed the pictures of the bi-layer into a screen. Use of thinner Teflon sheets and apertures with larger diameters is a possible way of reducing the edge effect. However, if to use a thinner Teflon sheet and a large aperture for lipid bi-layer formation, the quality of the aperture has to be very good as both will reduce the robustness of the aperture to facilitate a nano-scale film. With punching method this level of quality cannot be achieved. If pentane has been contaminated with pentane, the conductivity of pentane is

expected to reduce form its nominal value. However, there is no any easy method for the estimation of conductivity change of lipid due to mixing with n-pentane.

Short lifetime of the lipid bi-layer might be mainly due to the low quality of the aperture on the Teflon sheet. Another prominent factor behind this might be pulsation of the KCl flow due to stepper motor pulses in the syringe pump. Since the measurement uncertainty of current is only 0.5% the measurement errors are less likely to cause such a big discrepancy between observed values and values reported in the literature.

5. CONCLUSION AND FUTURE DIRECTIONS

Conclusions drawn from the study and the opportune areas based on the results of this study are listed in the following sections.

5.1 Conclusion

A novel microfluidic device for synthesis of lipid bi-layer was developed with borosilicate glass wafers and a Teflon sheet, and the lipid bi-layer synthesis was performed using a novel approach of continuous buffer flow. However, further testing might require for the verification of the experimental results as the specific resistance observed for the bi-layer was about three to five times the value given in other literature. A closed system by design, the new device of the size 49 × 45 × 6 mm is portable and easy to handle. The novel process can be automated and, together with the device, is suitable for outer-space applications.

The device was designed to miniaturize and automate the artificial planar bi-layer formation. The developed microfluidic flow model suggested a tradeoff between the flow control and miniaturization; for low operation pressures deeper channels were preferred but that would increase the amount of analyte usage. Further, flow rates for buffer and Pentane were established to ensure a laminar flow using the flow model. The fabrication process was optimized by selecting and refining various applicable fabrication methods at each stage of the development of the device. 1:1:10 of 49% of HF: HCl: BOE (50:1) was found to be a moderate borosilicate glass etchant. SU8 50

photoresist was not suitable as etch mask for etching Pyrex. The quality of the device against the cost and time were considered when designing and selecting the fabrication methods; even though the metal masks gave better features, its cost was not justifiable. The experiment measurement setup was designed to capture pico scale current signals. Four major areas of study were addressed in this study: Biophysics, Microfluidic, Microfabrication techniques and Electronic Measurements.

5.2 Future Directions

For verifying the experimental results the apparatus for burning quality apertures on Teflon using a high voltage spark can be implemented. With a quality aperture performance of the device can be expected to improve significantly; high flow rates and hence short bi-layer formation time might be possible; more stable bi-layers might be achieved. Use of better photoresist masks and thicker metal masks, which can give better features while withstanding strong etchants, might be another area to explore to remove channel depth barrier. Use of anisotropic dry etching of Pyrex will provide benefits of superior surface quality and strength of Pyrex to the device. Use of pulseless syringe pumps would be a possible way of improving the procedure. Hardware notch filter at 60Hz will be a good option for filtering high amplitude system noise. Hence instead of using a high-pass filter, a low-pass filter can be applied from the current amplifier. Finally, membrane protein experiments can be performed using the device.

NOTES

1) Final height selected for the device.
2) Directly taken from the reference.
3) Derived from the data given in the reference.
4) Resistance across the aperture. bi-layer was supposedly present.
5) Only the accuracy of resistance is considered.

REFERENCES

Bachman M (2000) Glass etch wet process. INRF Application notes, Retrieved 18:37, May 10, 2007, from <http://www.ampel.ubc.ca/nanofab/index.html#Documents>

Bien D, Rainey P, Mitchell S, Gamble H (2003) Characterization of masking materials for deep glass micromachining. J. Micromech. Microeng. 13:34-40

Brown M F (1996) Membrane structure and dynamics studies with NMR spectroscopy. In: Merz K Jr., Roux B (ed) Biological membranes, Birkhäuser, Boston.

Ciprian I, Francis E, Tay A, Jianmin M (2007) Strategies in deep wet etching of Pyrex glass. Sensors and Actuators A 133 (2007) 395–400

Corman T, Enoksson P, Stemme G (1998) Deep wet etching of borosilicate glass using an anodically bonded silicon subtrate as mask. J. Micromech.Microeng. 8:84-87

Darling R B, Negative photoresist - Tutorials for EE-527. Center for Applied Microtechnology, Department of Electrical Engineering, University of Washington, Retrieved 17:05, June 23, 2007, from <http://www.ee.washington.edu/research/microtech/cam/PROCESSES/NEWtutorial.html>

Darling R B, Photolythography - Tutorials for EE-527. Center for Applied Microtechnology, Department of Electrical Engineering, University of Washington, Retrieved 17:02, June 23, 2007, from <http://www.ee.washington.edu/research/microtech/cam/PROCESSES/NEWtutorial.html>

Darling R B, Positive photoresist - Tutorials for EE-527. Center for Applied Microtechnology, Department of Electrical Engineering, University of Washington, Retrieved 17:04, June 23, 2007, from <http://www.ee.washington.edu/research/microtech/cam/PROCESSES/NEWtutorial.html>

Euclid Research, Stepper Motor Dynamic Analyzer. San Jose, CA, Retrieved 14:25, Nov 26, 2007, from <http://www.euclidres.com/apps/stepper_motor/stepper.html>

Funakoshi K, Suzuki H, Takeuchi S (2006) Lipid bilayer formation by contacting monolayers in a microfluidic device for membrane protein analysis. Anal. Chem. 78: 8169-8174

Goodfellow Corp., PA, Polytetrafluoroethylene PTFE, Retrieved 11:25, July 13, 2007, from <http://www.goodfellow.com/csp/active/static/A/Polytetrafluoroethylene.html>

Guerin L J, SU8 Homepage, Retrieved 10:15, June 24, 2007, from <http://www.geocities.com/guerinlj/>

Hanke W, Schlue W R (1993) Planar lipid bilayers methods and applications. In: Sattelle D B (ed) Biological techniques: A series of practical guides to new methods in the modern biology, Academic Press, New York.

Jia Z, Fang Q, Fang Z (2004) Bonding of glass microfluidic chips at room temperatures. Anal. Chem. 76: 5597-5602

Kang X, Cheley S, Allison C, Rice-Ficht A, Bayley H (2007) A storable encapsulated bilayer chip containing a single protein nanopore. Journal of American Chemical Society, 129: 4701 – 4705.

Kang X, Gu L, Cheley S, Bayley H (2005) Single protein pores containing molecular adapters at high temperatures. Wiley-VCH 69451 Weinheim, Germany

Kelly J, Philipsen H (2005) Anisotropy in the wet-etching of semiconductors. Solid State and Materials Science 9: 84–90

Kelly R T, Woolley A T (2007) Microchip capillary electrophoresis systems for DNA analysis. In: Wang W, Soper S A (eds) Bio-MEMS technology and applications, CRC Press, New York.

Li P C H (2006) Microfluidic lab-on-a-chip for chemical and biological analysis and discovery, Chromatographic Science Series, Vol. 94, Taylor & Francis Group, New York

Malmstadt N, Nash M A, Purnell R F, Schmidt J J (2006) Automated formation of lipid-bilayer membranes in a microfluidic device. Nano Letters, 6.9: 1961-1965

Matsuzawa T, Mniwa A, Hasegawa N, Sunami H (1987) Two-dimensional simulation of photolithography on reflective stepped substrate. IEEE Trans. CAD 6-3:446-451

McGeer P and Duus H (1952) Effect of pressure on the melting point of Teflon tetraflluroethylene resin. The Journal of Chemical Physics 20: 1813-1814

MicroChem, NANO^{TM} SU8 negative tone photoresist formulation 50-100, Retrieved 13:04, June 24, 2007, from <http://www.microchem.com/products/su_eight.htm>

Mourzina Y, Steffen A, Offenha¨usser A (2005) The evaporated metal masks for chemical glass etching for BioMEMS. Microsystem Technologies 11:135–140

Peterman M, Ziebarth J, Braha O, Bayley H, Fishman H and Bloom D (2002) Ion channel and lipid bilyaer membranes under high potentials using microfabricated apertures. Biomedical Microdevices 4.3: 231-236

Resnick P, Buck W (1999) Teflon®AF: A family of amorphous fluoropolymers with extraordinary properties. In: Hougham *et al.* (ed) Fluoropolymers 2: Properties, Plenum Press, New York

Schmitt E, Vrouenraets M, Steinem C (2006) Channel activity of OmpF monitored in Nano-BLMs., Biophysical Journal, 91: 2163–2171

Singer S J, Nicolson G (1972) The fluid mosaic model of the structure of cell membranes. Science 175.4023: 720- 731.

Stouch T R, Bassolino D (1996) Movement of small molecules in lipid bilayers: molecular dynamics simulation studies. In: Merz K Jr., Roux B (eds) Biological membranes, Birkhäuser, Boston.

Suzuki H, Tabata K, Kato-Yamada Y, Noji H and Takeuchi H (2004) Planar lipid bilayer reconstitution with a microfluidic system. Lab Chip 4:502 – 505.

Tu Y, Lin Y, Yantasee W, Ren Z (2005) Carbon nanotubes based nanoelectrode arrays: fabrication, evaluation, and application in voltammetric analysis. Electroanalysis, 17.1: 79-84

Zheng Z., Cheng W., Huang F. and Yan B. (2007) 3D Microstructuring of pyrex glass using the electrochemical discharge machining process. J. Micromech. Microeng. 17: 960–966

Zhuang D, Edgar J (2005) Wet etching of GaN, AlN, and SiC: a review. Materials Science and Engineering R 48:1–46

APPENDIX A

SIGNAL PROCESSING PROCEDURE

The DSP procedure for application of digital signal filters to existing datasets using MATLAB SPTool is as follows. Demonstration is carried out using MATLAB 7.4.0 (R2007a) on Windows Vista™ Enterprise Edition.

1. Starting SPTool

MATLAB application can be opened by selecting MATLAB icon from the start menu.

SPTool window can be opened by typing ‘sptool’ in MATLAB command window.

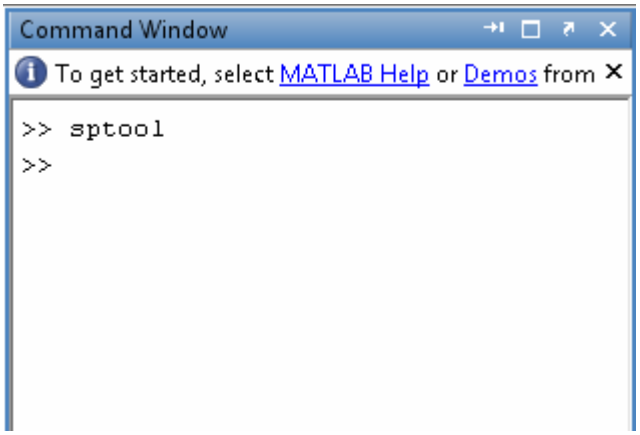

Figure 66: MATLAB command window

The SPTool will appear as below:

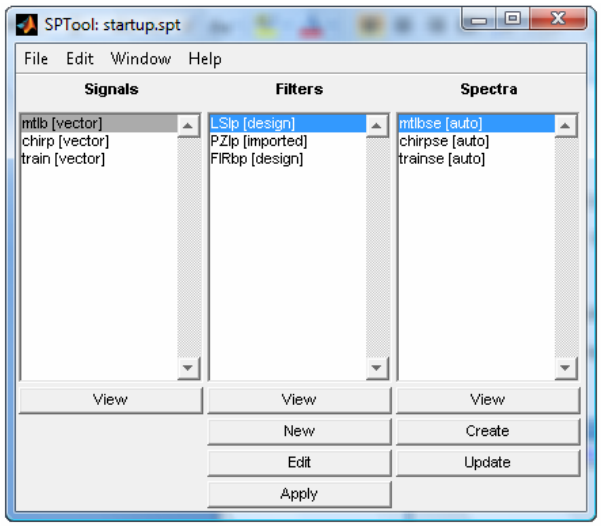

Figure 67: SPTool window initial view

2. Designing a Filter

A new filter can be designed using 'New' button under Filters in the SPTool window. For example a Filter can be created with the name 'LP_Filter'.

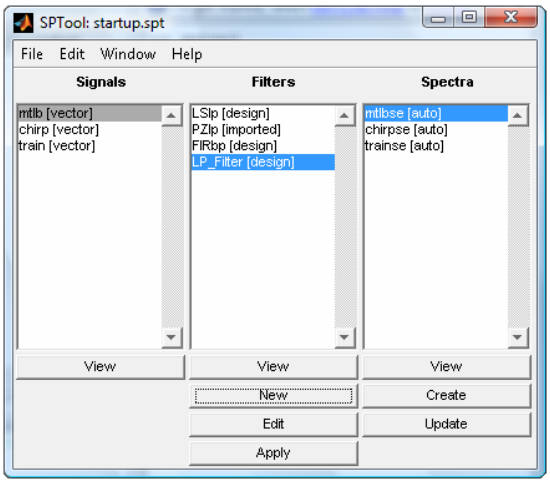

Figure 68: SPTool window: creating a new filter

LP_Filter can be configured by selecting LP_Filter [design] from Filters field and pressing 'Edit' button under Filters in SPTool window. The Filter Design and Analysis Tool window will appear.

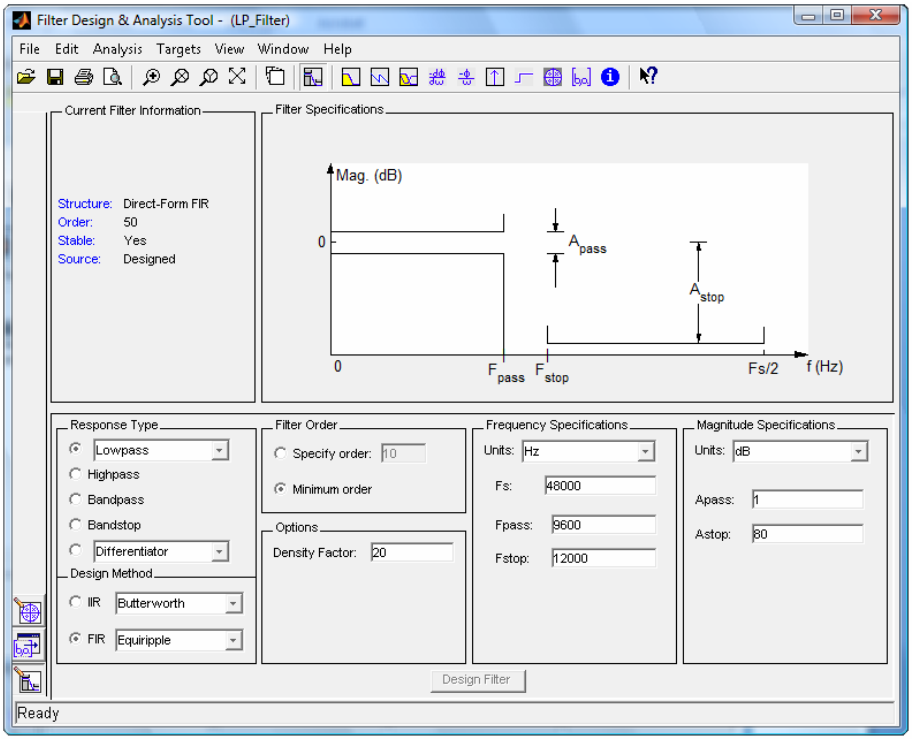

Figure 69: Low-pass filter design specifications in Filter Design and Analysis Tool

To design a low-pass filter Response Type has to be set to Lowpass. Sampling frequency has to be specified in the filed against Fs. Sampling frequency is the frequency at which data are captured. In other words inverse of the time between two data points in the time data series to be processed. F_{PASS}, the highest frequency to be pass through the filter, A_{PASS}, the signal amplitude ratio range in dB at frequencies below F_{PASS}, F_{STOP}, the lowest frequency that should be filtered, and A_{STOP}, the

amplitude ratio range in dB after F_{STOP}, have to be defined. When the Design Filter button is pressed MATLAB will designed the Filter. The low-pass filter used in the report will look as shown below:

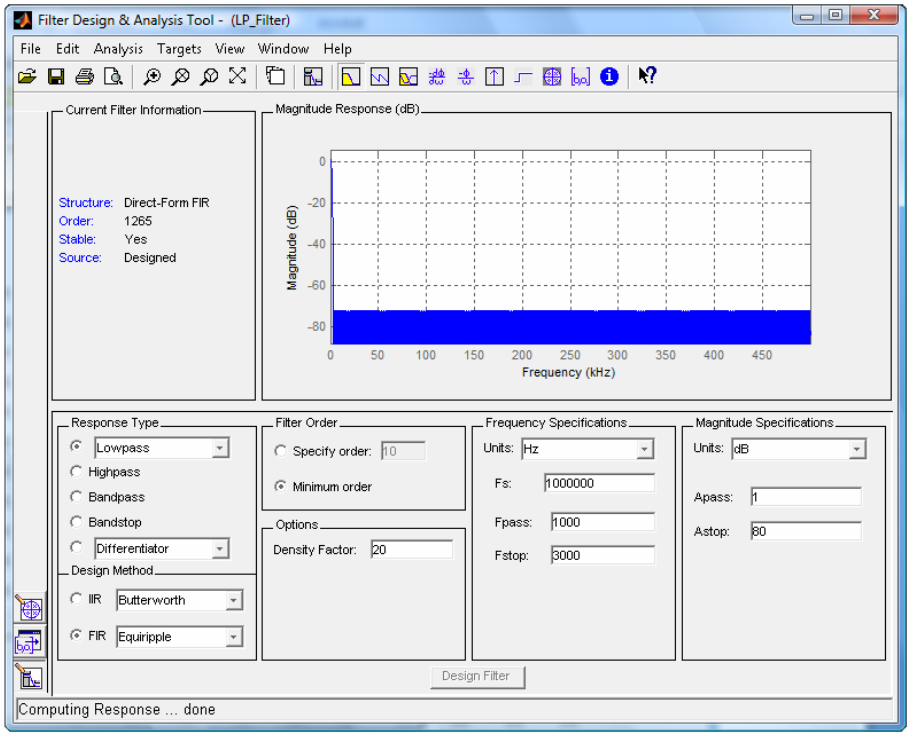

Figure 70: Designed low-pass filter in Filter Design and Analysis Tool

Using the 'View' button under Filters in SPTool window, a selected filter can be viewed as follows:

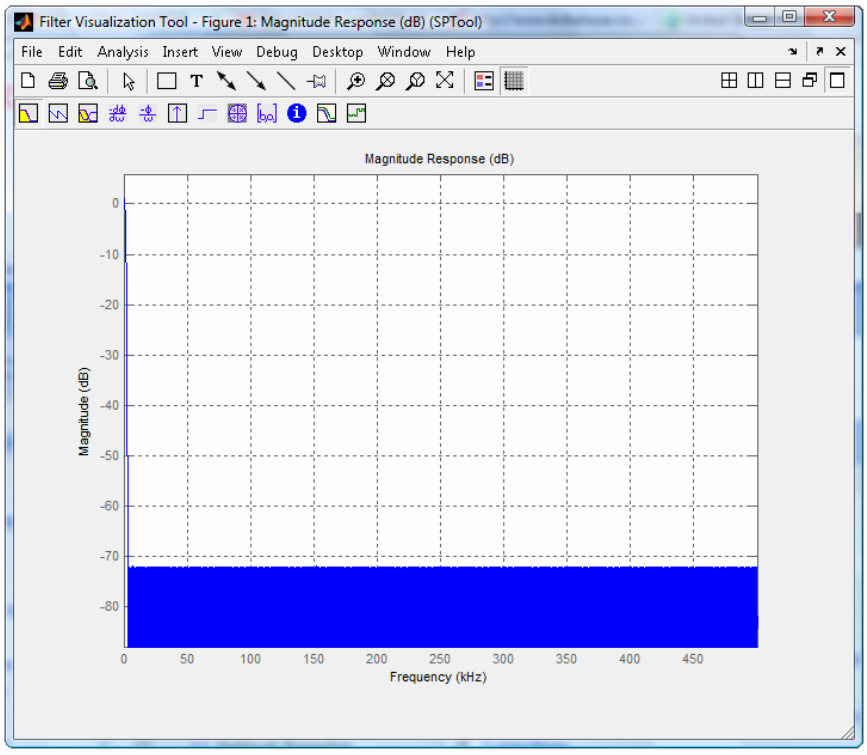

Figure 71: Visualization of low-pass filter

3. Importing a Time Data Series

Time data series to be processed can be imported into MATLAB workspace as a column matrix. To import a dataset from a Microsoft Excel sheet by selecting 'Import Data…' from File drop down menu on the MATLAB window.

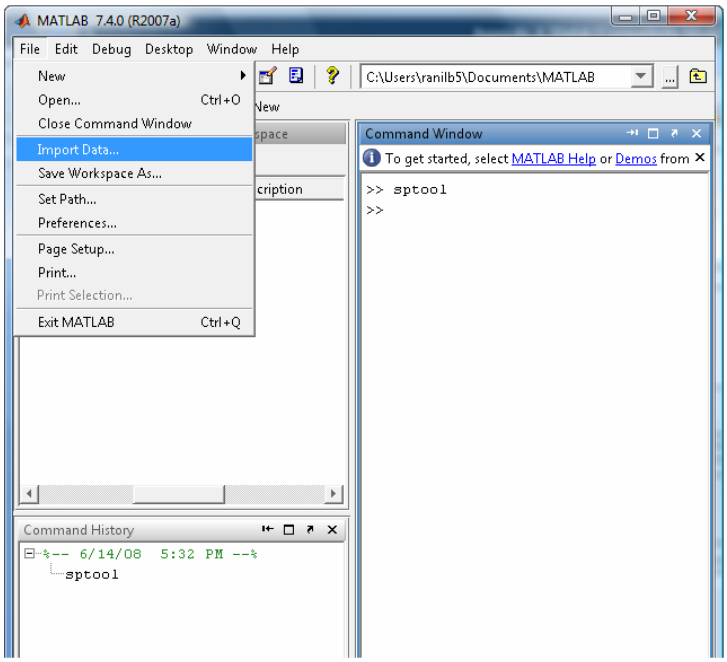

Figure 72: Import data option in MATLAB main menu

The file to be open can be browsed using the Import Data window that appears.

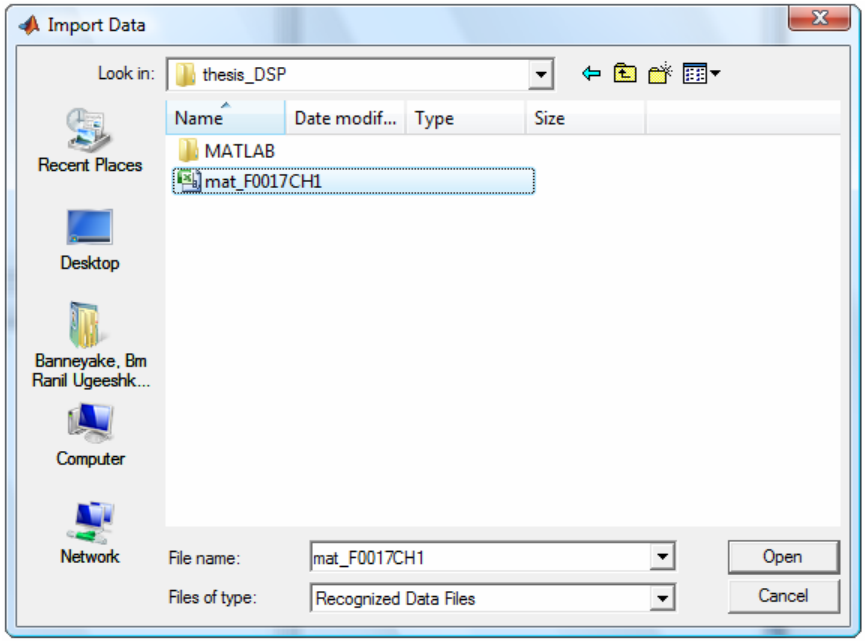

Figure 73: Import data browser

By pressing the ‘Open’ button after selecting the file to be open, the Import Wizard can be prompted.

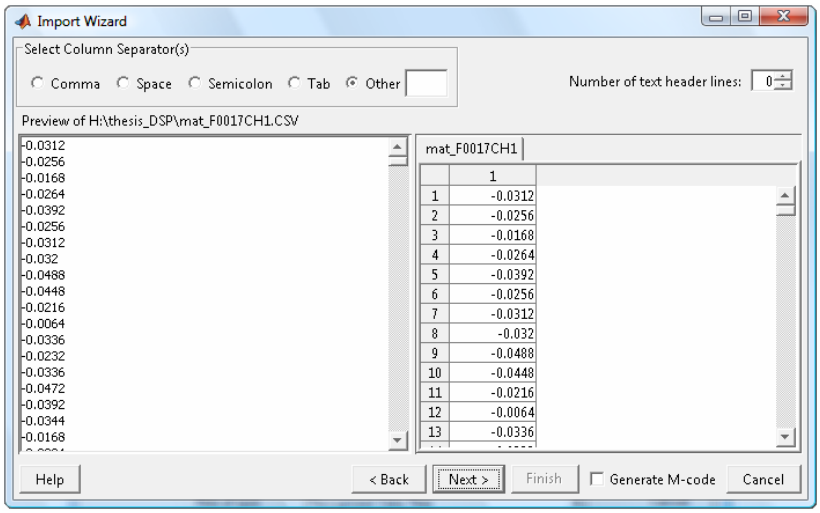

Figure 74: Data Import Wizard

By selecting different options the required data series can be selected in Import Wizard. Then by pressing the ‘Next’ button and pressing ‘Finish’ in the next appearing page a column matrix (vector) can be created in the MATLAB workspace.

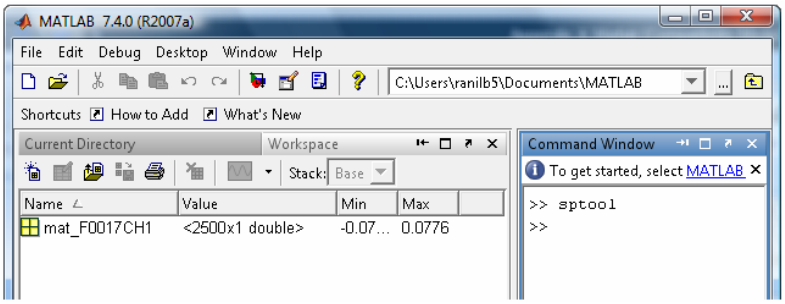

Figure 75: Imported dataset appears in MATLAB workspace as a matrix

In SPTool window, by selecting ‘Import’ from File Menu Import to SPTool window can be opened.

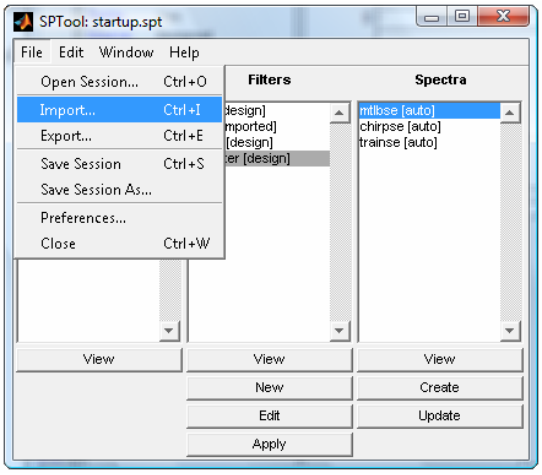

Figure 76: Importing a dataset into SPTool

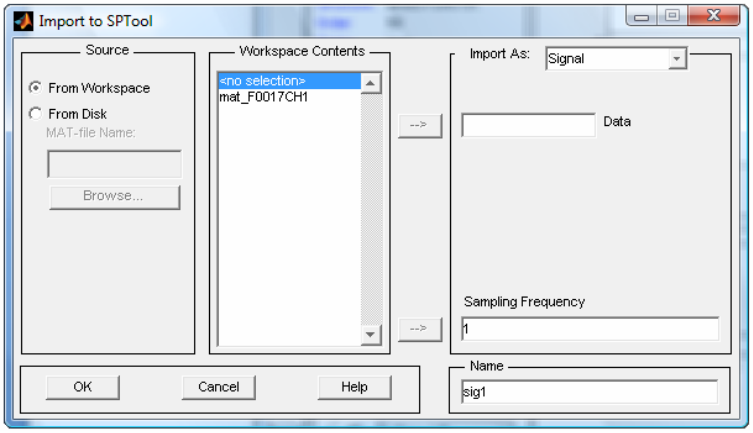

Figure 77: Import to SPTool window

In Workspace Content field a list of all the available datasets can be seen. After selecting the required dataset to be imported and pressing the arrow adjacent to Data field, dataset name can be seeing in the Data field as below. Sampling frequency for the dataset has to be entered. This should be compatible with Fs value defined when designing the filter.

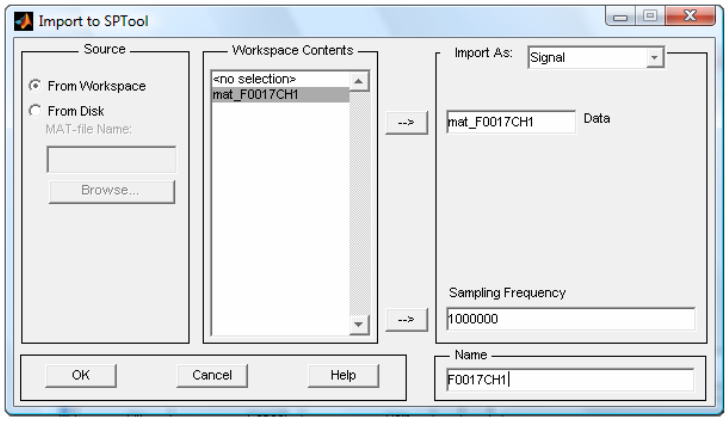

Figure 78: Sampling frequency specification for dataset

A name to recognize the dataset can be typed into Name field and the OK button can be pressed to complete the importing procedure. Then the name of the dataset appears in the Signals field in the SPTool window.

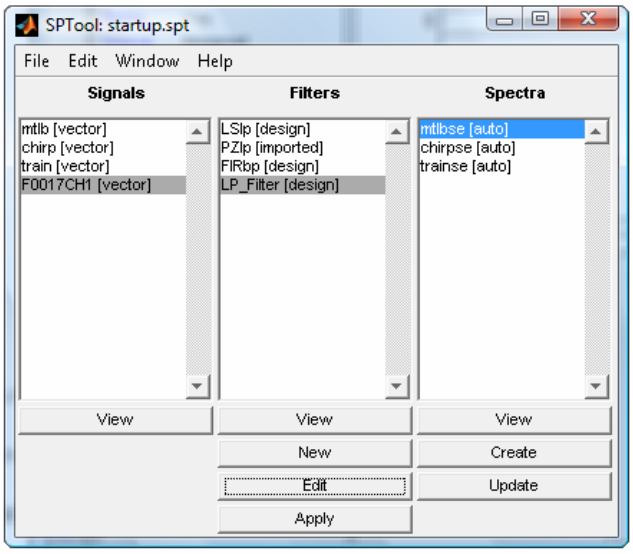

Figure 79: SPTool ready for filtering the dataset

Raw dataset can be viewed by pressing The View button in the Signals field of the SPTool window.

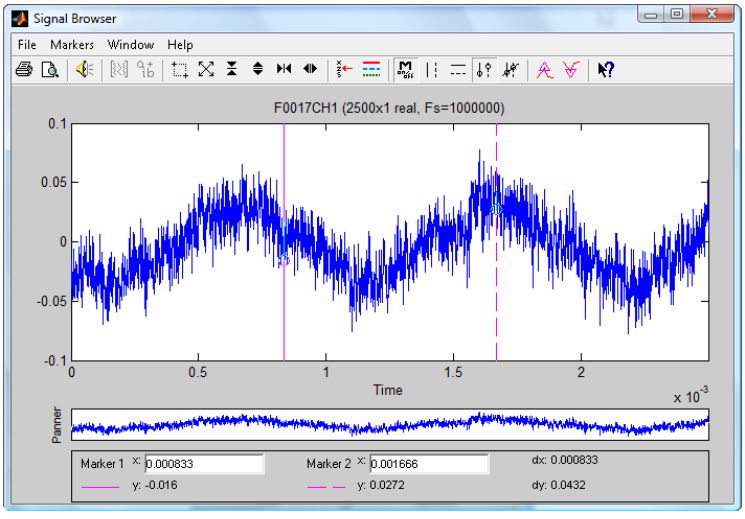

Figure 80: Signal Browser for viewing raw data

4. Applying the Filter to the Time Data Series

After selecting both the data series and the filter in Signals and Filters fields in the SPTool window the ‘Apply’ button has to be pressed to apply the filter to the time data series. In the appearing Apply Filter window a name for the filtered signal can be assigned.

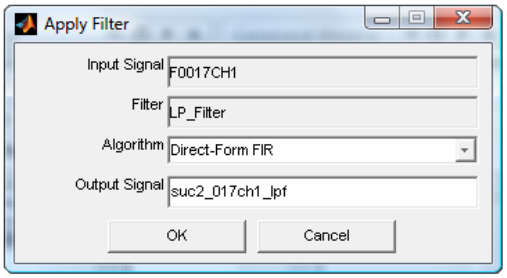

Figure 81: Apply Filter window

When pressed OK in Apply Filter window, the data series will be applied the filter and a new data series with the given name, suc2_017ch1_lpf in this case, will be generated into the Signals field in SPTool window. This can be viewed on Signal Browser by pressing the ‘View’ button under Signals field.

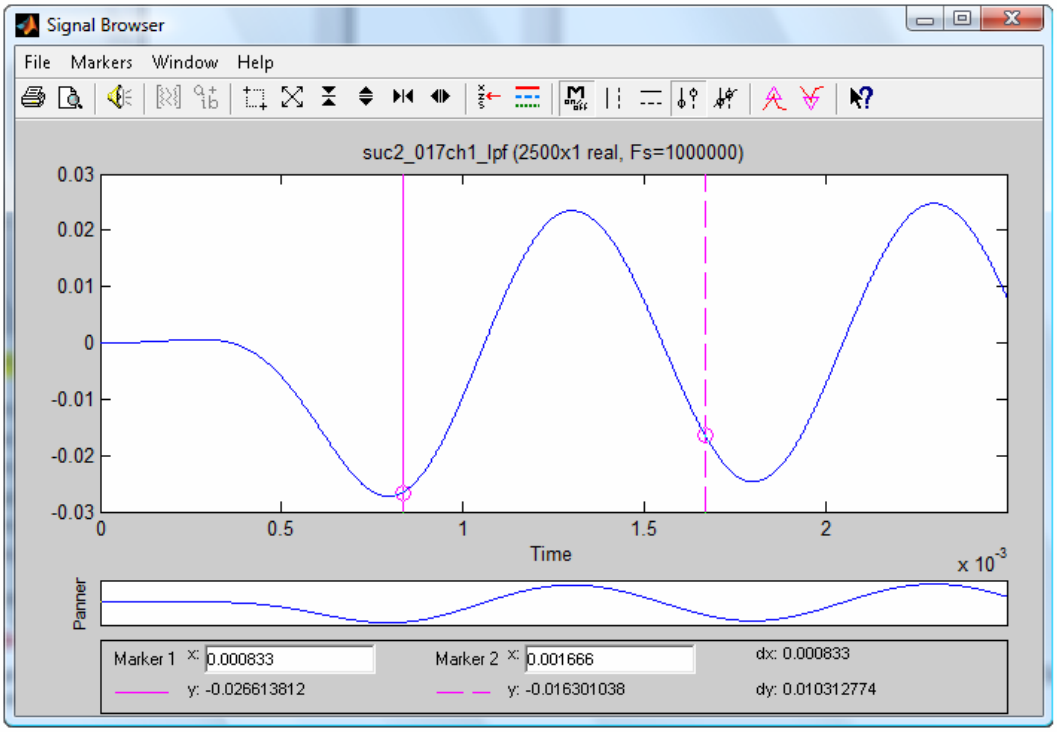

Figure 82: Filtered dataset (signal)

Signal Amplitude can be measured by placing the two cursors at an adjacent peak and a valley, and reading the ‘dy’ value. Then ‘dx’ will show the half-period of the signal.

VITA

Banneyake Mudiyanselage Ranil Ugeeshkumara Banneyake received his Bachelor of Science degree in production engineering from University of Peradeniya, Sri Lanka in December 2005. He entered the mechanical engineering graduate program at Texas A&M University in September 2006 and received his Master of Science degree in December 2008. His research interests include control systems and robotics, FEA, MEMS fabrication techniques, and microfluidics.

Mr. Banneyake may be reached at 19/2 Padiwatta, Kundasale, Sri Lanka. His email address is ranilb5@yahoo.com.